NASA-CR-194215

MCAT Institute
Final Report
94-005

8P

Planetary Entry Experiments

Roger Craig

July 1994

NCC2-762

MCAT Institute
3933 Blue Gum Drive
San Jose, CA 95127

JUL 1 4 1994
To CASI

Radiometer Window Design Definition:
April 1, 1992 To August 31, 1993
Objective:
Identify and document the critical new instrument technology
of window design for radiometric measurement of the forebody
radiative heating experienced by atmospheric entry spacecraft.

Results:
Objective has been met and the completed paper is being
published as a NASA TM[1]. A draft copy is attached.

Planetary Atmospheres:
Objective:
Complete a survey of the current state of understanding of
chemical species on selected solar system bodies. Assess the
importance of measurements with regard to vehicle
environment and with regard to understanding of planetary
atmospheres with emphasis on Venus, Mars and Titan.

Results:
This work was performed in collaboration with G. Carle, Chief
SSS. The assessment has been made and a report submitted to
G. Carle. This report was the basis for a proposal for
instrumentation of a Discovery class mission to Venus. This
proposal was submitted by G. Carle and R. Craig. In addition a
survey was made of planetary atmospheric experiments
ongoing in code SSS and a report prepared of possible
beneficially collaborative activities with code RT. This report
was submitted to G. Carle, and a copy was submitted to the
MCAT office.

VUV Arc jet Test
Objective:
Measure and analyze the radiation (VUV to near-IR) from the
shock heated gas cap of a blunt body in an Ames arc Jet wind-
tunnel facility.

Results:

---

[1]Craig, Davy, and Whiting, "Science Objectives and Performance of a Radiometer and
Window Design for Atmospheric Entry Experiments", NASA TM, 1994

The experiment was performed during the summer of 1992. The initial results covering the wavelength range from the UV to the near IR have been presented by Dr. Craig at an international meeting of the ISA[2]. A copy is attached. The VUV results have been identified as Commercial Sensitive Technology and have been presented to NASA for publication as a NASA TM[3] with CST restrictions. A copy is attached.

Collaborative work has completed calibrations of the arc-jet data and these results are the basis for research on the aerothermodynamics of the arc-jet wind tunnel. This work has been published and includes a comparison of the experimental results with theoretical calculations[4]

Planetary Atmospheres:
August 31, 1993 to May 31, 1993

Objective:
a) Explore the possibility that electrical interference on the Pioneer Venus probes was caused by reactions between exposed conducting elements on the probe and chemical species in the lower atmosphere of Venus.

b) Conduct research on the chemical composition of the lower atmosphere of Venus with emphasis on the complex equilibrium chemistry under scenarios of introduction of volcanic effluent.

c) Re-examine the PVGC 1978 in-situ data with emphasis on reported levels of molecular oxygen.

d) Conduct research on the aerosol formation in the atmosphere of Titan.

Results:

---

[2]Palumbo, Craig and Carrasco, "Spectral Measurements of Shock Layer Radiation in an Arc-Jet Wind Tunnel", Proc. of the 39th International Instrumentation Symposium, Sponsored by the Instrument Society of America, Albuquerque, N.M., 1993
[3]Craig, Palumbo and Carrasco, "VUV Shock Layer Radiation in an Arc-Jet Wind Tunnel Experiment", NASA TM 108796, 1994.
[4]Craig et. al., "Measured and Calculated Spectral Radiation from a Blunt Body Shock Layer in an Arc-Jet Wind Tunnel", submitted for the AIAA 32th Aerospace Sciences Meeting, January 10-13, 1994, Reno Nevada

a) Species calculated to exist at equilibrium, but not detected experimentally, were examined for possible chemical or electrical interactions. The effects of introducing metals vapors such as would be generated by degradation of the Venusian surface rocks were computed. The results of this work were presented at the PIONEER VENUS PROBE 12.5 KM ANOMALY WORKSHOP held at Ames on Sept 28-29, 1993, at which I participated as a working member, and as the portion of the Proceedings of this workshop[5] on the chemistry of the lower atmosphere of Venus. A copy of my report is attached.

b) The effects of introduction of volcanic gases has been studied. Measurements of gases from the Merapi volcano are used a model. Complex chemistry has been calculated from the mixing of these gases with the atmosphere of Venus. An example of the results of adding aluminum for a volcanic event is included as a graph. Various condensed species are seen as well as the evolution of SO3 and molecular oxygen. The results are being prepared for publication as a monograph.

c) Examination of the archived 1978 spacecraft data, together with a literature survey, has resulted in increased confidence of the originally reported data. This is of great significance because of the lack of acceptance of this data and its importance to the understanding of the atmosphere of Venus. This information has resulted in a proposal submission (4/15/94) to continue to study this problem[6]. A copy of this proposal is attached. In addition, identification of the need to develop the necessary computational techniques to conduct this work resulted in a proposal for DDF support. A copy of this proposal is attached.

d) Experimental results have been compared with theoretical results and the need to develop a laboratory data base of the growth rates of aerosols in Titan's and other atmosphere has been identified. The experimental program to perform this research has been developed. This program has been proposed for overguideline RTOP support. A copy of the proposal intent

---

[5]Seiff, Sromovsky, Borucki, Craig, Juergens, Young, and Ragent, "Report of the Pioneer Venus 12.5 km Anomaly Workshop", 1994 in preparation.

[6]Determination of Molecular Oxygen Abundance in the Lower Atmosphere of Venus, Roger Craig, PI., response to NRA 94-OSS-01.

(submitted in response to a call from SS) is attached. The complete proposal is due in response to a HQ call expected in August, 1994.

APPENDIX - A

07 3a5
32a9l0   76p

Science Objectives And Performance Of A Radiometer And Window Design For Atmostspheric Entry Experiments

Roger Craig
MCAT Institute
Moffett Field
California

DRAFT

Science Objectives and Performance
of a
Radiometer and Window Design
for
Atmospheric Entry Experiments

ROGER A. CRAIG[1], WILLIAM C. DAVY[2] AND ELLIS E. WHITING[3]

ABSTRACT

The Radiative Heating Experiment, RHE, aboard the Aeroassist Flight Experiment, AFE, (now cancelled) was to make in-situ measurements of the stagnation region shock layer radiation during an aerobraking maneuver from geosynchronous to low earth orbit. The measurements were to provide a data base to help develop and validate aerothermodynamic computational models. Although cancelled, much work was done to develop the science requirements and to successfully meet RHE technical challenges. This paper discusses the RHE scientific objectives and expected science performance of a small sapphire window for the RHE radiometers. The spectral range required was from 170 to 900 nm. The window size was based on radiometer sensitivity requirements including capability of on-orbit solar calibration. Window contamination from

[1] MCAT Institute
Work performed under NASA Cooperative Agreement NCC2-762
NASA Ames Research Center
Moffett Field, CA 94035

[2] Eloret Institute
Work performed under NASA Cooperative Agreement NCC2-XXX
1176 Maraschino Drive
Santa Clara, CA 94057

[3] Eloret Institute
Work performed under NASA Cooperative Agreement NCC2-XXX
1176 Maraschino Drive
Santa Clara, CA 94057

DRAFT

spacecraft material (volatiles or particulates) is a concern, especially for ultraviolet performance, and requires careful identification and control. The window described can withstand the aeropass heating pulse and maintain optical performance to meet the objectives.

I-INTRODUCTION

The advent of the Space Station Freedom will usher in a new capability for planetary exploration and utilization of Earth/moon space. Lunar and planetary mission vehicles could be assembled, deployed, and retrieved on this platform without ever returning to earth. New, efficient, space transportation systems are needed to exploit this capability. A promising technique is aeroassist-- an Aeroassisted Space Transportation Vehicle, ASTV, is a vehicle equipped with a lightweight, low L/D, forebody heatshield. An ASTV, returning from a mission, would need to decelerate and alter its orbital parameters to rendezvous with the space station. These orbital changes would be achieved during a pass through the upper atmospheric (figure G). By controlling pitch and roll, the forebody aerodynamic forces would be directed to exit the ASTV into the desired orbit. The STS could then provide the link with earth.

Aeroassist can reduce or eliminate the need to carry decelerating retro-rockets and their fuel on a mission. There is potential for substantially lower space transportation costs if light weight, efficient heat shields can be designed. The present capability for predicting the ASTV heat protection requirements is based on the present capability to model aerothermodynamic processes. These models are of necessity based on many approximations and need validation data to reduce uncertainties. This is especially true for predictions of the heat load from the shock layer radiation. These uncertainties need to be resolved before we can design heat shields with minimum conservatism to degrade the benefits.

DRAFT

A NASA Aerocapture Technology Working Group was formed in 1980 to meet this challenge. This group identified specific technical issues which must be addressed to develop the design capability for routine use of aeroassist to modify orbits. The group agreed that a technical data base from a flight experiment was required. This data base would be used to improve and validate computational models which would form the basis for ASTV design codes. Radiative heating was identified as a critical heating source to be understood and an experiment, the Radiative Heating Experiment (RHE), reference K, was identified to help answer the radiation questions. A flight test vehicle was defined, the Aeroassist Flight Experiment (AFE, reference A), to be instrumented to gather, in-flight, the needed data base. The AFE, depicted in figure B, was small aerobrake, STS deployed into low earth orbit (LEO) and rocket driven into the Earth's upper atmosphere at the velocity and entry angle of an ASTV maneuvering from geosynchronous earth orbit (GEO) to LEO. The AFE would perform the aeropass, exit and return to the LEO for STS recovery and return to ground.

The AFE was given new-start approval in 1987. Although cancelled in 1991 due to funding limitations much work was accomplished to solve technical challenges. The Radiative Heating Experiment goals and engineered design were well matured. Many RHE design challenges were successfully met and results of these efforts should have application elsewhere. From the computational standpoint, a specification of the data needed to help validate predictive heating models incorporating radiation transfer was developed. Experiment objectives and flight instrument requirements were developed. The harsh flight environment required development of a window which would withstand the aeropass heating pulse and transmit the needed spectral radiation information to the transducer. Several window concepts were examined and viable designs were tested. The purpose of this paper is to present the RHE experiment objectives and rational, the results of the window development and the expected science return. It is expected that these results will be of interest and use to

3

DRAFT

designers of other spacecraft mission experiments involving
atmospheric entries.

II-FLIGHT MISSION

ASTV FLIGHT PATH

The flight path of a maneuvering ASTV is compared with those
of the STS and the Apollo in figure A. The ASTV entry is
initially similar to the Apollo entry since both would be
returning from relatively distant missions (GEO or lunar). But
the ASTV is maneuvered away to decelerate and change its
orbital parameters, mainly between 75 and 90 KM, and leaves
the atmosphere in an orbit accessible to the STS. Although the
STS and Apollo trajectories pass through the ASTV
maneuvering altitude, neither substantially alters its velocity
there. These vehicles are designed to withstand their major
aerodynamic heating at lower altitudes. Their heat shields are
overly conservative for their passage through the ASTV
altitude and their experience offers little information on which
to develop efficient ASTV design codes.

The AFE shape is given in Figure B. It is shaped like an
operational ASTVs but at 1/4 scale. It was designed to fly at a
constant trim angle of 17° to produce drag and lift and fly a
trajectory of an ASTV maneuvering from GEO to LEO. The
planned trajectory is shown in Figure F. The atmospheric entry
velocity is 9.89 km/sec at 122 km altitude. Navigation control
was to be by rolling the spacecraft to redirect the lift/drag
vector. The orbit engineers optimized the flight profile around
the two indicated velocity/altitude points. The trajectory, from
entry to exit would take 600 seconds. Details of the AFE flight
are found in Reference M.

III-EXPERIMENT SCIENCE OBJECTIVES

An ASTV would be distinguished from other spacecraft by the
incorporation of a large, blunt, aerobrake surface. An ASTV
would meet the atmosphere head-on at hypersonic speed and

be exposed to substantial surface heating. This heating would include a radiative component perhaps equal to the convective heating. Accurate predictions of this heating requires the solution of the real gas conditions of the flow field environment of the vehicle. Predictive codes, incorporating realistic gas properties, are being developed at Ames and elsewhere. Predictions of the AFE shock layer properties, from an Ames two temperature aerothermodynamic code, are shown in figure C from reference B. The calculation is for the conditions of peak heating (9.5 km/sec and 77 km altitude). The vehicle size, velocity, and altitude result in a shock predicted to be composed largely of thermally non-equilibrated gas. This is evidenced by the large difference between the high translational temperature, T_t, and the vibrational temperature, T_v, near the shock. This difference diminishes toward the surface to a more nearly equilibrated state. The initial collisions which form the shock convert the kinetic energy of the impact velocity of the air directly into random motion (T_t). Just after the shock T_t is very high, about 50,000 K. Subsequent collisions and other kinetic processes distribute this energy into other internal modes. N_2^+ is formed, N_2 and O_2 dissociate, and reactions proceed to produce NO. The vibrational levels of the molecules eventually are populated and T_v is seen to approach the decreasing T_t. The temperatures relaxes toward each other to about 8500 K as the gas equilibrates. At the low densities of a maneuvering ASTV this relaxation process occupies a significant portion of the shock layer.

An important objective of the AFE was to generate a data base to validate predictive models of radiative heating at the ASTV forebody stagnation region As seen in the figure this heating is predicted to be dominated by emission from the nonequilibrated gases near the shock. The thickness of this region is determined, approximately, by the collisions which drive the gas kinetic processes. For the same maneuver this thickness, and hence the radiative flux from the nonequilibrated regions, is approximately constant with vehicle size (Reference R).. This zone merges with the cooler boundary

DRAFT

layer on small configurations at high altitude conditions (Reference I). This would apply to the size of models which could be used in ground based tests (ballistic ranges, shock tubes, or arc-jet wind tunnels), namely much less than one meter. Validating data from this kind of test would be hampered by a distorted relationship between the kinetic processes as compared with a full scale ASTV. In addition modelling the shock layer of these small shapes would necessitate solving the merged boundary layer also- a different boundary condition from the full scale case. Extrapolation from ground based test results to full scale conditions would involve many uncertainties and require large conservatism. Further, some 3-D calculations have indicated important- processes with relaxation times on the order of the AFE shock layer residence time (Reference H). This phenomena would never be observed on a small test configuration. In contrast, the shock layer of full sized vehicles flying at low altitudes (higher densities) will be mostly equilibrated gases with a very thin, nonequilibrated region at the shock. Apollo and the STS experience most of their heating under this condition. An instrumented subscale ASTV, such as the AFE, flying an ASTV maneuver, was needed to meet the technical requirements. The AFE diameter, limited to the dimensions of the STS cargo bay, was 4.26 meters. This diameter would be adequate to provide a isolating zone of nearly equilibrated gas between the non-equilibrated region of the shock layer and the cooler boundary layer and would provide a suitable platform to develop the data base to help resolve the radiative heating and other ASTV design issues.

SHOCK LAYER RADIATION
The radiating shock region contains a mixture of gases over a large range of conditions and involves many kinetically limited processes (Reference F). The surface flux, even though spectrally resolved, would contains emissions from a complicated source. Surface flux measurements of molecular band systems, for example, would be the aggregate emissions, along lines-of-sight, from the populations of excited molecules over a range of thermodynamic and molecular conditions. Although apparent temperatures (kinetic, rotational and vibrational) would be indicated in the data, they would, in

DRAFT

reality, be the summation of a variety of concentrations and conditions and possibly include absorption. Analysis of this data to understand the conditions within the shock layer would require companion computational models to correlate the measurements with a realistic representation of the physical principles of coupled high speed flight and radiation (spectroscopy). This correlating model would be, of course, an important step toward a validated ATSV design code.

Preliminary codes describing the radiating shock layer of an ASTV have been developed at the ARC. These codes were the basis for developing the science objectives for the RHE. Predictions of the radiant flux onto the surface of the maneuvering AFE were done for species which were expected to be important. Results of these calculations are contained in reference J. Figure E is the calculated spectrum of the radiative flux onto the surface of the AFE near peak heating assuming an optically thin shock (reference B). Molecular systems as well as atomic lines are evident. Atomic nitrogen and oxygen lines are seen in the vacuum ultraviolet, VUV, (100 nm to 180 nm), with the Birge-Hopfield system, (BH-1), of molecular nitrogen as the underlying background. Molecular bands from nitric oxide[4] are seen from 190 nm to 300 nm. Molecular nitrogen[5] systems contribute energy from 280 nm on and then merge with other, stronger molecular bands systems[6] which then dominate the molecular radiation from 300 nm to the infrared. Atomic lines are also seen in the infrared. Very little radiative heating is expected from the infrared beyond one micron.

Because of the subscale size of the AFE, radiative heating is predicted to represent only about 10% of the total heating and is therefore not of overwhelming concern to the AFE. Therefore the RHE was not configured to measure and assess the radiative heating to the AFE, but rather to gather a radiative flux data base to identify the important radiators and

---

[4] NO_γ, $A^2S^+ - X^2P$, and NO_β, ≡≡≡≡≡≡

[5] $N_2(2+)$ bands, XXXXXXXXXXX

[6] $N_2^+(1-)$, $B^2S_u^+ - X^2S_g^+$, CN_v, $B^2S - X^2S$, and $N_2(1+)$, $B^3\Sigma_g - X^3\Sigma_u^+$

DRAFT

to validate the calculated gas properties of the flow field calculations including radiative transport. Such a validated model could then be used to establish the requirements for an efficient full scale ASTV heat protection system.

<u>Vacuum Ultraviolet:</u>
Some of the atomic lines in the VUV are extremely intense and are the subject of concern. Various models of these line emissions predict widely different radiative heating levels ranging from insignificant amounts to levels dominating the overall heating (references B, C, and D). Since the VUV emissions are from transitions to the ground states a description of the surface flux is complicated by spectral absorption from a range of condition of the absorbers between the emitters and the surface. A realistic, predictive model must include accurate details of the absorption and emission. Calculations at the ARC (reference B) indicate that if the VUV line radiation would reach the surface unabsorbed, the resulting heating would be vastly more than the convective heating. The VUV emission is from the nonequilibrated regions close to the shock. Here the spectral lines are strongly doppler broadened by the high kinetic temperature. The cooler parts of the shock and boundary layer are calculated to absorb these strong features directed toward the surface. But these cooler absorption regions have spectrally narrower absorption features resulting in the curious effect that the intense region at the line center is absorbed and only the energy in the wings reaches the surface with any heating significance. The total line emission can be calculated reasonably precisely. But the problem of the overall absorption is difficult because accurate spectral distributions of energy over the emission line shape, and over the absorbing line shape are needed to properly determine the ultimate energy reaching the surface. The Ames model predicts that absorption will reduce the VUV flux by 99.8% to represent about 25% of the radiative heating of the AFE, but errors in the calculated line shapes could result in disproportionate errors in the prediction of surface heating rates.

DRAFT

ARC predictions (reference B) of the total flux from all of the VUV atomic lines over the AFE trajectory are plotted in figure J together with predictions of the total radiative surface flux and the flux from the group of 174 nm atomic nitrogen lines. The predictions are not accurate at the low densities where the intensities are low ($0<t<60$ seconds, and $t>250$ seconds) and are represented herein only as qualitative. The total radiation from the VUV lines is predicted to be controlled by self absorption, and become optically thick, throughout the period of significant radiant heating. The importance, and perhaps spectral details, of the heating from these intense VUV lines needs to be ascertained. The lines at 174 nm contribute substantially to the total VUV and they too become optically thick. Of primary importance is to obtain measurements of these lines during the initial portion of the aeropass, while the radiation is at low optical density, the increase to optically thick conditions, and adequately into the subsequent optically thick region to establish its intensity. Also important, but secondarily, would be the analogous measurements on the outward leg of the trajectory to establish the transition from optically thick conditions to as far as the intensity would permit. These measurement periods are seen from figure J to be from entry to 100 seconds, and from 200 seconds to exit

UV-Visible:
Most of the heating of a maneuvering ASTV is predicted to come from the strong $N_2^+(1-)$ and CN_v molecular band systems in the near UV and visible regions of the spectrum. From the viewpoint of heating this spectral region is probably optically thin. Measurements of the detailed spectral radiative flux in this region would help identify unexpected, but important, radiators in the shock layer, and would be the basis to validate predictions of the conditions of the importantly radiating gases. Code validation of these measured molecular spectral features would be a very powerful validation of the predictive capabilities.

Infrared:
Rich and diagnostically important atomic line radiation is predicted from oxygen and nitrogen in the infrared. These

DRAFT

lines also emanate from the hot regions near the shock. The range of intensities of these lines is from weak (unabsorbed) to moderate (partially absorbed) levels. Measurements of the unabsorbed lines would yield information, unmodified by absorption, about the emission phenomena which is from the gas near the shock. Measurements of the flux from the partially absorbed lines would yield information about the absorption properties of the intermediate, cooler gases

Under the conditions of a maneuvering ASTV electronic excitation of these atoms is by electron collisions. Measurements of the IR line intensities would help validate predictions of ionization levels and electron gas temperatures. The absolute measurements of the intensities of these lines could also help determine the atomic density profiles through the shock.

IV-RHE INSTRUMENT PERFORMANCE

The objective of the AFE was gather flight data to help develop the design technologies needed for efficient ASTVs, and the RHE objective was to provide data to address the radiation issues. Since the radiating medium was complex in composition and state, surface flux measurements alone would not be useful. The RHE relied on companion predictive codes to develop the objectives, and would also rely, in turn, on these codes for post flight data interpretation. This experiment/code relationship concept was successfully employed in a pioneering flight experiment, the PAET (Reference L). PAET was an Earth entry experiment which measured shock layer radiation with none spectrally resolved radiometers. The data was combined with results from a computational model to determine properties of the ambient gas. This test was designed to demonstrate the potential to obtain data during the high speed entry of a planetary probe which could be used to determine the atmospheric composition.

Successful predictions of the observed RHE quantities by the physics of the gas chemistry and spectroscopy incorporated in

DRAFT

the computational codes would require matching of many observed quantities. Consistency of the results would in turn result in confidence in the predictions of the details of shock layer gas conditions. The RHE was to make absolute spectral measurements of the stagnation region surface flux, under conditions of important radiative ASTV heating, to validate the VUV and longer wavelength radiation calculations, and to help determine the shock layer gas conditions (concentrations, Tk, Tv, Tr and Te).

In each case measurements would be made at several locations through windowed penetrations of the AFE stagnation region heat shield.

These objectives, with predictions of the surface radiative flux, (see figures C, J and E) formed the basis for the RHE instrument performance requirements. The requirements were, in part, as follow below:

Obtain spectrally resolved surface flux data from the AFE stagnation region gas cap. Measure the flux from the atomic nitrogen lines at 174 nm to provide assessment of the VUV calculations. Measure the range from 200 nm to 900 nm with sufficient spectral resolution for code validation;

Obtain spectrally integrated data using a wide band detector, such as a blackened thermopile, to measure the spectral radiation from the VUV to the IR. This data would provide a level of redundancy with the spectral instrument, and would help determine the sufficiency of the spectral data to provide validation for overall radiative heating;

Provide a windowed aperture to isolate the detector from the shock layer gases. The window to be mounted flush with the spacecraft surface so as to not disturb the boundary layer flow; and

Obtain a broad band measurement and a complete spectrum every 3 seconds during the 600 second AFE trajectory.

11

DRAFT

These requirements formed the basis for a Request for Proposal and a fully competed contract was awarded to Martin Marrietta Corporation, Denver, CO.

V- RHE INSTRUMENTS

The contractor developed the design of the instruments and completed a CDR for all but the windowed aperture. The final design is summarized as follows.

The contractor determined that instrument requirements could be met using a small, grating spectrograph (0.125 meter focal length) with a ‾scanning, linear photocathode array detector. The UV spectral sensitivity of a sample, windowless, commercially available, array detector was measured to extend to below 160 nm by the contractor team (reference N) . Their measurement result is shown in Figure H. Spectral resolution of 0.6 nm from 174 nm to 800 nm was thereby attainable. Their sensitivity measurements, together with predictions of the radiation intensities, showed that this setup was adequate to meet the scientific objectives including intensity measurements of the 174 nm atomic nitrogen lines.

Sensitivity and dynamic range requirements for the spectrally integrated data were met with a thermopile detector. The spectral response of such a detector, for purposes herein, would only be limited by the window transmission.

FLIGHT WINDOW DESIGN
The window design was not matured to a CDR level at the time of program termination. Although a flight article had not been designed and tested, considerable progress had been made. Viable designs, which would survive the aeropass and meet all or part of the experiment objectives, had been developed and tested. The results indicated window configurations which have a high likelihood of flight worthiness. This section describes these designs and their expected science return.

<u>Requirements:</u>

DRAFT

Window design requirements included adequate optical performance to meet the scientific objectives and survivability to not compromise mission safety. The scientific objectives required, in part, that the window transmit radiation over the range of interest, e.g., from 174 nm to several microns, over important portions of the trajectory. The widow and its mounting would experience high convective heating rates which might include heat liberated from catalytic reaction of recombining atoms diffusing to the surface, and thermal shocks.

Sapphire was determined to be the material of choice for the window (Reference O).

Spectral transmission:
Sapphire, at room temperature, transmits ultraviolet radiation from well below 174 nm to well into the IR. The short wavelength cutoff of sapphire's transmission is due to the long wavelength edge of a broad absorption band. At elevated temperatures this band widens. Thus the shortest VUV wavelength transmitted increases with temperature. A discussion of this phenomenon, from the standpoint of glasses, is in Reference Q. The maximum sapphire window temperature which would be useful for measurements at 174 nm was measured by us (Reference O) to be about 800 C (1472 F). This was done by measuring the 174 nm transmission of a heated specimen window. The measurement results are shown in Figure L.

The short wavelength cutoff of sapphire infrared transmission, about 5 microns, insures that the aeropass heating will not degrade the optical transmission at the IR wavelengths of interest herein (e.g., 1 micron).

Window heating:
The AFE aeropass heating rate is shown in figure D. This heating pulse would rapidly raise an uncooled window to temperatures well above 800 C. Indeed, during simulated aeropass heating testing in an arc-jet wind tunnel, uncooled sapphire reached its melting temperature (2040 C) and

13

ablation was observed. Because of sapphire's low infrared emissively radiative cooling does not significantly help maintain the desired temperature. The minimum design requirement, which could meet the science objectives, is that the window maximum temperature not exceed 800 C for at least the first 100 seconds of the entry, and then if possible during the period after 200 seconds with a desired goal of maintaining the temperature below 800 C for the entire aeropass.

To achieve the required ultraviolet performance the entry heating would have to be offset by a thermal mass to maintain a manageable temperature.

Window designs:
A development program was conducted and several designs concepts were built and subjected to laboratory tests. These tests consisted of exposing the windows and their mounting configurations to various heating loads simulating the AFE entry heating and included aggressive, overly conservative, testing in an arc-jet wind tunnel (reference O). Successfully surviving these tests would insure that the design would survive the aeropass and not pose a risk to spacecraft or the experiment. Some of the tests specimens were instrumented with thermocouples to develop computational models of the in-depth thermal response of the window and its mount during the arc-jet tests (reference P). These models were in turn used to predict the thermal response during the flight mission.

Two design, one uncooled and one cooled, were shown to be promising as bases for design of a flight window which would survive the AFE entry environment and yield scientific data. Both designs used niobium in the construction of the mounting hardware. The regions of the niobium which could be exposed to the shock heated air were coated with a silicide coating to protect them from chemical erosion (reference P).

A design, called the uncooled design, employing thermal isolation between the sapphire and the mount was configured. Alumina paper and fibrous insulation (FRCI-15, STS type heat

14

DRAFT

shield material) was used to reduce the thermal conductance between the sapphire and its mount as shown sketched in Figure O. This design was instrumented and tested in the arc-jet wind tunnel Windows of 13.7 mm diameter and of thicknesses from 1 mm to 3 mm were not damaged during the arc-jet tests.

Predictions of the thermal performance of the uncooled design during the AFE aeropass are shown in figure M. This window would be adequate to gather data UV-VIS and IR spectral regions over the entire trajectory. However the hottest portion of the window is predicted to reach 800 C at about 130 seconds into the trajectory. This would allow measurements of the 174 nm region for the initial portion of the trajectory but would be too hot during the period after 200 seconds.

Two cooled designs were evolved by the contractor. Both windows were cooled by conduction through a copper element to the metallic mounting and thence to a heat sink. High thermal conductivity was assured by a copper element which was brazed with a eutectic bond (developed by Martin Marrietta Aerospace Group) to the inner surface of the sapphire and in turn was brazed to the upper end of the support tube (reference O). One configuration employed a 14.5 mm diameter window with a copper screen, 50% open, bonded to the surface as the copper element. A smaller window configuration was 10.7 mm diameter and a copper washer bonded to the flat edge of the window. Both of these configurations were built and were not damaged during the arc-jet tests. Both designs would transmit the same amount of radiation and would satisfy aperture requirements of the experiment.

These cooled configurations are shown sketched in Figure K.

Predictions of the performance of the cooled designs in the configuration of the test specimens were not made. Instead a recommended cooled design was developed based on these test results. This design is shown sketched in figure P Note that this design shields the silicide coated areas of the holder by

DRAFT

overlapping the heat shield material. This would reduce the problem of possible window contamination from the coating. This problem is discussed below under "Window Contamination". Predictions of the thermal performance of this design during the AFE aeropass are shown in Figure N. The maximum temperature of this window remains below 800 C for the entire aeropass so this window would meet the thermal goal. The scientific objectives could be met over the entire aeropass.

SOLAR CALIBRATIONS

In order that the RHE data be useful, it must be credible. Experience with absolute measurements of radiation teaches the value of calibrating before and after a measurement. But the RHE instrumentation would not be available for laboratory testing for a substantial period before the flight, perhaps as long as one year, and for a substantial period after the flight. The sun would provide a useful calibration source which would be available just before and just after the aeropass. The source strength can be well characterized and there is no problem with atmospheric interference. The UV-Vis to IR spectral region would be well calibrated but scattered light problems within the spectrograph would make calibration at 174 nm difficult. A spectrally selective filter would probably be required during this calibration.

Calibrations using the sun were deemed to be important to insure credibility of the data. However these calibrations required spacecraft resources to be expended to point each radiometer in turn at the sun. In addition the radiometer view field needed be adequate to accommodate errors in navigation, pointing accuracy, and spacecraft drift during the calibration time. In the AFE case a circular, radiometer view field of 22 millisteradians was be required to guarantee capture of the entire sun's disc without vignetting. The radiometer mounting requirements behind the heat shield dictated a window diameter of 14.7 mm to achieve this viewfield. The arc-jet tests suggested that an uncooled window this size would suffice at the cost of the later period VUV data. The larger cooled window required a screen brazed over the entire under surface

of the sapphire, the presence of which would make it difficult or impossible, to guarantee what fraction of the sun was obscured by the opaque portion of the screen.

<u>Window lens:</u>
The maximum window diameter (based on performance requirements) with the minimum distance from the window to the instrument aperture (based on spacecraft requirements) will not subtend an adequate viewfield for solar calibrations needs. The view field of the small, edge cooled window could be increased to without compromising the radiometer objectives by fashioning the inner surface of the sapphire into a negative lens. The effect would be to increase to viewfield of the for solar calibration purposes without decreasing the sensitivity with respect to the shock layer radiation from that of the flat cooled windows. With respect to the radiometer the radiating shock layer is an relatively uniform, extended source but the sun is a discrete source. Such a lens will slightly alter the region of the shock being measured but would not change the shock layer flux reaching the radiometer. An illustrative design, based on the dimensional requirements for the AFE, of a lens-apertured window is shown in Figure Q. A virtual image of the solar disk is formed within the extended field of view of the internal solid angle. The negative curvature required is very small and would have negligible effects on lessons learned during the arc-jet tests. Use of data gathered under this configuration would, of course, require a different geometrical interpretation of the radiating regions of the shock layer contributing to the signal.

WINDOW CONTAMINATION:
Window contamination is a serious concern to the credibility of the data. Trace window contaminates can significantly increase the uncertainty of radiometric data, particularly if the ultraviolet. Sensor windows can be fouled during all phases of the AFE mission by contaminants form a variety of sources. Any spacecraft experiment expecting to gather reliable radiometric data will have to be particularly critical of the presence and thoroughness of a contamination control activity to identify, assess, and control the problem. An estimate of the

DRAFT

expected contamination, from an inventory of known contaminants, is important to help assess the validity of the solar calibrations and the data. Three types of window contamination, their sources, and implications for this kind of mission application are discussed below.

Particulates (i.e., dust)

Sources include dust-laden air after the "last access" point when no further cleaning or inspection is permitted, launch vehicle (i.e., STS or other carrier) payload bay dust dislodged during launch, orbit operations in the vicinity of the launch vehicle, and particulates ejected by maneuvering rockets, RCS, from either the launch vehicle or the spacecraft.

Protective covers should protect the windows during most ground operations. After final cover removal and cleaning, a characterized clean room environment should be maintained. Vertically positioned radiometer windows will reduce agglomerate of particulates to about 5% of the horizontal rate in a one G environment. The mission activity is different. During the launch of the STS, for example, payload bay dust, including dust from companion payloads, is violently agitated and then "settles" uniformly of all exposed surfaces.

The particulates from the RCS activities can be ameliorated simply by avoiding the spray pattern of the RCS engine. Monopropellant grade hydrazine can contain as much as 1 mg/liter of particulates and a high purity grade is available if required.

The effect of contamination from these particulates should be fairly non-wavelength sensitive and an assessment would be possible from the solar calibrations.

Volatile contaminates (compounds of small molar mass, e.g., H_2O or NH_3):

These contaminates are threats to optical surfaces if they chemically attack the material, or if they are deposited as aerosols containing dissolved solutes that are left behind after evaporation. Potential sources are migration from saturated

DRAFT

surfaces, and from thruster motors venting and exhaust products. Air-borne aerosols, particularly of NaCl in water, could be a problem, for example, at Kennedy Spacecraft Center due to its proximity to the ocean.

Nonvolatile contaminates (nonvolatiles of large molecular mass such as polymeric compounds, including silicone derivatives.:

This class of contaminant is the most deleterious to the radiometry experiments. They can be derived from a variety of sources. They are difficult to remove and in general are strong radiation absorbers, particularly of UV photons. Sources of these contaminants are the spacecraft itself, the payload bay, and companion payloads. The are generated primarily from polymeric compounds, i.e., plastics that are used as matrix binders, in circuit boards, films, adhesives, or coatings. With respect to the AFE silicones were very worrisome in this regard because they are used extensively in the heat shield bonding and they will probably bond strongly to the window material. Solar heating of the spacecraft, and the resulting increase of production of these contaminants, in the vacuum before atmospheric entry, poses a special situation to be assessed. The firing of a major rocket motor can also be a source of nonvolatile fouling as well as the thermal degradation of the polymeric insulation liner after shutdown. During the aeropass contaminants generated from the heat shield by the atmospheric heating will be carried in the boundary layer flow and possible deposit on the windows. In order to quantify the sensitivity to this form of contaminant as estimate was made of the allowable level of film thickness of nonvolatile contaminants. To limit beam attenuation to less than 1.5% at 200 nm, the maximum allowable film thickness is 0.5 nm assuming the reasonable value for the extinction coefficient of 0.0002 nm^{-1}. Considering the probably molecular size of these compounds this value undoubtedly represents a less than monomolecular layer.

Silicide coating contamination:

As seen in figures O and K, the designs of the arc-jet wind tunnel test specimens included a silicide coating on the metallic portions of the window mount which would be exposed to the

DRAFT

flow. Spacecraft experience has shown that this coating is effective in eliminating the metal erosion during atmospheric entries. This coating could likely be part of the design of the flight windows. It was therefore of interest to address possible material from this coating contaminating its adjacent window. The environment of the arc-jet free stream contains contaminants from the arc heater so examination of the window was not conclusive. Several tests were conducted to compare emission spectra from the radiating region near the window with and without a silicide coated holder. Material ejected from the silicide, entering the boundary layer, should show added spectral features. The setup is shown in Figure R. Spectra were taken from XX nm to XXnm and no differences were noted. This test was encouraging but not exhaustive enough to validate flight design performance. Further work would be required if this material were to be used.

The high importance of controlling contaminants requires that a high priority be given to this at every phase of the experiment, spacecraft and mission design.

VI- CONCLUSIONS

Experiment objectives for the Radiative Heating Experiment of the Aeroassist Flight Experiment are described. Although the project was cancelled, the design of the experiment were well matured. The instruments, with the exception of the windowed aperture, had successfully completed a Contractors Design Review. The experiment goal was to develop a data base characterizing the radiation flux incident on the stagnation region surface of an aerobrake returning from GEO mission. The purpose of the data base was to refine and validate aerothermodynamic computational models for these vehicles. The experiment objectives, based on this goal, was to obtain stagnation region surface flux, with 0.6 nm spectral resolution, from 174 nm to 900 nm, during the aeropass. There are serious questions about the importance of the VUV radiation from atomic lines. To help answer this concern data from the atomic nitrogen at 174 nm is shown to be required from entry until about 100 seconds into the trajectory and from about 200 seconds on. Instrument

DRAFT

performance specifications were generated from these requirements were a small grating spectrograph using a UV sensitive linear array was found to meet the specifications. Special, windowless arrays, were found to be useful at 174 nm.

Although the window had not reached the maturity of the instruments, considerable progress had been made. The entry environment of high heating and exposure to the shock layer plasma present special problems. Sapphire was chosen as the material of choice. Window temperatures needed to be below 800 C for use at 174 nm. Small sapphire windows, both cooled and uncooled were built. The former were conductivity cooled through a copper screen or washer brazed to the sapphire. The latter were insolated by ceramic material from the heat sink. Both of these kinds of windows successfully withstood overly conservative arc-jet wind tunnel testing. Scientific performance predictions of these windows were made based on theoretical models of the radiant flux during the entry, and on window thermal performance models based on instrumented arc-jet tested specimens. Three designs are described which would partially or totally meet experiment objectives and would form the basis for the design of a flight window. A recommended design is described.

The importance of credibility of the data is discussed in the context of absolute calibrations and window contamination. Solar calibrations were designed as part of the mission scenario. The influence of these calibrations on window requirements is discussed and the use of a lens instead of a flat window is shown to be possibly required. Window contamination is important and requires special consideration by the experiment and mission designers.

References

Reference A
Williams, L., Putnam, T., Morris, R., "Aeroassist Flight Experiment", Aeronautics Division, Headquarters, National Aeronautics and Space Administration, Washington, D.C.

Reference B
Whiting, Ellis E., and Park, Chul, " Radiative Heating at the Stagnation Point of the AFE Vehicle", NASA TM 102829, November 1990.

Reference C
Carlson, L. A., "Approximation for Hypervelocity, Non-equilibrium, Radiating, Reacting, and Conducting Stagnation Regions", AIAA Thermophysics, Plasmadynamics and Laser Conference, June 27-29, 1988, San Antonio, TX, AIAA Paper 88-2672.

Reference D
Moss, J. N., "Non-equilibrium Thermal Radiation for an Aeroassist Flight Experiment Vehicle", AIAA Paper 88-0081, Jan. 11-14,1988.

Reference E
Palumbo, G., "Shock Layer Vacuum UV Spectroscopy in an Arc-Jet Wind Tunnel" NASA TM 02258, January, 1990.

Reference F
Park, C., "Problems of Rate Chemistry in the Flight Regimes of Aeroassisted Orbital Transfer Vehicles", Reprinted from "Thermal Design of Aeroassisted Orbital Transfer Vehicles", H. F. Nelson ed., Progress of Astronautics and Aeronautics, 96, 1985.

Reference G
Palumbo, Giuseppe , Craig, Roger and Carrasco, Armando., "Spectral Measurements of Shock Layer Radiation in an Arc-Jet Wind Tunnel"

Reference H

Reference which showed the AFE radiation peaking along the surface (Chandler)

Reference I
For the same manuveur this thickness, and hence radiative heating from the nonequilibrated regions, is approximately constant with vehicle size. In the cases of small, ground based test shapes, tested at high altitude conditions, this zone merges with the cooler boundary layer (reference I).

Reference J
Whiting and Craig "Handbook of AFE Stagnation Region Radiant Flux Calculations"

Reference K

Davy, W .C., Park, C., Arnold, J. O., and Balakrishnam, A., "A Radiometer Experiment for the Aeroassist Flight Experiment", AIAA Paper   85-0967, June 1985.

Reference L
PAET

Reference M
Data Book Documentation: AFE Aerobrake Aerothermodynamic Data Book for Baseline V Trajectory, prepared by the Lockheed Engineering and Sciences Company under contract NAS 9-17900 for the Aerosciences Branch, Advanced Programs Office, Lyndon B. Johnson Space Center NASA, Houston Texas, JSC-23623, April 1989.

Reference N
Private communication: Laura Wood and XXX for measurements of the VUV response of the array.

Reference O
Terrazas-Salinas, Imelda, "Development of Radiometer Windows for Atmospheric Entry Vehicles", Paper 93-142, Proceedings of the 39th International Instrumentation Symposium, pps 1031 to 1049, Albuquerque, New Mexico, May 2-6, 1993

Reference P
Private communication: A. Stewart and Thomas Squire to James O. Arnold, RTM:234-1, 9/92.

Reference P
Private communication: Silicide coating for niobium

Reference Q
Wedding, Brent, "Measurement of High-Temperature Absorption Coefficients of Glasses", J of the American Ceramic Society, 58, no 3-4, pages 102 to105, Mar-Apr, 1975

Reference R
Binary scaling rule

Figures

Figure A. Flight path of a maneuvering ASTV is compared with those of the STS and the Apollo

Figure B. The AFE shape

Figure C Calculated stagnation region properties, from reference B)

Figure D Calculated aeropass heating rates for the AFE

Figure E, Prediction of the important surface heating radiation flux onto the surface of the AFE from reference B.

Figure F Predicted flight of the AFE spacecraft. Show pylons.

Figure G Artists depiction of an ASTV maneuvering through the Earth's upper atmosphere

Figure H Measured MM uv response of the linear detector.

Figure J Prediction of the surface intensity of the 174 nm atomic nitrogen lines, all VUV lines, compared with the overall radiative surface flux over the AFE trajectory. The regions important to acheive the VUV data are indicated.

Figure K
Test specimens of cooled Sapphire radiometer window designs. One utilized a XXXmm diameter window brazed to a perforated copper heat transmission plate, and the other utilized a XXXXXmm diameter lens edge cooled.

Figure L
Sapphire transmission as a function of temperature.

Figure M

Temperature history of uncooled window during the entry.

Figure N

Temperature history of cooled window during the entry.

Figure O

Sketch of thermally isolated sapphire window assembly

Figure P

Sketch of recommended cooled RHE window design. The window holder is shielded from the shock region gases by overlapping the coating.

Figure Q

Sketch of lens aperture.

Figure R

Sketch of setup to mearsure radiation from material removed from the silicide coating.
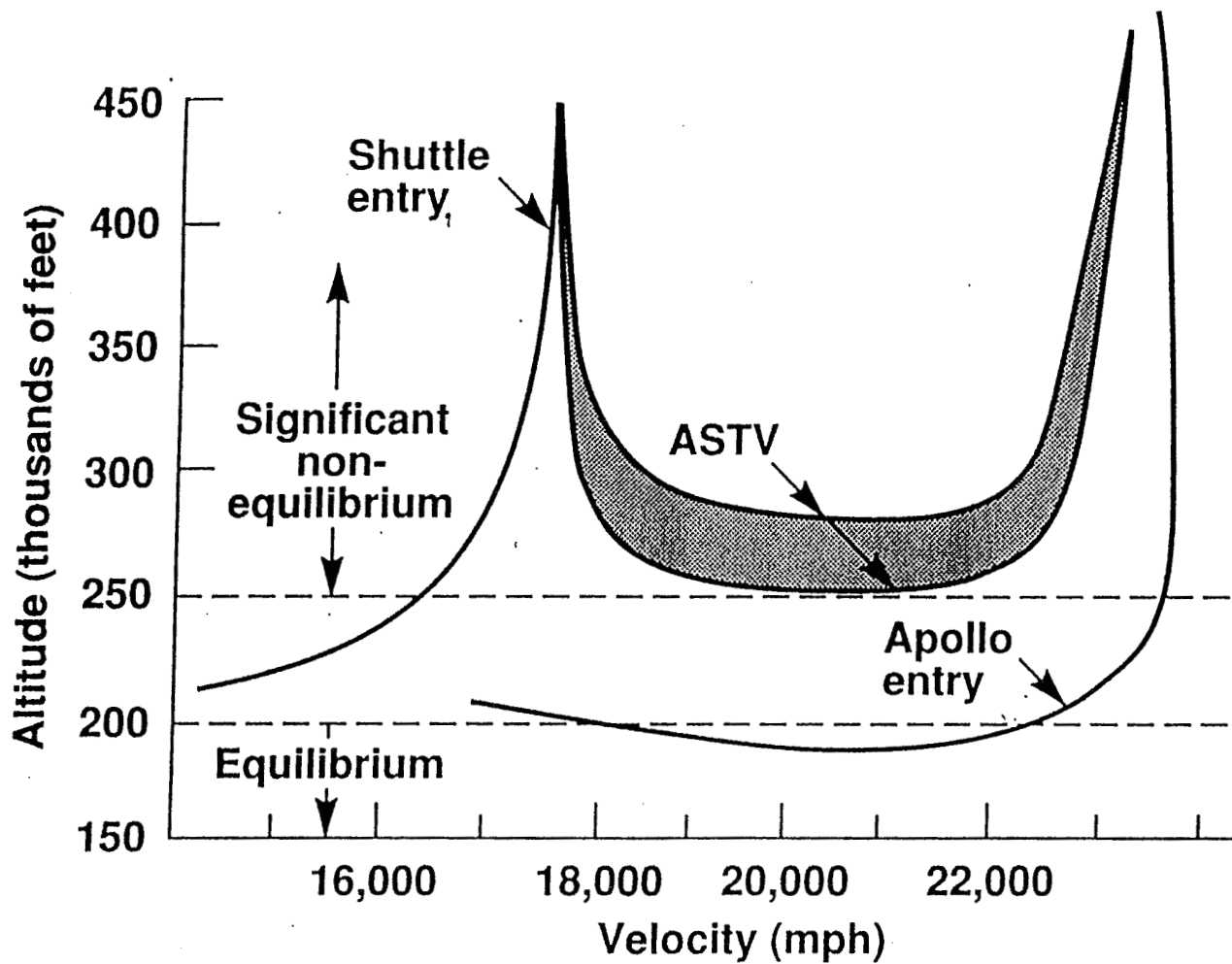
FIGURE A

ASTV FLIGHT REGIME COMPARED WITH STS AND APOLLO
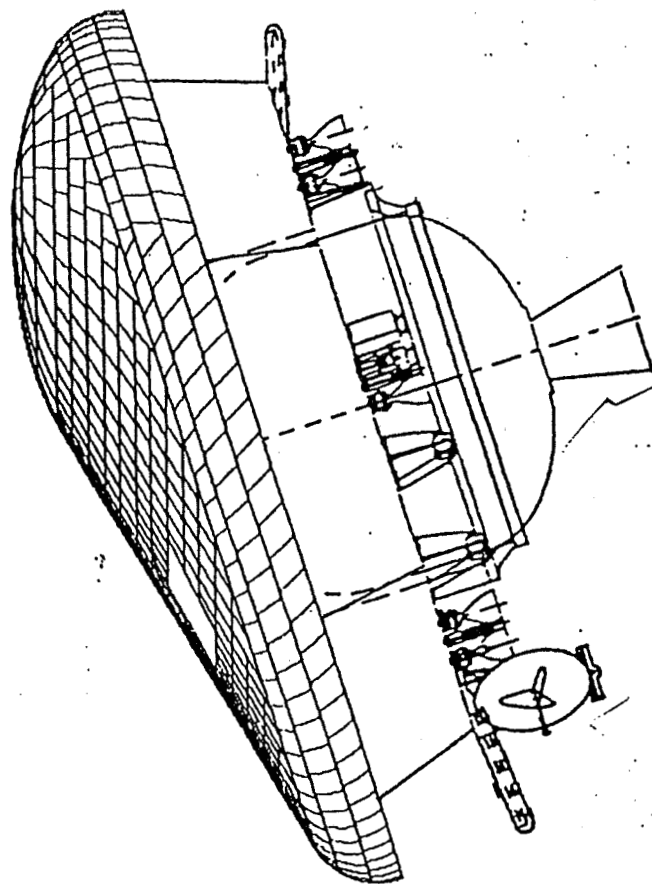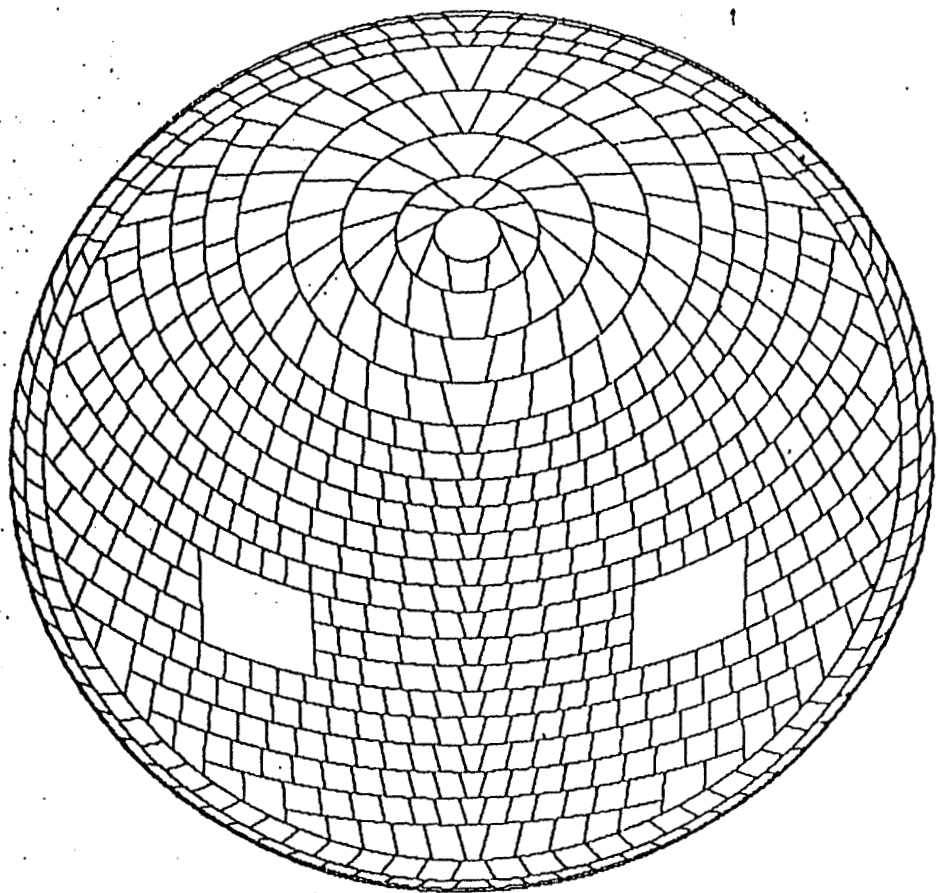
FIG   B

AEROASSIST FLIGHT EXPERIMENT
SPACECRAFT   SHAPE
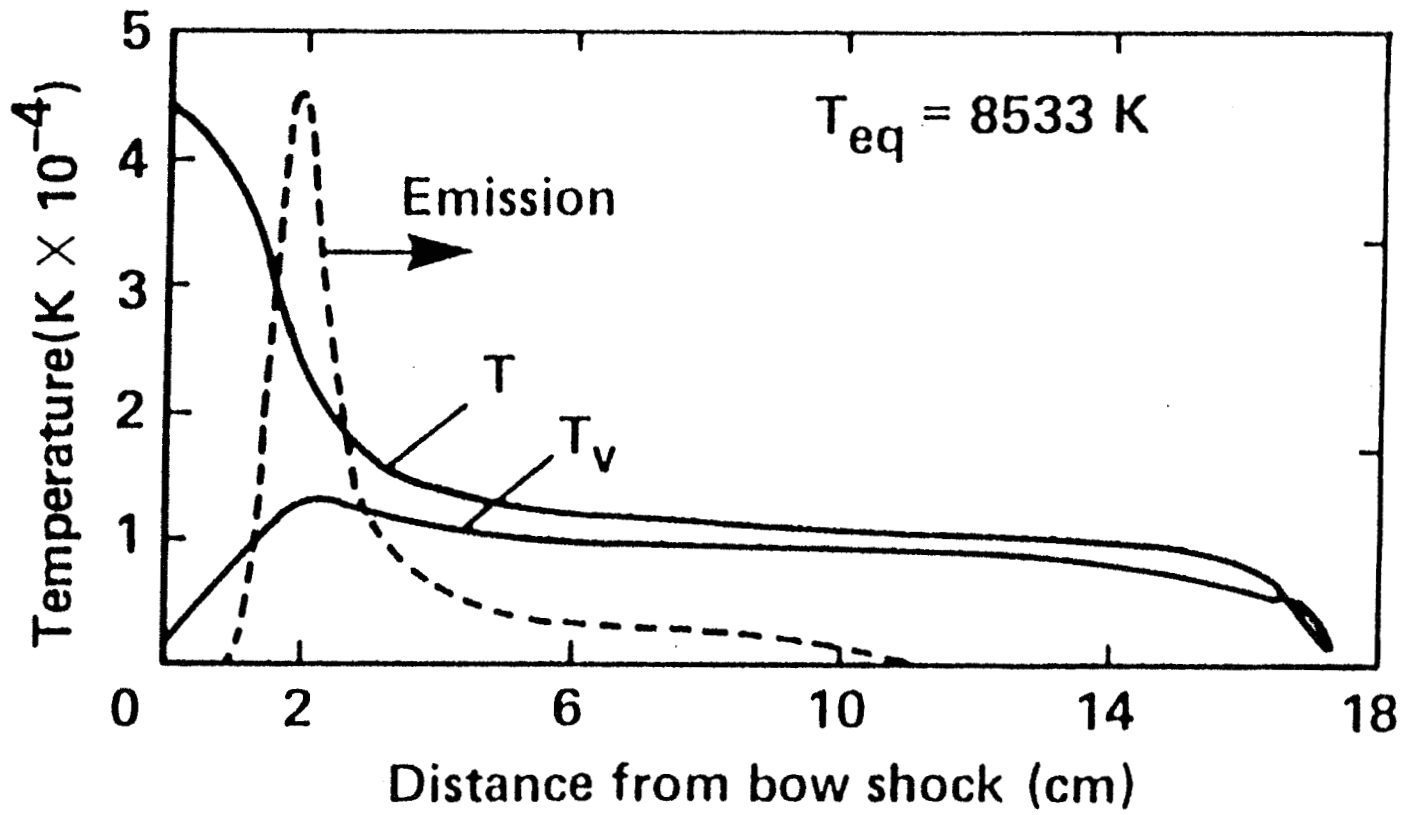
FIGURE C

AFE Aeropass Heating Rates
Baseline V

Typical Locations
Stagnation Point   (1)
Ellipsoid-Cone Interface (2)
Cone-Skirt Interface   (3)
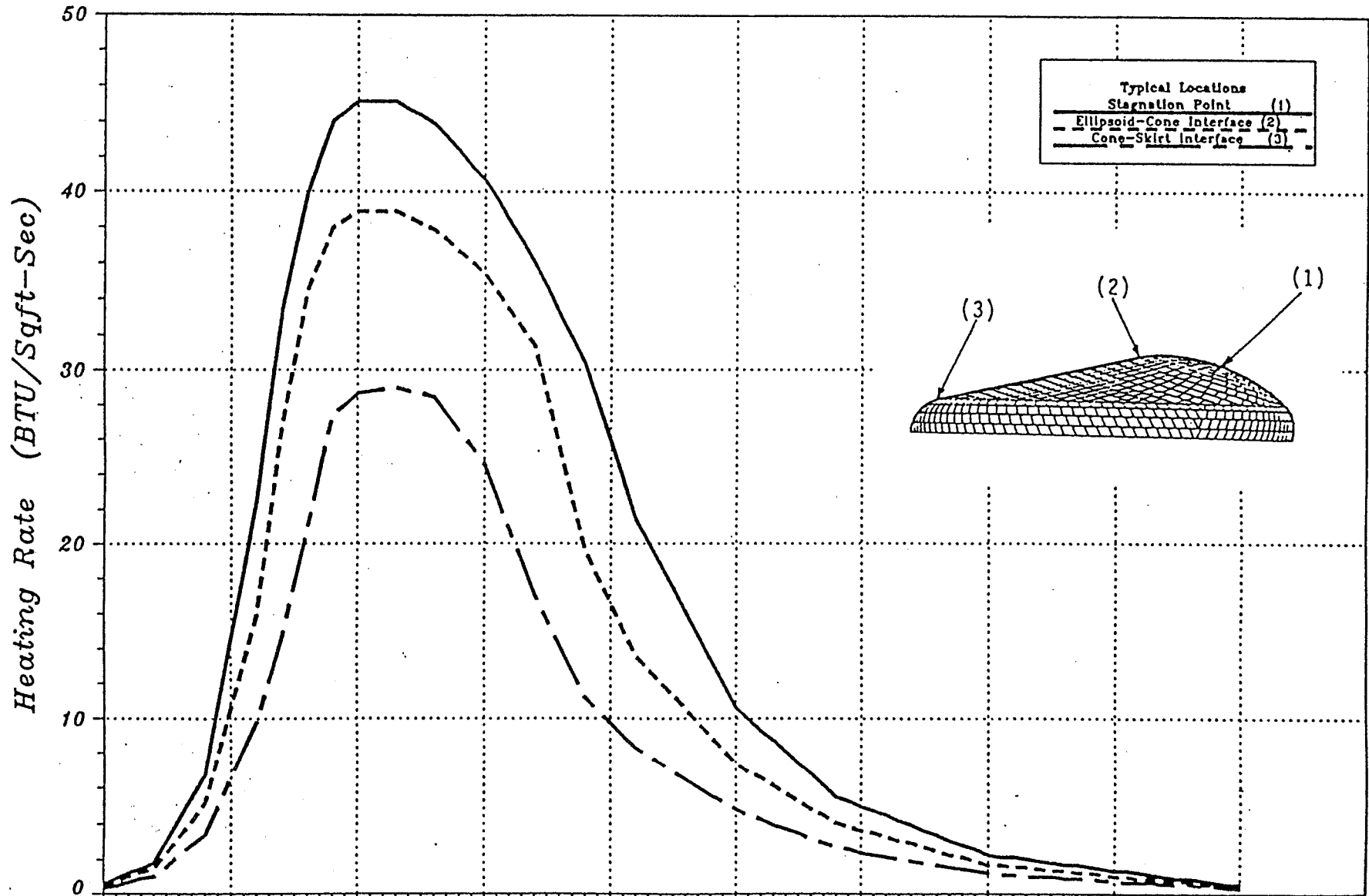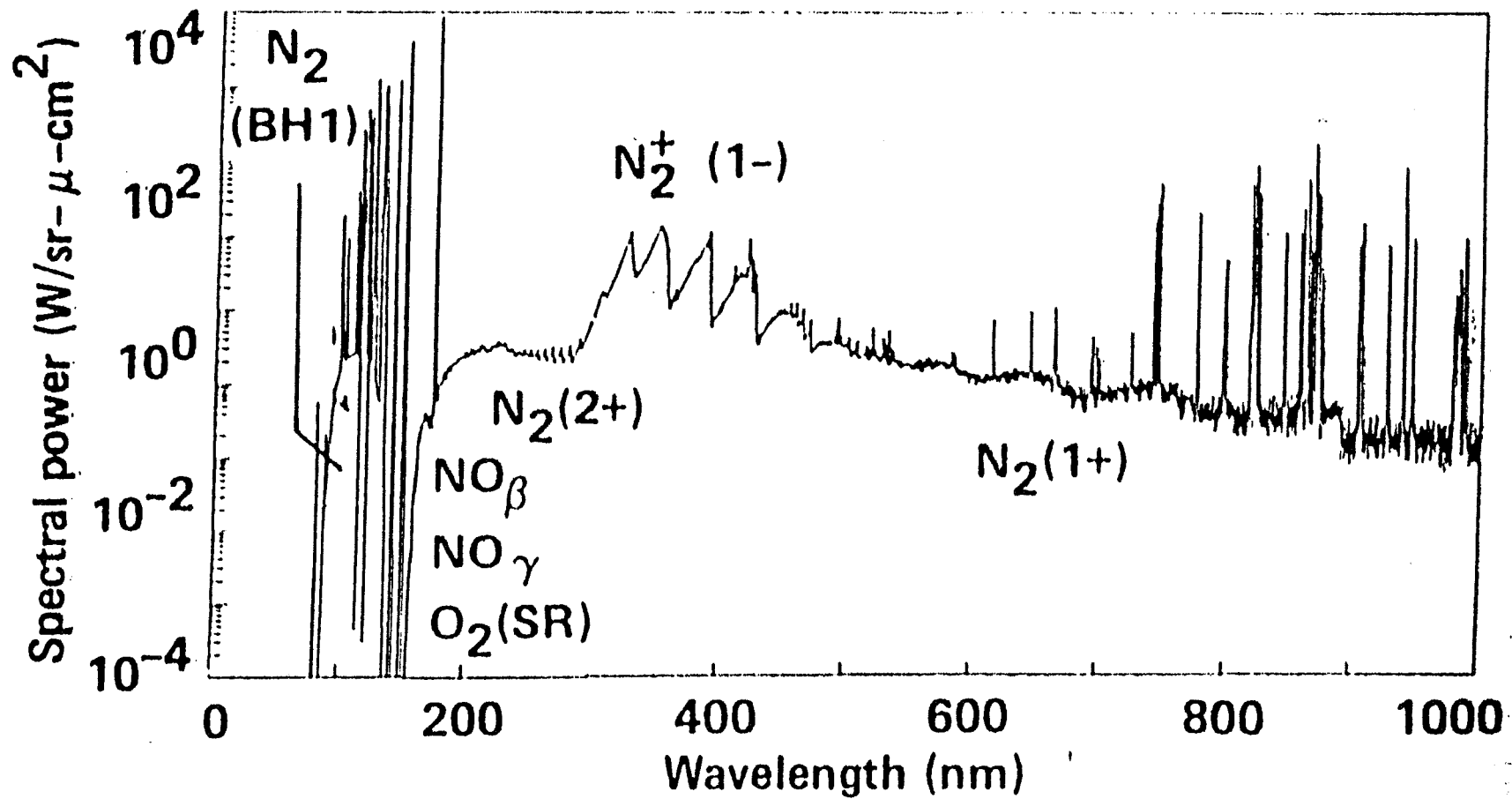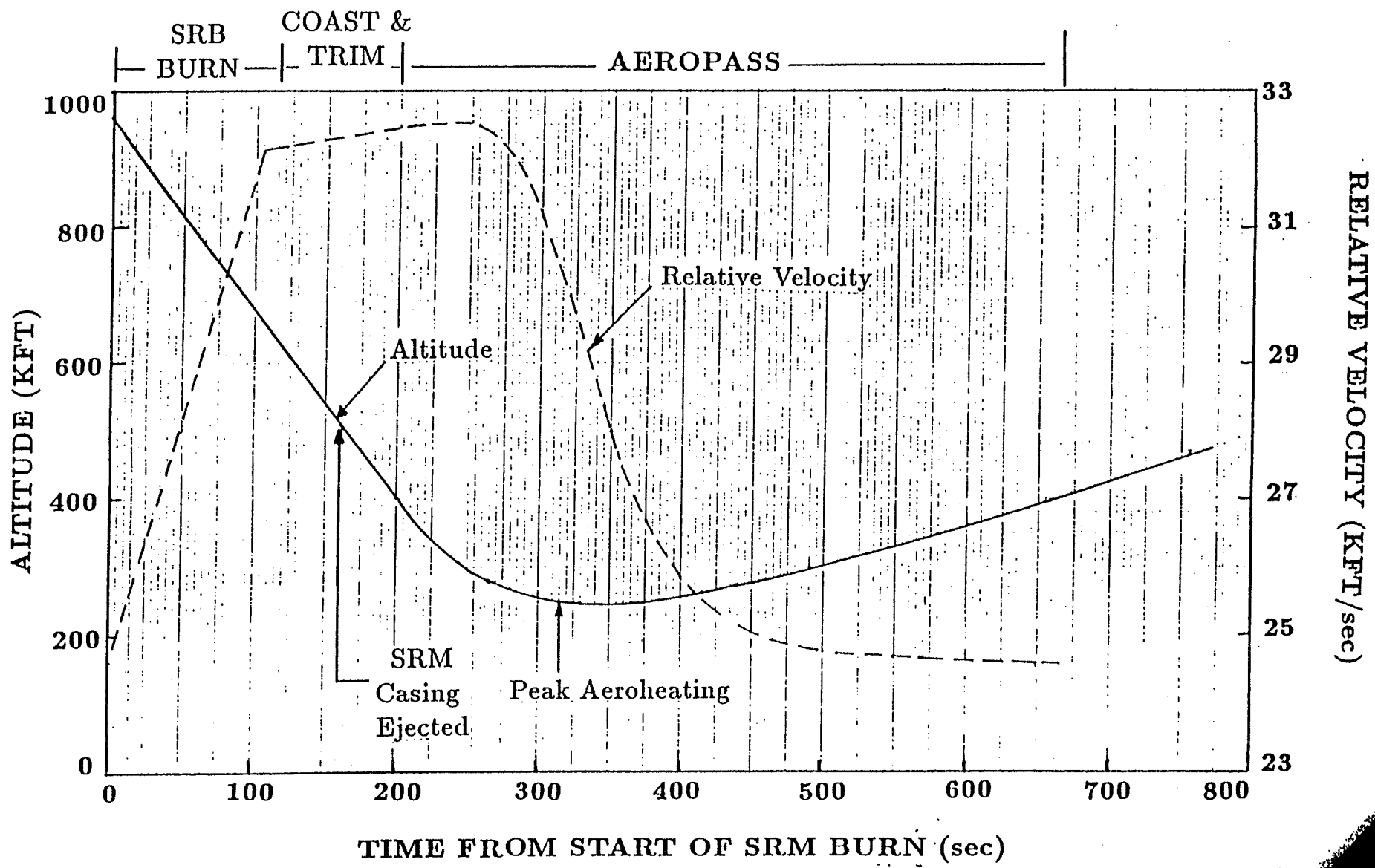
FIGURE E

Figure 3.1: AFE Trajectory During STAR 63FD SRM Burn and Aeropass for a 4100 lb. Vehicle. The Aeropass Trajectory is the Baseline 5, 3-sigma Trajectory.

FIG 9

windowless array
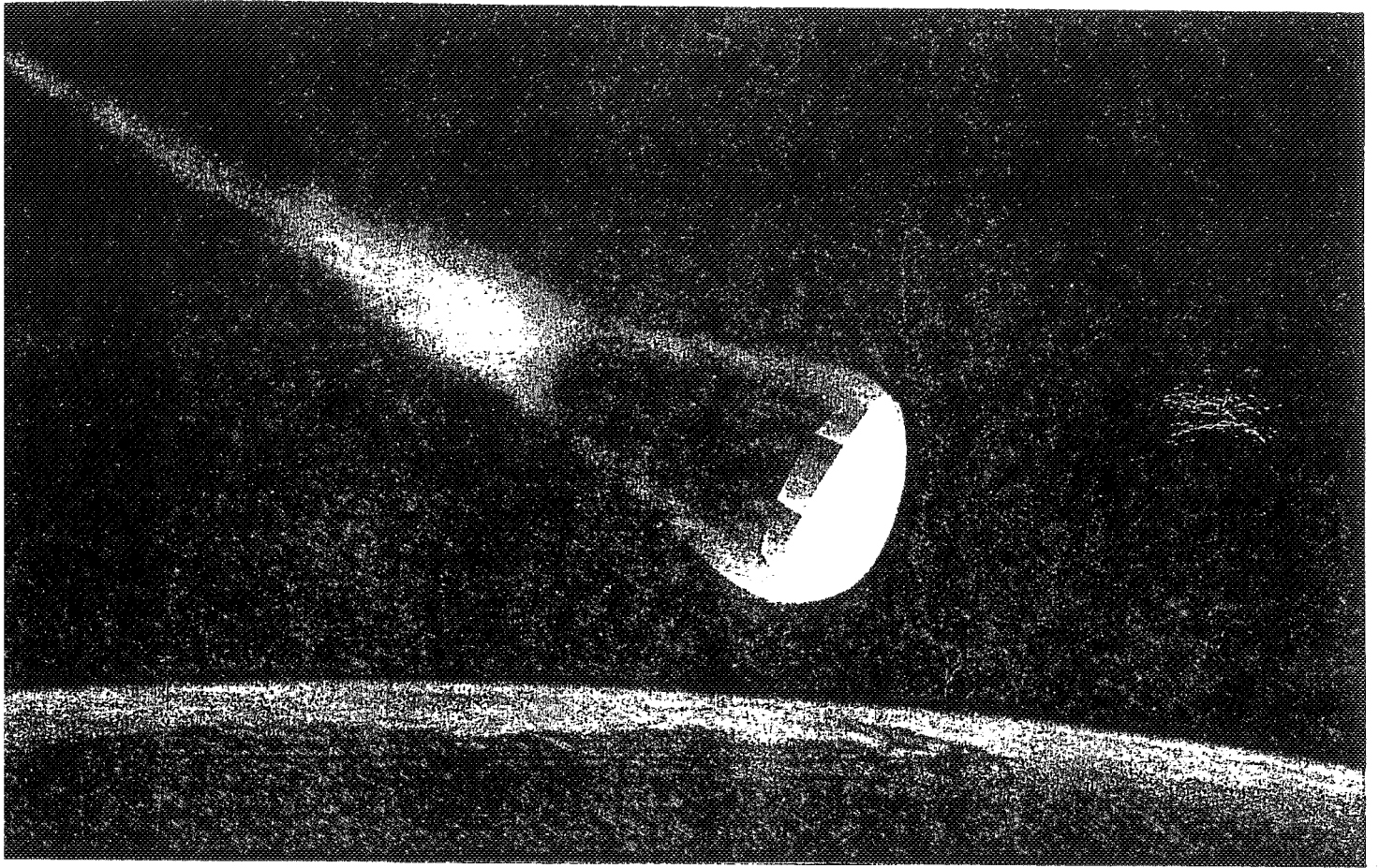
NORMALIZED RETICON RESPONSE (PMT STD)
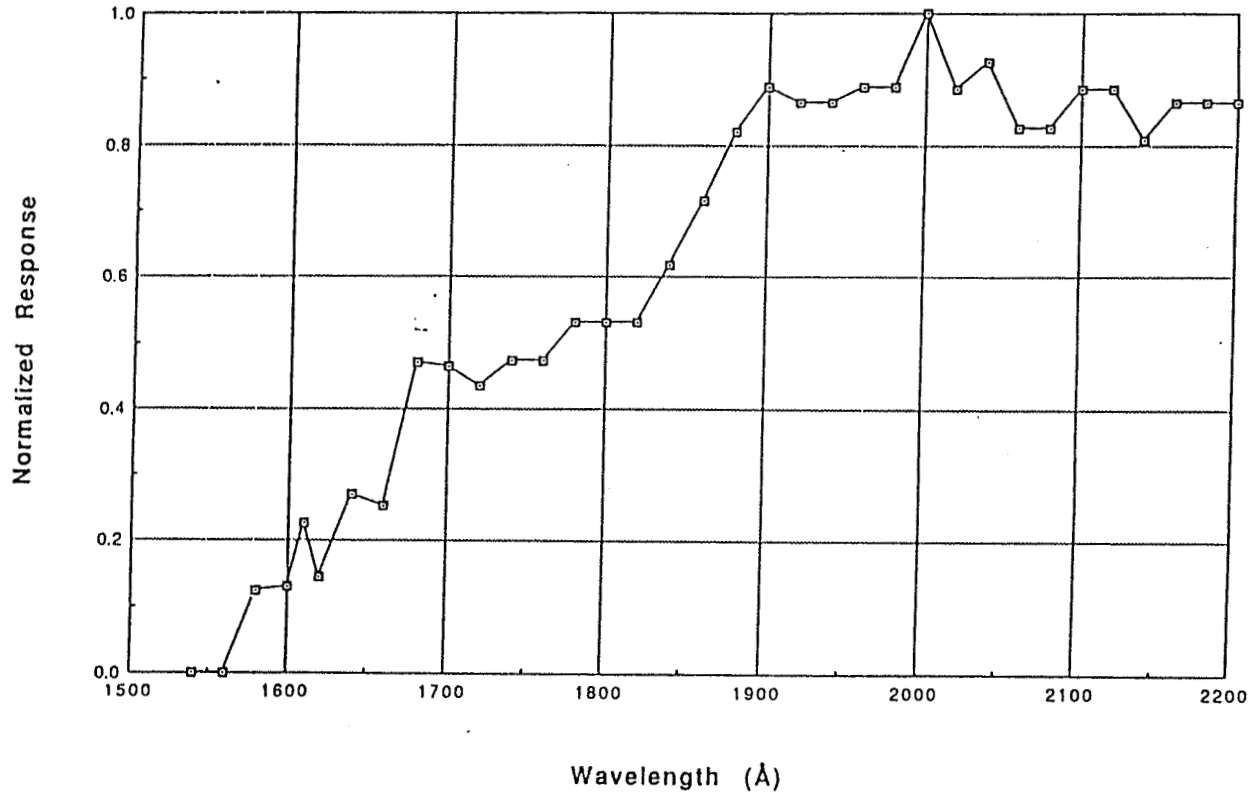
Wavelength (Å)

Figure H

Figure J

Photo

Fig K
Test specimens of coiled
windings

FIG L

T/T_0

$(740 \text{Å}^{\circ} \text{C}$

Temp

Sapphire T vs Temp

RCG COATING

ALUMINA PAPER

SAPPHIRE

FRCI-15

L1-2200

NIOBIUM WITH

VH109 COATING

S.S. STEEL
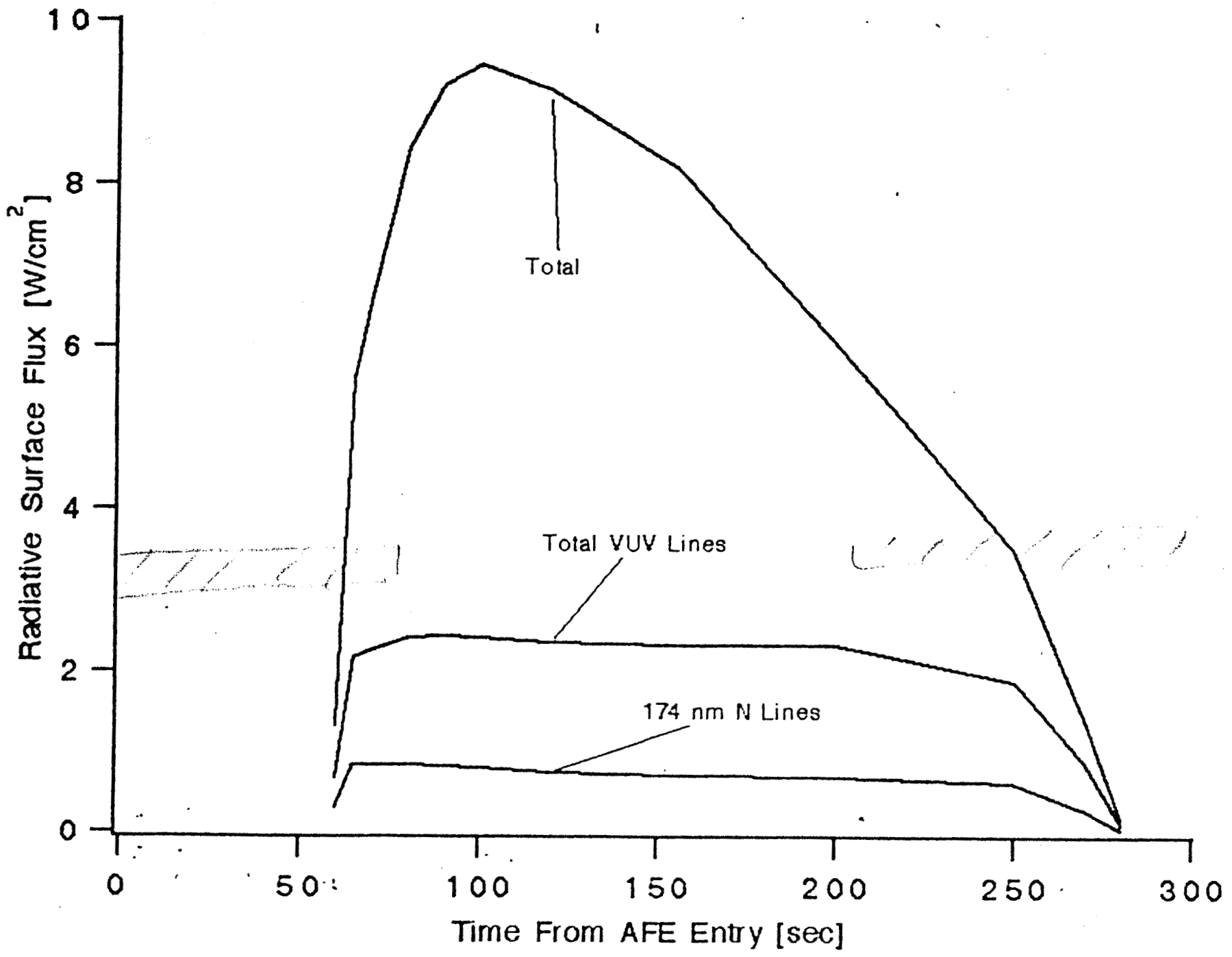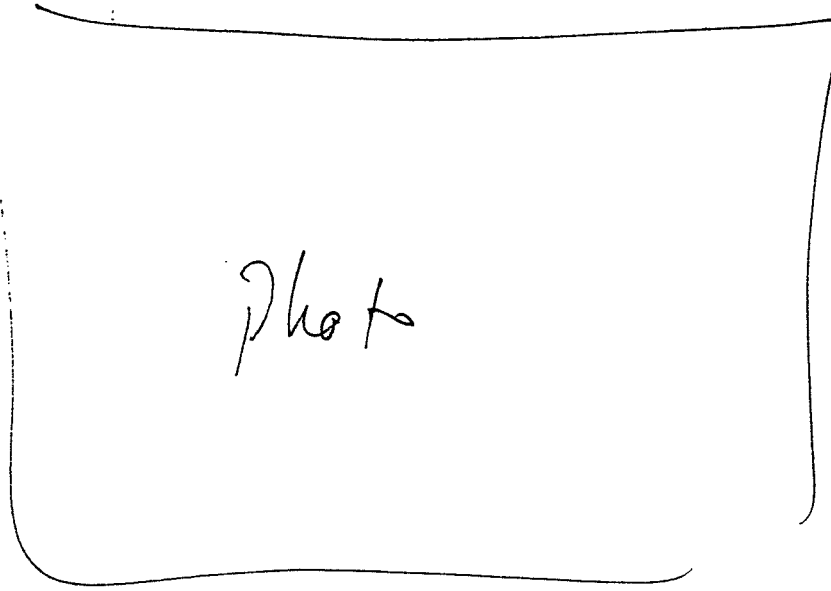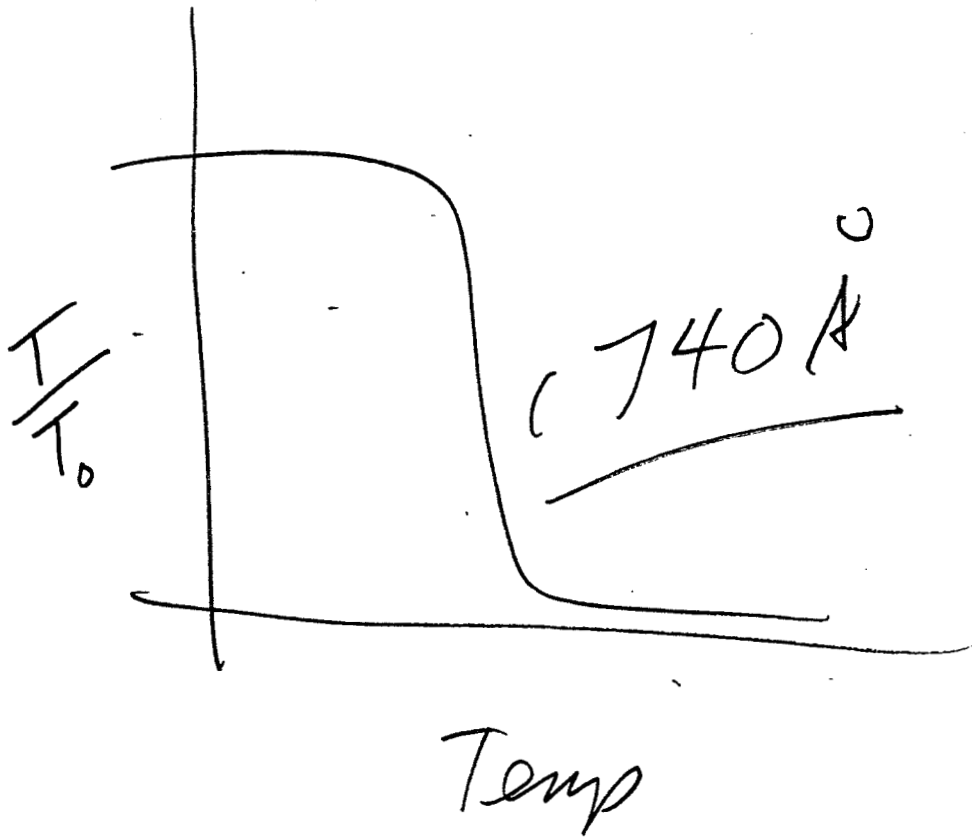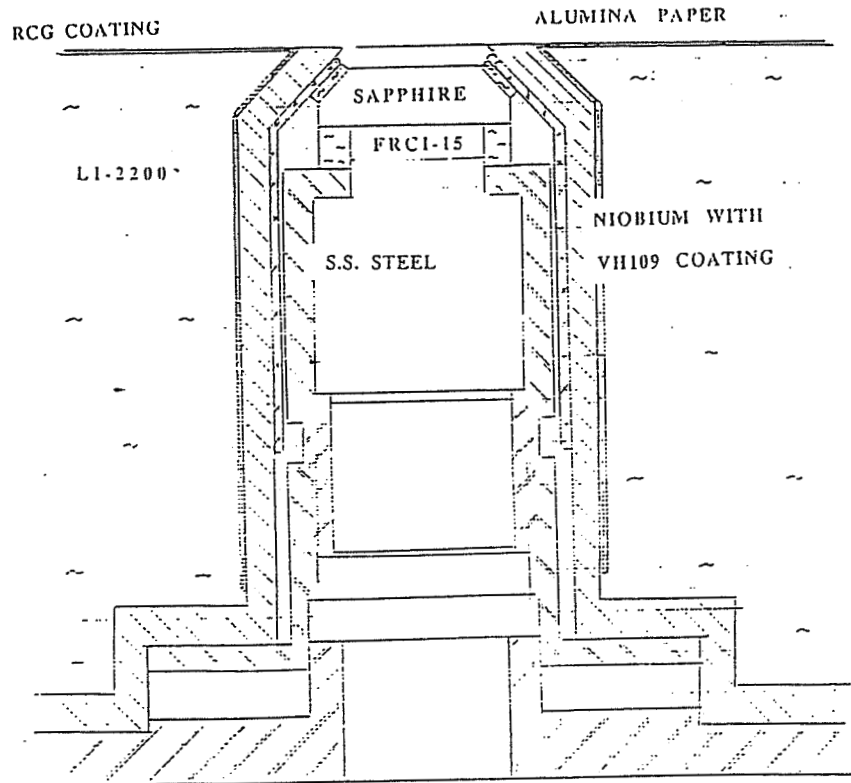
needs leaders to clarify materials

Figure O

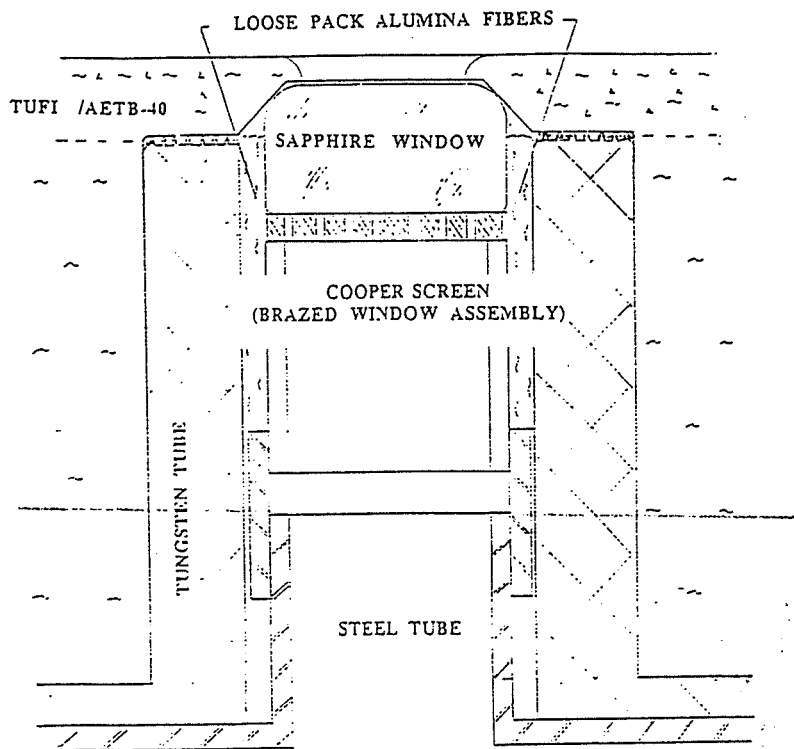Sketch of test article for the themally isolated sapphire window.

Figure P
Sketch of recommended RHE window design. Heat is transmitted to the copper element, a screen for larger diameters, and a washer for small diameters. The metal window holder is shielded from the shock region gases by overlapping the coating.
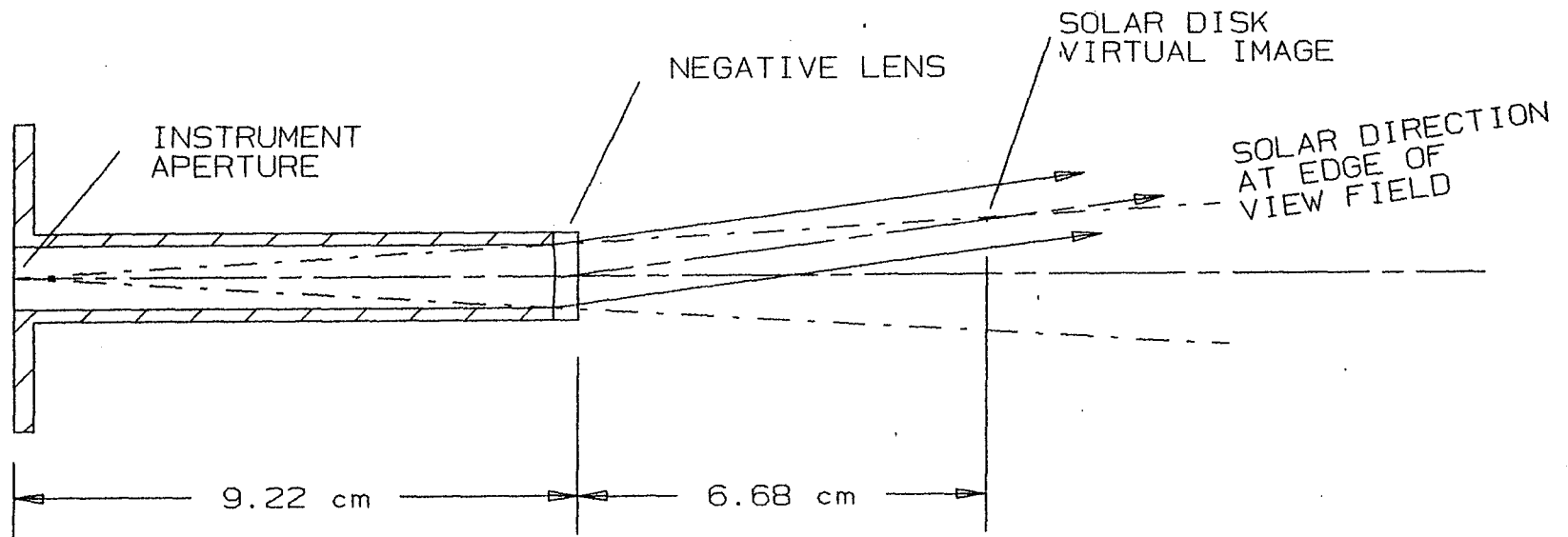
SOLAR DISK
VIRTUAL IMAGE

NEGATIVE LENS

SOLAR DIRECTION
AT EDGE OF
VIEW FIELD

INSTRUMENT
APERTURE

|←——— 9.22 cm ———→|←——— 6.68 cm ———→|

Figure Q
Sketch of a lens-apertured window based on AFE dimensional
requirements. The viewfield in increased by shaping the inner
surface of the window into a negative lens. A virtual image of the
solar disk is formed within the field of view of the instrument
aperture. The larger viewfield requirements for the solar
calibrations is thereby accommadated.

APPENDIX - B

Spectral Measurements of Shock Layer Radiation in an Arc-Jet Wind Tunnel

Roger Craig
MCAT Institute
Moffett Field, California

Spectral Measurements of Shock Layer Radiation in an Arc-Jet Wind Tunnel

Giuseppe Palumbo,[1] Roger Craig[2] and Armando Carrasco[3]

KEY WORDS

Spectroscopic Analyzers, Optical Instrumentation, Radiation Instrumentation, Ultraviolet (UV) Instrumentation

ABSTRACT

Measurements were made of the radiating gas cap of a blunt body in an NASA-Ames 20MW arc-jet wind tunnel. The test gas was air. Spectra of the flux incident on a small aperture centered at the stagnation region were obtained. A helium-cooled, magnesium fluoride window transmitted flux into an evacuated collimating system that focused the aperture onto the entrance slit of a spectrometer. Data were obtained with films and by photomultipliers. *The range covered was 120 nm* to 1000 nm and the resolution was 0.05 nm to 0.5 nm. This paper presents preliminary results from the experiment. *Representative spectral records from 200 nm to 1000 nm are shown.* The spectra show the atomic lines from oxygen and nitrogen in the IR, as well as the molecular systems of NO, N_2, N_2^+, and CN. Copper, as a contaminant, and carbon are tentatively identified. Planned subsequent laboratory work will result in calibration of spectral sensitivity and refined wavelength determinations.

[1] Eloret Institute
Work performed under NASA Cooperative Agreement NCC2-653
1176 Maraschino Drive
Santa Clara, CA 94057

[2] MCAT Institute
Work performed under NASA Cooperative Agreement NCC2-762
NASA Ames Research Center
Moffett Field, CA 94035

[3] Thermo-Physics Facilities Branch
NASA Ames Research Center
Moffett Field, CA 94035

INTRODUCTION

Arc-jet wind tunnels, simulating conditions of high speed flight, are likely to be more and more important for aerospace research in the future. Computational modelling replacing the work of low speed wind tunnels, wherein real gas effects do not dominate, is becoming a reality. However, high speed flights, such as earth entry from a space mission (low earth orbit, LEO, or further), involves flowfield gases which are not in thermochemical equilibrium (references 1 and 2). This can include important levels of transport of radiative energy (reference 3). At present we cannot accurately predict the environmental conditions surrounding these spacecraft. Figure 1 shows flight regimes experienced for the entries of the Shuttle, Apollo and a proposed Aeroassisted Space Transfer Vehicle (ASTV). An ASTV is a conceptual vehicle which utilizes aerodynamic forces to decelerate and alter orbit parameters to rendezvous with the Shuttle or a space station (reference 1). The design of future, highly efficient heat-shields (i. e., not overdesigned) for these vehicles, and others, requires the capability of making accurate heating predictions. This fact is acknowledged by the inception of the Aeroassist Flight Experiment (reference 4). This experiment utilized a vehicle designed to be deployed and recovered by the Shuttle. It was to fly a trajectory which simulated an ASTV maneuver from geosynchronous earth orbit (GEO) to LEO for rendezvous with the Shuttle or a space station. The objective was to gather a data base for development of the ASTV and other advanced space transportation systems. The program was recently canceled due to funding limitations. Although the activity was cancelled the technical requirement remains.

Real gas computational models are being developed (reference 5) but validating data are lacking. Various models predict widely different radiative heating levels. *For example, predictions of ASTV radiative heating from only the VUV atomic lines range from insignificant amounts to levels dominating the overall heating (references 6, 7 and 8).*

Arc-jet wind tunnels can produce the enthalpy and pressure conditions simulating these high speed entries. These facilities generally consist of an arc heater, a supersonic nozzle, a test box, a model holder and the necessary equipment to deal with the extreme heat transfer and the exhaust. Reference 9 describes arc-jet wind tunnels in some detail. In the past their main use has been for heat shield development. Future uses will include aerothermodynamic testing for spacecraft flight. Also these facilities can be used to conduct experiments to validate computational codes. Even though the size scale cannot

be simulated, a flow-field rich in non-equilibrated, radiating gas can be generated. Computational models can be exercised on arc-jet test conditions for comparison with experimental results. There are some major difficulties in this approach, however. The free stream plasma flow conditions (enthalpy, species distribution, energy states distribution, etc.) in an arc-jet are not well understood. Initial conditions for shock layer computational models can only be estimated. At present there are efforts to calculate the model test environments using computational models starting with the arc column, continuing with the conical or contoured expansion nozzle, and culminating in the flow field of a model located in the exit flow from the nozzle (reference 10). Experimental results are needed to support the theoretical work. A review of techniques used to study arc-jet wind tunnel flow is given in reference 11.

This paper reports on initial results of an arc-jet wind tunnel experiment. The experiment measured the spectral radiative flux emanating from the shock layer and incident on a blunt model placed in the supersonic stream. *Data was taken from 120 nm to 900. This paper presents wavelength results from 200 to 900 nm. The VUV (120 nm to 200 nm) results will be reported on elsewhere.* The purpose was to gather data to help characterize the stagnation region shock layer flow. Understanding this flow would be valuable for development and validation of advanced arc-jet wind tunnel design codes and help extend the capability of this class of facility to advanced aerothermodynamic testing.

The data shown in this paper are preliminary and do not benefit from final calibrations. The flux was spectrally resolved and over a wide range. The data will be analyzed and used to identify important radiating species and help determine the state of the gas and the operating characteristics of arc-jet wind tunnels.

EXPERIMENTAL SETUP

The experimental setup is as described in reference 12 except that the model diameter was increased to 6 inches. Figures 2 and 3 are from this reference and are included here. Figure 2 is a schematic plan view of the experiment. Supersonic flow from the arc is produced in the nozzle and the model is placed in the free stream. The standing shock layer over the model is indicated. Figure 3 is a schematic view of the model. The model face is a 6" diameter flat disk and the entire model is water cooled. A small aperture centered on the forward face admits the surface radiative flux. A helium cooled window, shown immersed in a cavity below the aperture, transmits the surface flux into the optical system. The optical system consists of a flat mirror, directing the

optical path to a concave mirror, which in turn collimates the beam to another concave mirror shown at the top of figure 2. This mirror focuses the aperture, via a flat turning mirror, onto the slit of the spectrograph. The spectrograph was a 0.5 meter instrument using a modified Czerny-Turner optical layout with the provision for operating either as a scanning monochromator or a film spectrograph . The portions of the system exposed to the plasma were all water cooled. Figure 4 shows the model arrangement in the test box. The nozzle exit can be seen at the left, and the aperture can be seen centered on the model face. The optical axis in front of the model was canted 15° from the centerline to reject radiation from the arc column.

TEST CONDITIONS

The test was conducted in the Ames 20 Megawatt Aerodynamic Heating Facility. The facility was operated with a supersonic nozzle with a 1.5 inch diameter throat and an 18" exit diameter. The facility operating parameters were as follows:

> Test gas mixture: 80% air* and 20% Argon by mass,
> arc current: 1000 amperes,
> arc column pressure: 15psia,
> nozzle pressure: 7.5psia,
> test box pressure: 0.2 to 0.3 mm Hg, and
> stagnation pressure: 9mm Hg.

The resulting free stream conditions for the present experiment is approximate as indicated in by the circle in figure 1. The velocity is deduced from an estimate of the free stream enthalpy which was, in turn, derived from the heating rate of a small sphere placed in the stream. It should be noted that the arc-jet free stream enthalpy, although repeatable, is not well characterized. Indeed, one of the objectives of this experiment is to help quantify this and other arc-jet wind tunnel performance characteristics.

Figure 5 is a photograph taken during a test. The shock is seen well formed over the flat model face. The intense radiation from the high temperature shock layer gases is clearly evident.

The experiment consisted of a series of 10 minute runs during each of which a specific spectral region was examined. The length of a run was limited by the heating loads on the test box. Data were obtained using film and

---

* Dried and filtered ambient air

photomultiplier tubes. The photomultiplier signal was processed with synchronous amplification. Readout was on a chart recorder and digitally recorded.

The instrument configurations used in the tests are summarized in Table 1.

DIGITAL DATA ACQUISITION

Four signals were recorded digitally during the experiment tests: stagnation pressure on the model face, *optical system vacuum pressure*, photomultiplier high voltage, and photomultiplier output signal. The stagnation pressure, vacuum pressure, and the high voltage were recorded at one hertz with an analog mixer. The photomultiplier output signal was recorded at forty hertz.

Figure 6 shows the configuration of the data recording system for the time history of the pressure, vacuum, and high voltage signals. The system used a multiplexer and a controller configured with a portable personal computer. Twisted and shielded grounded cables were used to transmit the signals. The data acquisition and instrument control software were configured to record the data during each run at one hertz and concurrently display it on the monitor.

Figure 7 shows the configuration of the data recording system for the photomultiplier records. The system consisted of a controller, a scanning A/D converter, and a 16 channel isolated input rack connected to an NB-DMA board contained within the personal computer system. The data acquisition and control software was set to record at 40 Hertz.

The photomultiplier data presented here were manipulated for display purposes using graphic and analysis software.

RESULTS AND DISCUSSION

Computed Spectral Details.

The development of computational codes to predict the shock layer radiation, such as that measured by this experiment, is a parallel, ongoing activity at the Ames Research Center. These codes are based on calculations of the arc process, the expansion in the nozzle and the shock layer processes. The radiating shock region is very non-homogeneous and involves many kinetically controlled processes. Substantial radiation emanates from the nonequilibrated regions immediately behind the shock. Here the kinetic temperature is extremely high, approaching 50,000K. The spectral line radiation is strongly

Doppler broadened by this high temperature. The cooler parts of the shock will partially absorb the strong features directed toward the surface, but absorption will occur only at around the line centers because the absorption lines are narrow due to the low kinetic temperature. The surface radiative heating flux is thus seen to be the aggregate radiation from regions of very different conditions and estimates from computational codes involve consideration of complex interactive and kinetic processes. At present these codes exist as separate codes but the goal is to couple them together and validate the result as a reliable code for predicting arc-jet wind tunnel conditions. Figure 8 is a calculated spectrum. NO bands are seen from 190 nm to 300 nm. N2(2+) bands contribute energy from 280 nm on and merge with the stronger N2$^+$(1-) and N2(1+) bands which dominate the molecular systems from 300 nm to the infrared. Rich and diagnostically important atomic line radiation is predicted from oxygen and nitrogen in the infrared.

Test Results

As indicated above the data were taken with film and with photomultiplier tubes. The data presented herein are not corrected for instrument spectral response. This correction will be done with future work. The photomultiplier data was digitized in-situ. The film spectra density will be subsequently digitized.

Ultraviolet-visible results.

Data was acquired in the spectral region from 200 nm to 500 nm by both film and photomultiplier tube. Figure 9is a print from a film record taken on 8/10/92. The spectral range is from 330 nm to 450 nm. The uppermost spectrum is from the shock layer radiation and includes N_2^+(1-) $B^2\Sigma_u^+ - X^2\Sigma_g^+$ and CNv $B^2\Sigma - X^2\Sigma$ band systems and atomic lines from nitrogen and oxygen. The other spectra are mercury line calibrations. Figure 10 is a densitometer scan of the 360 nm to 395 nm region of figure M in which details of a portion of the N_2^+(1-) system are shown. The vib-rot structure can be seen in detail. This and the other film records will be digitally analyzed for subsequent use. Photomultiplier data were obtained in this region also. Figure 11 shows photomultiplier data of the spectral details from 200 nm to 300 nm. This spectral region is dominated by the NO_γ $A^2\Sigma^+ - X^2\Pi$ bands. Figure 12 is the photomultiplier data from 250 nm to 500 nm. These data were recorded digitally in-situ as well as with chart recorder backup. As with the VUV data, there is no correction to these figures to account for instrument spectral response. This correction awaits further laboratory work.

Visible-infrared results.

Noise limitations prohibited use of photomultiplier tubes beyond 700 nm. Film spectra, however, were obtained with great detail. Figure 13 is a print of the film taken from the 7/23/92 test. It covers the spectral range from 300 nm to 1000 nm with a resolution of approximately 0.1 nm. Figure 14 is a densitometer trace of this record. The details which overlap with the photomultiplier record can be seen. The important atomic oxygen and nitrogen emission lines are well resolved. Figure 15 is an densitometer trace of an expanded portion of this film indicating the resolution of the atomic lines. Several features await identification. Calibrations of the non-linearities of the film system will result in a data base allowing comparison of the intensities of these features with theoretical results. Their relative intensities will help understand the electron density of the plasma.

CONCLUSIONS

The spectra have been obtained from the flux incident on the stagnation surface of a flat model placed in the supersonic stream in an arc-jet wind tunnel. The preliminary data set shown is detailed at high resolution from 200 nm to 1000 nm. Important radiators are evident. The data set will be further developed and used to help refine and calibrate computational models of the aerothermodynamics of entry and of arc-jet wind tunnels.

ACKNOWLEDGMENTS

TABLE 1

I-TESTS USING FILM

Date	Grating Ruling, *l/mm*	Blaze Wavelength *nm*	Slit *microns,*	Exposure, *seconds*	λ range *nm*
7/8/92	60	300	20	100	200 to 500
7/15/92	180	150	20	60, 300	200 to 500
7/16/92	300	500	20	10, 50, 300	300 to 1000
7/23/92	300	500	20	100, 390	300 to 1000
7/24/92	1200	150	20	100, 600	200 to 400
3/10/92	1200	150	20 -	10, 100, 480	300 to 500

II-TESTS USING PHOTOMULTIPLIER TUBE

Date	Grating *l/mm*	Blaze *nm*	resolution, *nm*	spectral features	λ range, *nm*
3/4/92	2400	150	0.4	$N2^{+}(1-)$	300 to 500
3/4/92	2400	150	0.1	$N2^{+}(1-)$	300 to 500
3/5/92	2400	150	0.4	NOγ	200 to 290
3/5/92	2400	150	0.1	NOγ	200 to 290

11. Scott, Carl D., "Intrusive and Nonintrusive Measurements of Flow Properties in Arc Jets", Invited paper for the Workshop on Hypersonic Flows for Reentry Problems", co-organized by INRIA-Sophis Antipolis and GAMNI-SMAI, January 22-26, 1990, Antibes, France.

12. Palumbo, G., "Shock Layer Vacuum UV Spectroscopy in an Arc-Jet Wind Tunnel" NASA TM 02258, January, 1990.

FIGURES

Figure 1.
Flight regimes of mission returns for ASTV, Shuttle, and Apollo. The point indicated by the circle is an estimate of the altitude and velocity simulated by the arc-jet conditions used during the present tests.

Figure 2.
Schematic diagram of experimental setup. The arc column is to the left of the nozzle.

Figure 3.
Schematic diagram of model showing the aperture and window and orientation of the bow shock. Radiation incident onto the surface is reflected by the turning mirror to the concave mirror and thence to the spectrograph. Vacuum was maintained <0.01μ for the VUV tests.

Figure 4.
Photograph of model in test box. The optical system is protected by the water cooled coils shown as well as internal water cooling. The aperture can be seen in the face of the model. The nozzle exit can be seen at the left.

Figure 5.
Photograph of model during test. The stagnation shock is seen well formed over the model face and the intense radiation from the shock heated air is evident.

Figure 6.
Data acquisition system block diagram for recording the stagnation pressure on the model face, optical system vacuum pressure, photomultiplier high voltage.

Figure 7.
Data acquisition system block diagram for recording the photomultiplier output signal.

Figure 8.
Preliminary calculation of the spectral surface flux from the stagnation region of a model placed in an arc-jet wind tunnel.

Figure 9

Print from a film record taken on 8/10/92. The spectral range is from 330 nm to 450 nm. The uppermost spectrum is from the shock layer radiation and includes N_2^+(1-) $B^2\Sigma_u^+ - X^2\Sigma_g^+$ and CNv $B^2\Sigma - X^2\Sigma$ band systems and atomic lines from nitrogen and oxygen. The other spectra are mercury line calibrations.

Figure 10

Densitometer trace of the 360 nm to 395 nm region of the film record of figure M is shown. This region includes a portion of the N_2^+(1-) $B^2\Sigma_u^+ - X^2\Sigma_g^+$ band system. The vibration-rotation lines are seen to be well resolved. The atomic oxygen line at 394.8 nm is also shown.

Figure 11

Photomultiplier record of spectrum from 200 nm to 300 nm. This spectral region is dominated by the NO_γ $A^2\Sigma^+ - X^2\Pi$ bands.

Figure 12.

Photomultiplier record of spectrum from 250 nm to 500 nm. The molecular spectra from NO_γ $A^2\Sigma^+ - X^2\Pi$, N_2^+(1-) $B^2\Sigma_u^+ - X^2\Sigma_g^+$ and CNv $B^2\Sigma - X^2\Sigma$ are in this region as well as atomic lines from oxygen and nitrogen and copper (contamination from the arc electrodes).
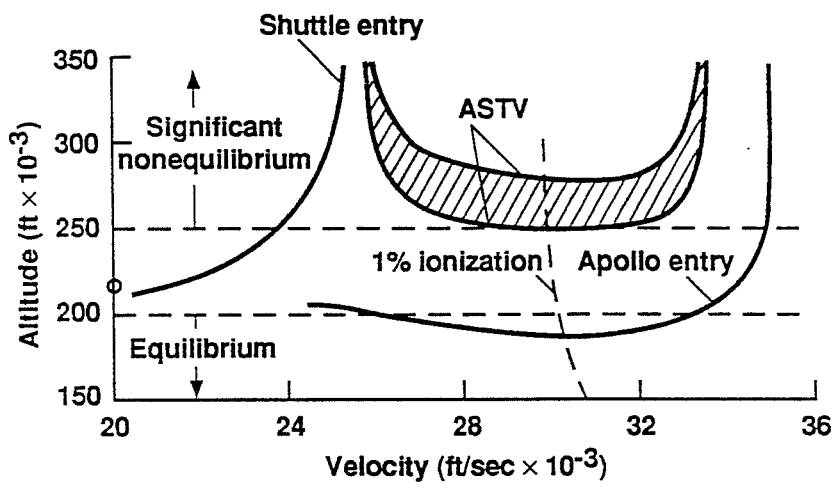
Figure 13.

Photographic print of 7/23/92 film spectrum from 300 nm to 1000 nm. Two different duration exposures of the shock layer emission were taken. Exposure A is a short exposure of emission from the shock layer and an overlapping calibration exposure from a Hg lamp. Exposures B and D are Hg lamp calibration exposures. Exposure C is a long exposure without overlapping Hg lamp calibration. Selected Hg emission lines in the first, second and third orders, are indicated.
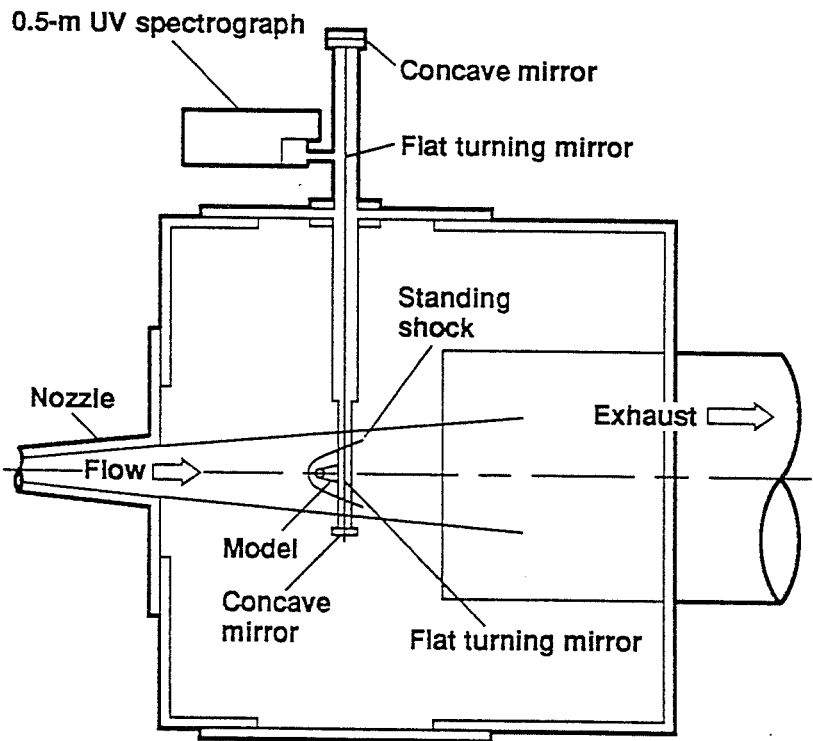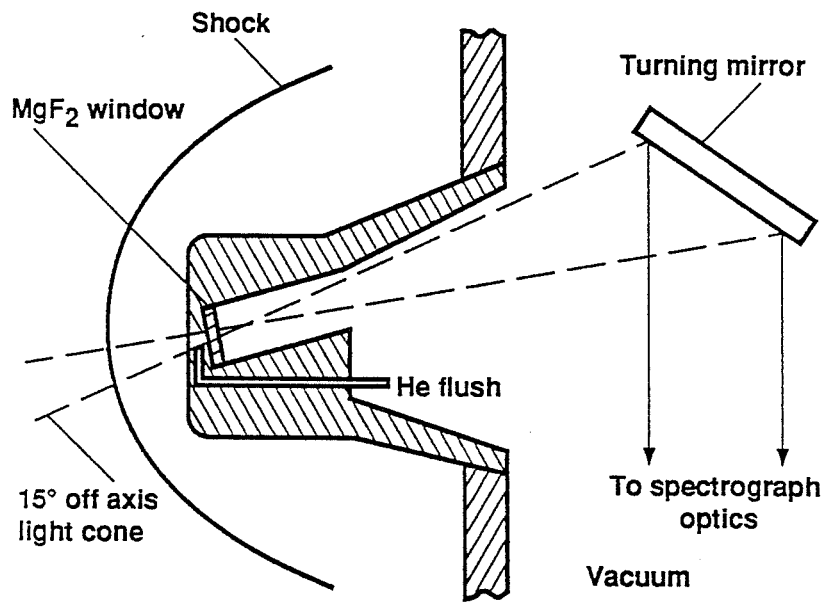
Figure 14.

Densitometer trace of 7/23/92 film spectrum from 500 nm to 1000 nm. The important atomic oxygen and nitrogen emission lines are well resolved. Also seen are the copper lines at 324.7 nm and 327.4 nm in the second and third orders.
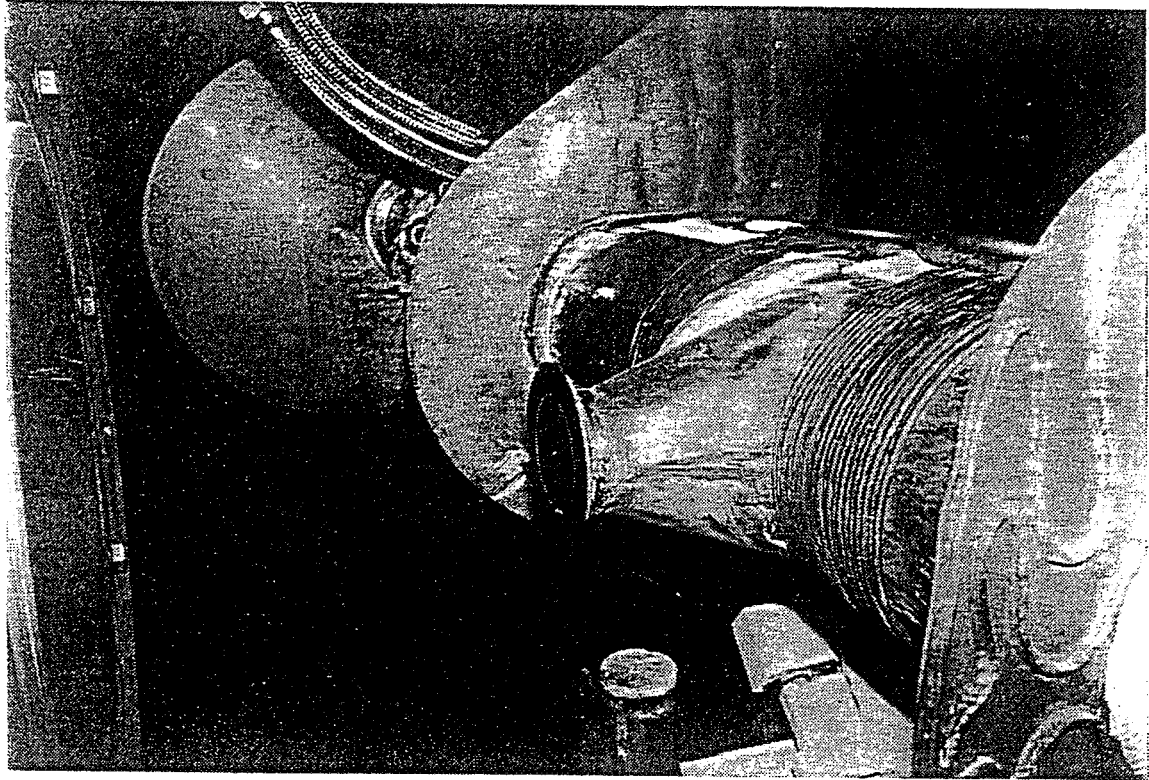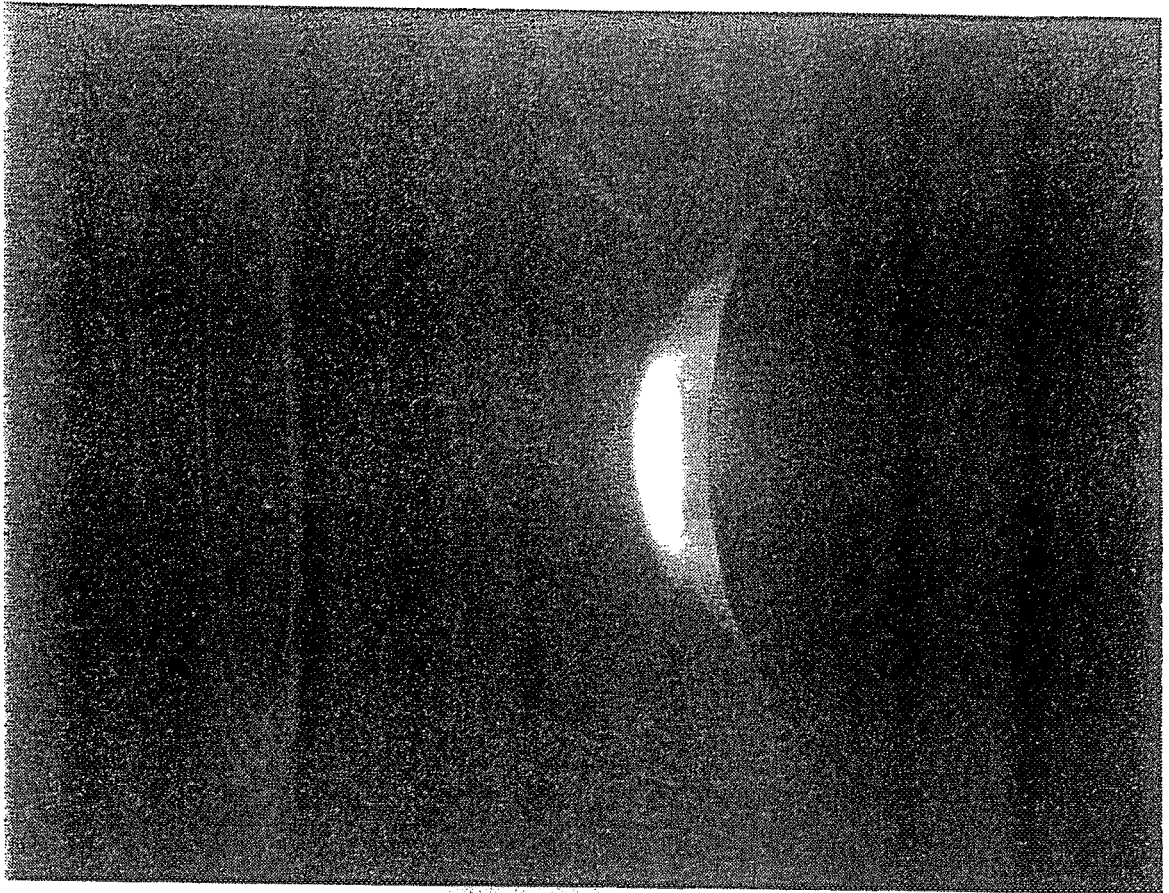
Figure 15.

Expanded portion of the 7/23/92 film spectrum densitometer trace showing the atomic lines near between 800 nm and 880 nm. Several features await identification.
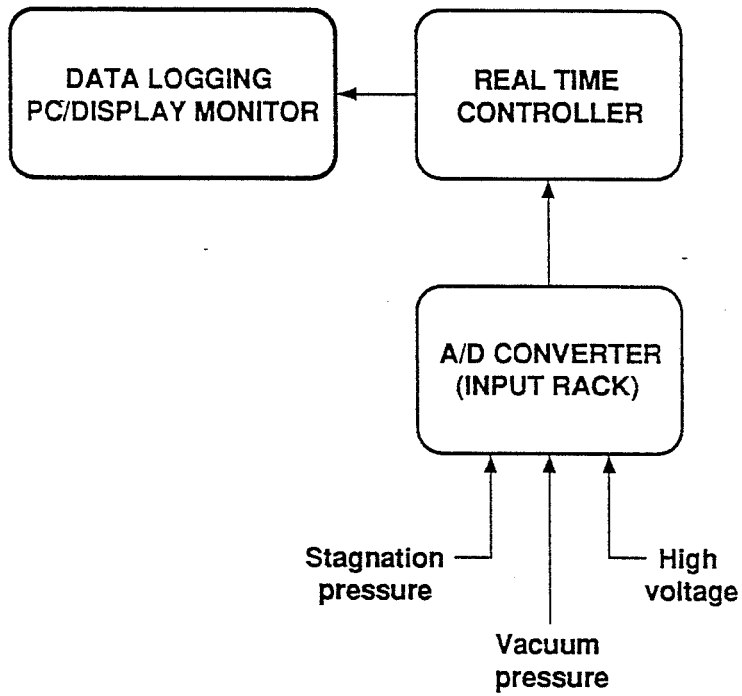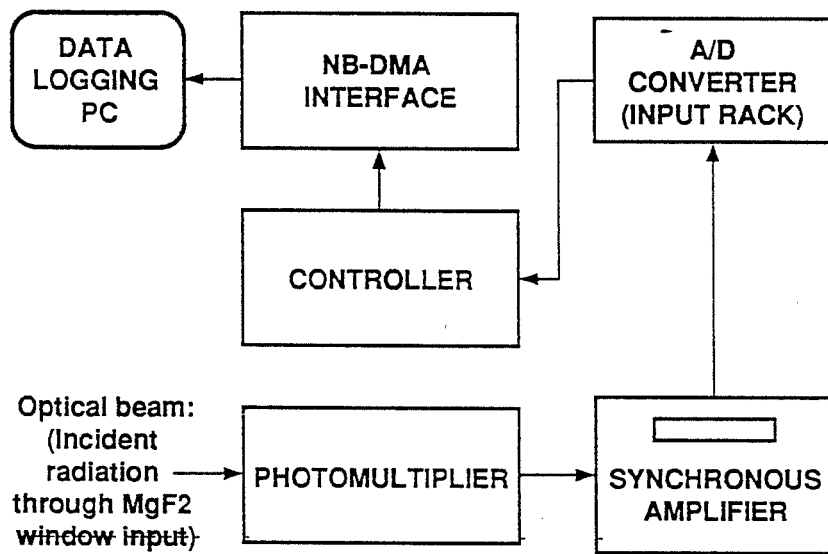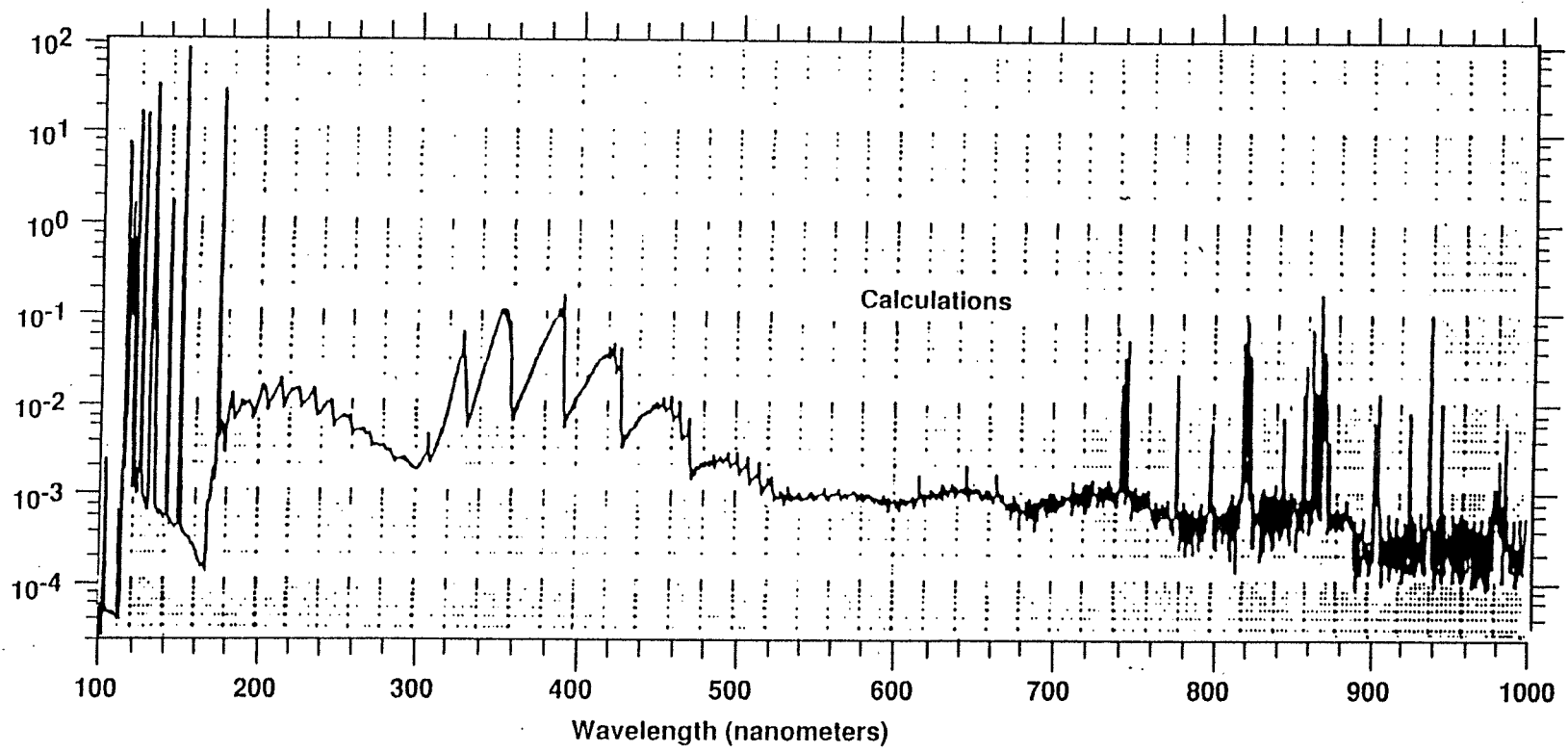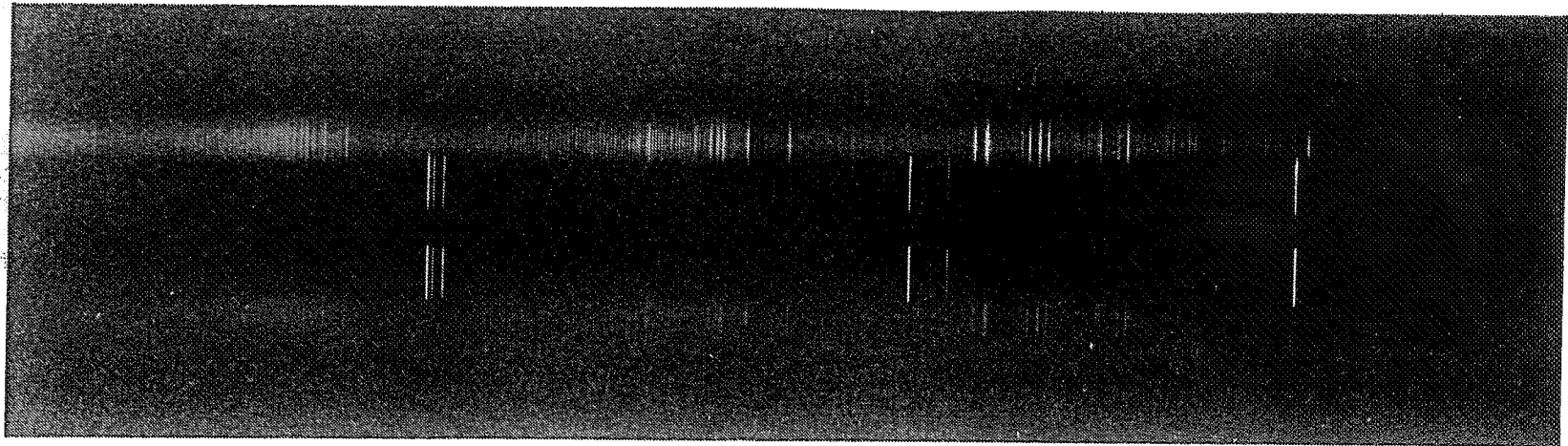
Palumbo-1

0.5-m UV spectrograph

Concave mirror

Flat turning mirror

Standing shock

Nozzle

Exhaust

Flow

Model

Concave mirror

Flat turning mirror

Palumbo-2

Shock

MgF$_2$ window

Turning mirror

He flush

15° off axis
light cone

To spectrograph
optics

Vacuum

Palumbo-3

4

5

Palumbo-6

Palumbo-7

Calculations

Wavelength (nanometers)

Palumbo-8

Wavelength (nanometers)
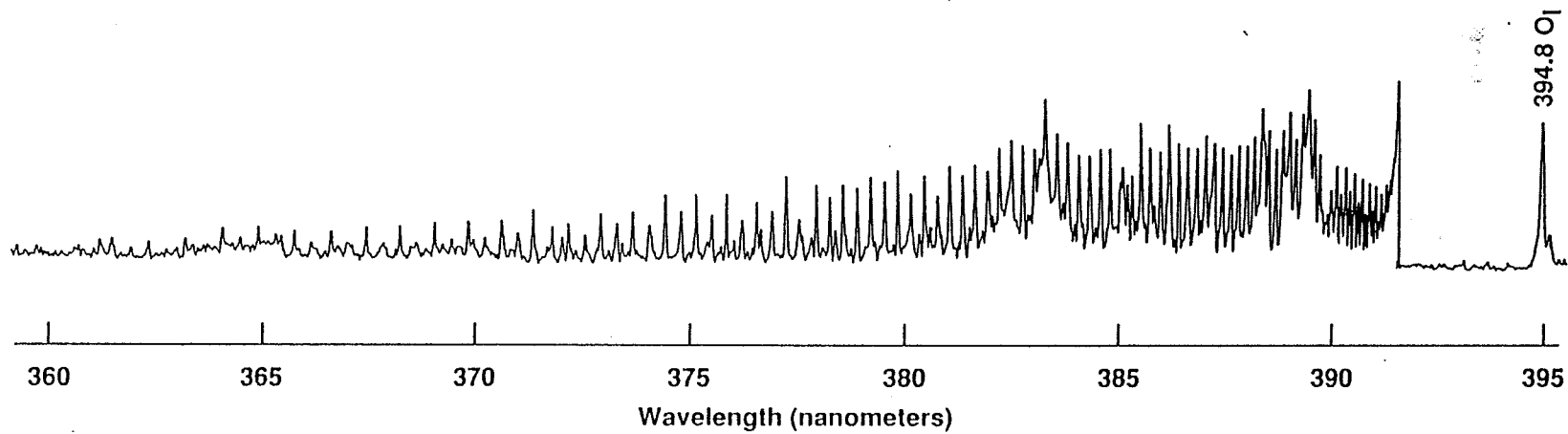
330   340   350   360   370   380   390   400   410   420   430   440   450

365.6

435.8

Hg lines

Palumbo- 9

Wavelength (nanometers)

394.8 O_I

Wavelength (nanometers)

Wavelength (nanometers)

Labels on figure: Cu (2nd order), O$_I$, N$_I$ lines, O$_I$ line, N$_I$ lines, O$_I$ lines, N$_I$ lines, Cu (3rd order)

12-13

Palumbo-72-14

Wavelength (nanometers)

Palumbo-26 15

Spectral plot with horizontal axis "Wavelength (nanometers)" showing labeled emission peaks:

- 258.7
- 263.0
- 267.1
- 271.3
- NOγ (bracket grouping the above)
- 295.2 NOγ
- 315.9 NOγ
- 324.7 Cu
- 327.4 Cu
- 353.2 N₂⁺ (1-)
- 354.8 N₂⁺ (1-)
- 356.3 N₂⁺ (1-)
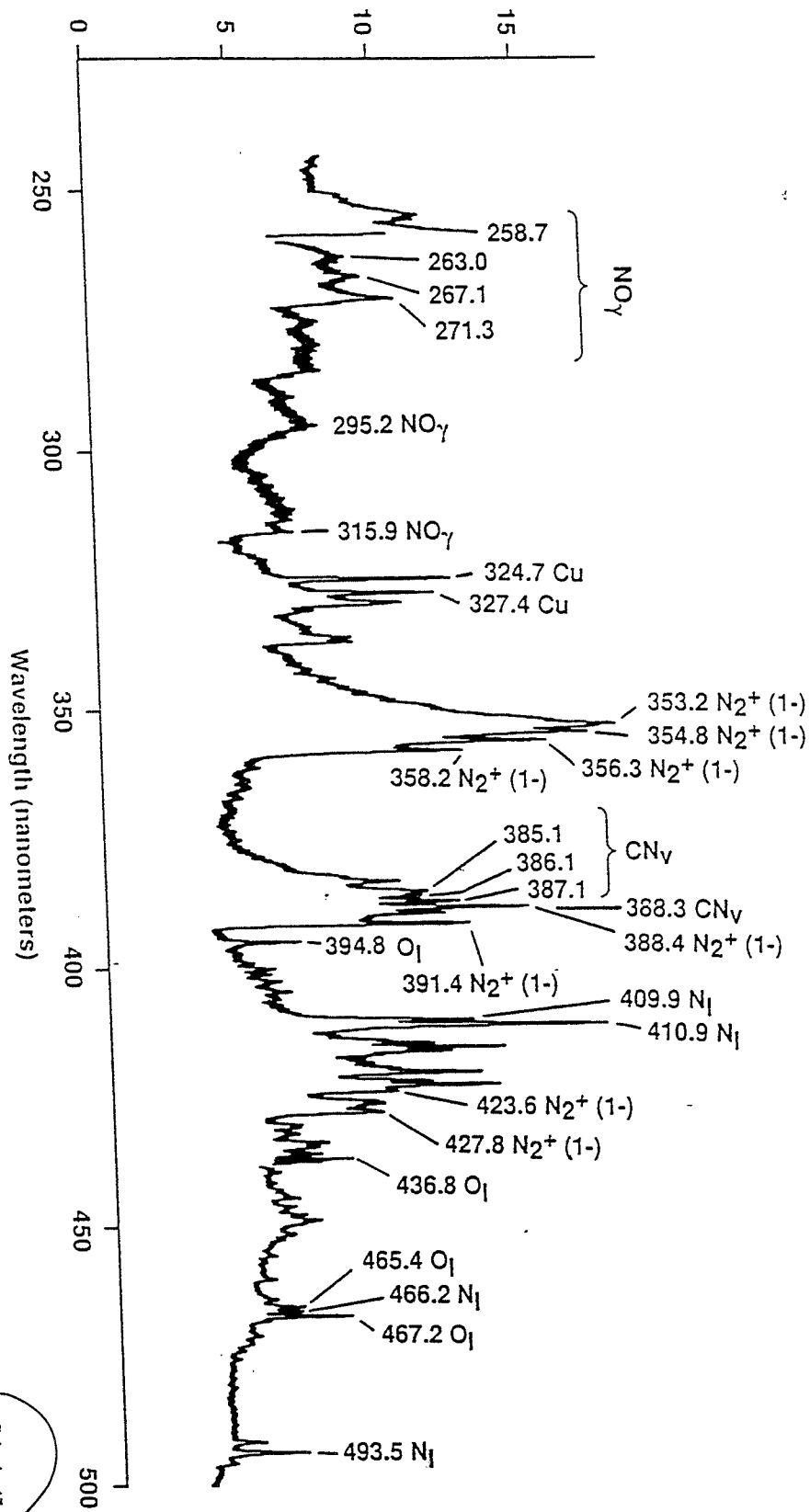- 358.2 N₂⁺ (1-)
- 385.1
- 386.1
- 387.1
- CNᵥ (bracket grouping 385.1, 386.1, 387.1)
- 368.3 CNᵥ
- 388.4 N₂⁺ (1-)
- 394.8 O₁
- 391.4 N₂⁺ (1-)
- 409.9 N₁
- 410.9 N₁
- 423.6 N₂⁺ (1-)
- 427.8 N₂⁺ (1-)
- 436.8 O₁
- 465.4 O₁
- 466.2 N₁
- 467.2 O₁
- 493.5 N₁

Palumbo-17

16

17.

Wavelength (nanometers)

450   500   550   600   650   700   750   800   850   900   950

A
B
C
D

435.8   253.6   312.6 313.0   365.0   253.1   312.6   313.0
         (2nd order) (2nd order)   (2nd order) (3rd order)   (3rd order)

Hg lines

394.8

Palumbo-18

APPENDIX - C

VUV Shock Layer Radiation in an Arc-Jet Wind Tunnel Experiment

Roger Craig
MCAT Institute
Moffett Field
California

VUV Shock Layer Radiation
in an
Arc-Jet Wind Tunnel Experiment

Roger Craig[1] Giuseppe Palumbo[2] and Armando Carrasco[3]

ABSTRACT

Measurements were made of the radiating gas cap of a blunt body in an NASA-Ames 20MW arc-jet wind tunnel. The test gas was air. Spectra of the flux incident on a small aperture centered at the stagnation region were obtained. A helium-cooled, magnesium fluoride window transmitted the flux into an evacuated collimating system that focused the aperture onto the entrance slit of a spectrometer. Data were obtained with films and by photomultipliers. The spectral ranges covered were the vacuum ultraviolet, VUV, (120 nm to 200 nm) and the ultraviolet to near infrared (200 nm to 900 nm) with resolutions from 0.05 nm to 0.5 nm. This paper presents the preliminary VUV results from the experiment. Results from the 200 nm to 900 nm spectral range have been presented elsewhere. Representative spectral records from 120 nm to 200 nm are shown. The intense atomic oxygen and nitrogen lines which are concern to hypersonic flight are measured. Carbon lines are are also seen. These results will be used to help develop and validate aerothermodynamic computational models of arc-jet wind tunnel performance and help to assess the importance of VUV heating to entering spacecraft.

INTRODUCTION

High speed flight, such as an earth entry from a space mission (low earth orbit, LEO, or further), involves flowfield gases which are not in thermochemical equilibrium *(references A and B)*. This can include important levels of transport of radiative energy *(reference C)*. *Figure A* shows flight regimes experienced for the entries of the Shuttle, Apollo and a proposed Aeroassisted Space Transfer Vehicle (ASTV). An ASTV is a conceptual vehicle which utilizes aerodynamic forces to decelerate and alter orbit parameters to rendezvous with the Shuttle or a space station *(reference A)*. The design of future, highly efficient heat-shields (i. e., not overdesigned) for these vehicles, and others, requires the capability of making accurate heating predictions. At present we cannot accurately predict the environmental conditions surrounding these spacecraft. Real gas computational models are being developed *(reference E)* but validating data are lacking.

The VUV radiative heating of an maneuvering ASTV is a subject of concern. Various models predict widely different radiative heating levels. For example, predictions of ASTV radiative heating from only the VUV atomic lines range from insignificant amounts to levels dominating the overall heating *(references F, G and H)*. There is no flight data to assist in choosing between, or refine, these conflicting theories. The Aeroassist Flight Experiment, now cancelled, was to be instrumented to measure the intensity of certain of these lines under large scale and realistic conditions, during the spacecraft entry, by an on-board experiment. These measurements would have provided a validating measurement for predictive codes. Although the present experiment was conducted in an arc-jet wind tunnel it is expected, as predictive codes are developed, that this VUV data set is important because of its uniqueness of providing a level of VUV validating data.

Arc-jet wind tunnels can produce the enthalpy and pressure conditions simulating these high speed entries. These facilities can be used to conduct experiments to validate computational codes even though the size scale cannot be simulated. A flow-field, rich in non-equilibrated, radiating gas can be generated. Computational models can be exercised on arc-jet test conditions for comparison with experimental results. There are some major difficulties in this approach, however. The free stream plasma flow conditions (enthalpy, species distribution, energy states distribution, etc.) in an arc-jet wind tunnel flow are not well understood. Upstream conditions for shock layer computational models can only be estimated. At present there are efforts at the Ames Research Center *(reference J)* to calculate the model test

environments using computational models. Preliminary estimates of the shock layer radiating have been made with a hybrid code starting with the arc column, continuing through the conical or contoured expansion nozzle, and culminating in the flow field of a model located in the exit flow from the nozzle. The radiation falling on the surface of a blunt model placed in this flow is a result culminating the entire modelling process. Experimental results, such as the spectra developed in this work, are needed to support the development of this important theoretical work.

This paper reports on results of an arc-jet wind tunnel experiment. The experiment measured the spectral radiative flux emanating from the shock layer and incident on the stagnation region of a blunt model placed in the supersonic stream. The data shown in this paper are preliminary and do not benefit from final calibrations. The flux was spectrally resolved from 120 nm to 900 nm. This paper presents the VUV results, from 120 nm to 220 nm. The results from 200 nm to 900 nm have been presented in reference N.

Reasonable agreement between the theoretical predictions and this data would be a very convincing test of the veracity of the modelling capability of the arc-jet wind tunnel processes. Understanding this flow would be valuable for development and validation of advanced arc-jet wind tunnel design codes and help extend the capability of this class of facility to advanced aerothermodynamic testing. Validating the capability to predict the VUV measurements in the arc-jet experiment would enable improved predictions of VUV aerothermodynamic radiative heating which are needed to answer the question of the importance of this heating.

EXPERIMENTAL SETUP

The experimental setup is as described in *reference N. Figures B and C* are from this reference and are included here. *Figure B* is a schematic plan view of the experiment. Supersonic flow from the arc is produced in the nozzle and the model is placed in the free stream. The standing shock layer over the model is indicated. *Figure C* is a schematic view of the model. The model face is a 6" diameter flat disk and has a small aperture centered on the forward face to admits the surface radiative flux. A MgF_2 window is immersed in a cavity below the aperture and transmits the surface flux into the optical system to be imaged onto the entrance slit of the spectrograph. The spectrograph was a 0.5 meter vacuum instrument and operated as a scanning monochromator and a film spectrograph. *Figure D* shows the model arrangement in the test box. The nozzle exit can be seen at the left, and the aperture can be seen centered on the

model face. The optical axis in front of the model was canted 15° from the centerline to avoid radiation from the arc column. The entire optical system, from the MgF$_2$ window to the transducer in the spectrograph, was evacuated to the order of 0.01 microns of Hg.

TEST CONDITIONS

The test was conducted in the Ames 20 Megawatt Aerodynamic Heating Facility. The facility was operated with a supersonic nozzle with a 1.5 inch diameter throat and an 18" exit diameter. The facility operating parameters were as follows:

> Test gas mixture: 80% air* and 20% Argon by mass,
> arc current: 1000 amperes,
> arc column pressure: 15 psia,
> nozzle pressure: 7.5 psia,
> test box pressure: 0.2 to 0.3 mm Hg, and
> stagnation pressure: 9 mm Hg.

The resulting free stream conditions for the present experiment is approximate as indicated in by the circle in *figure A*.

Figure E is a photograph taken during a test. The shock is seen well formed over the flat model face. The intense radiation from the high temperature shock layer gases is clearly evident.

Data were obtained using VUV film and a solar blind VUV (MgF$_2$ windowed) photomultiplier tube.

RESULTS AND DISCUSSION

Computed Spectral Details.

The radiating shock region is very non-homogeneous and involves many kinetically controlled processes. Substantial radiation emanates from the nonequilibrated regions immediately behind the shock. Here the kinetic temperature is extremely high, approaching 50,000 K. The VUV spectral line radiation is strongly Doppler broadened by this high temperature. These lines are from transitions to the ground state so there will be absorbers in the cooler parts of the shock and boundary layer. Absorption of strong features

---

* Dried and filtered ambient air

directed toward the surface will occur but only around the line centers because the absorption features are narrow due to the low kinetic temperature. The VUV surface radiative heating flux is thus seen to be the aggregate radiation and absorption from regions of very different conditions. Estimates from computational codes involve consideration of complex interactive and kinetic processes. *Figure H* is a calculated spectrum from 120 nm to 500 nm. The intense VUV lines are well represented. The Birge-Hopfield system (BH-1) of molecular nitrogen is the underlying background.

Test Results

Neutral atomic oxygen radiates at wavelengths as short as 81 nm, and neutral atomic nitrogen at 109 nm. To cover the entire spectral range would have necessitated windowless spectroscopy. Considering the energetics of the shock layer it was decided to conduct this experiment with a windowed design. MgF_2 was chosen for the window to permit measurements from the VUV to 1000 nm in the near infrared. The vender supplied, VUV spectral transmission curve for MgF_2 is shown in *figure I*. Also shown in the figure are estimates for the grating (150 nm blaze) efficiency, the spectral performance of the VUV photomultiplier tube and the losses due to the MgF_2 overcoated optical elements *(reference M)*. The optical system utilizes seven reflecting surfaces (including the spectrograph) and one MgF_2 window, and has an optical path of 3.5 meters. All reflecting surfaces have a MgF_2 overcoat.

The values shown in *figure I* were used to estimate the VUV spectral response of the system with the VUV tube as the transducer. This estimate, shown in *figure J*, shows useful VUV performance to 120 nm.

As indicated above the data were taken with film and with photomultiplier tubes. The film data presented herein are not corrected for instrument or film spectral response. This correction will be done with future work. The photomultiplier data has not been calibrated, but an estimated adjustment for spectral sensitivity was made based on generic data of *figure J*.

The VUV performance of the overall instrument was verified with VUV film by illuminating the model aperture with an air discharge lamp. Detailed spectra were obtained from 120 nm to 200 nm. Of special interest were the well resolved presence of the atomic oxygen and nitrogen lines at 130 nm, 149 nm and 174 nm.

The radiant flux incident on the aperture is shown in *figure K3*. This figure is a densitometer trace of a relatively low resolution, survey film record and show the spectrum from 120 nm to 500 nm. The sensitivity range in this record is from the VUV instrument limit to the VUV film limit. This figure should be compared with the calculated spectrum in *figure H* to put into context the features of the various radiating species. The spectral sensitivity of the overall system, including the film, varies over a large extent, therefore the film density should not be used to compare relative intensities of different spectral regions. To spite this shortcoming, the degree of similarity is encouraging- the predicted ,intense atomic lines are observed as well as the molecular systems of NO, N_2, and N_2^+. *Reference N* contains a more detailed identification of the features above 200 nm.

Figure K is a measurement of the surface flux spectrum from 120 nm to 210 nm. The spectral resolution is 0.13 nm. This record is from the photomultiplier output, with the estimated correction for spectral sensitivity described above. The important atomic line groups are well resolved from the background in this survey and are given below.

O and N	130 nm to 133 nm
N	141 nm
N	149 nm
N	174 nm

Other features can be seen. The feature at 166 nm is likely from atomic carbon lines grouped around 165.75 nm.

It is not possible to show on this figure the richness of details which are present in this data record. *Figure K2* is an expanded portion of this data set showing the spectral region around the 130 nm to 133 nm lines.

Because of the interest of the shapes of the lines, high resolution, low noise spectra were obtained over selected atomic lines during dedicated runs. *Figure L* shows the photomultiplier record from 173 nm to 175.5 nm. This spectral region was scanned to examine in detail the group of atomic nitrogen lines at 174 nm. These lines are predicted to be possibly important to the surface heating of a spacecraft (*reference F*). The two lines shown are each doublets separated by 0.001 nm. However, they are not separated at the resolution (0.05 nm) of this test. *References F and L* discuss the importance in evaluating the line wing shapes in assessing the heating importance of the VUV atomic line radiation. The shape of the line wings is distinguished from the background in this scan.

These details will be subsequently used to help verify the line shapes calculated by the predictive codes.

CONCLUSIONS

Spectra have been obtained from the flux incident on the stagnation surface of a flat model placed in the supersonic stream in an arc-jet wind tunnel. The resulting data set is detailed at high resolution from 120 nm to 220 nm. Important radiators are evident. The wing shape of the atomic N lines at 174 nm is shown. The data set will be further developed and used to help refine and calibrate computational models of the aerothermodynamics of entry and of arc-jet wind tunnels.

ACKNOWLEDGMENTS

REFERENCES

A. Walberg, Gerald D., "A Survey of Aeroassisted Orbit Transfer", J. Spacecraft, 22, 1, Jan-Feb 1985

B. Shinn, Judy L., and Jones, Jim J., "Chemical Nonequilibrium Effects on Flowfields for Aeroassisted Orbital Transfer Vehicles", J. Spacecraft, 22, 1, Jan-Feb 1985

C. Park, Chul, "Radiation Enhancement by Nonequilibrium in Earth's Atmosphere" J. Spacecraft, 22, 1, Jan-Feb 1985

E. Park, C., "Problems of Rate Chemistry in the Flight Regimes of Aeroassisted Orbital Transfer Vehicles", Reprinted from "Thermal Design of Aeroassisted Orbital Transfer Vehicles", H. F. Nelson ed., Progress of Astronautics and Aeronautics, 96, 1985.

F. Whiting, Ellis E., and Park, Chul, " Radiative Heating at the Stagnation Point of the AFE Vehicle", NASA TM 102829, November 1990.

G. Carlson, L. A., "Approximation for hypervelocity, Non-equilibrium, Radiating, Reacting, and Conducting Stagnation Regions", AIAA Thermophysics, Plasmadynamics and Laser Conference, June 27-29, 1988, San Antonio, TX, AIAA Paper 88-2672.

H. Moss, J. N., "Non-equilibrium Thermal Radiation for an Aeroassist Flight Experiment Vehicle", AIAA 26th Aerospace Science Meeting, Jan. 11-14, 1988, Reno NV, AIAA Paper 88-0081.

J. Babikian, Dikran, Gopaul, Nigel K. J. M., and Park, Chul, "Measurement and Analysis of NO Radiation in an Arc-Jet Flow", Proposed paper for AIAA 28th Thermophysics Conference, July 6-9, 1993, Orlando, FL.

L. Palumbo, G., "Shock Layer Vacuum UV Spectroscopy in an Arc-Jet Wind Tunnel" NASA TM 02258, January, 1990.

M. Lochte-Holtgereven, editor, "Plasma Diagnostics", page 356, North-Holland Publishing Co., Amsterdam, Holland, 1968.

N. Palumbo, Giuseppe., Craig, Roger, and Carrasco, Armando, "Spectral Measurements of Shock Layer Radiation in an Arc-Jet Wind Tunnel", ISA Paper

FIGURES

Figure A.
Flight regimes of mission returns for ASTV, Shuttle, and Apollo. The point indicated by the circle is an estimate of the altitude and velocity simulated by the arc-jet conditions used during the present tests.

Figure B.
Schematic diagram of experimental setup. The arc column is to the left of the nozzle.

Figure C.
Schematic diagram of model showing the aperture and window and orientation of the bow shock. Radiation incident onto the surface is reflected by the turning mirror to the concave mirror and thence to the spectrograph. Vacuum was maintained $<0.01\mu$ for the VUV tests.

Figure D.
Photograph of model in test box. The optical system is protected by the water cooled coils shown as well as internal water cooling. The aperture can be seen in the face of the model. The nozzle exit can be seen at the left.

Figure E.
Photograph of model during test. The stagnation shock is seen well formed over the model face and the intense radiation from the shock heated air is evident.

Figure H.
Preliminary calculation of the spectral surface flux from the stagnation region of a model placed in an arc-jet wind tunnel.

Figure I.
This figure shows vender supplied characteristics of the VUV transmission of the MgF_2 window, the spectral response of the VUV photomultiplier tube, and estimates for the grating efficiency (150 nm blaze) and reflection losses due to the MgF_2 overcoating on the optical surfaces.

Figure J.
Estimation of overall instrument spectral characteristics in the VUV with the photomultiplier tube. The estimate is based on the values given in figure G.

Figure K

VUV surface flux data from the arc-jet wind tunnel test. Atomic lines from nitrogen and oxygen are well resolved. The strong atomic nitrogen feature at 174 nm is seen to be off-scale. Carbon lines are tentatively identified.
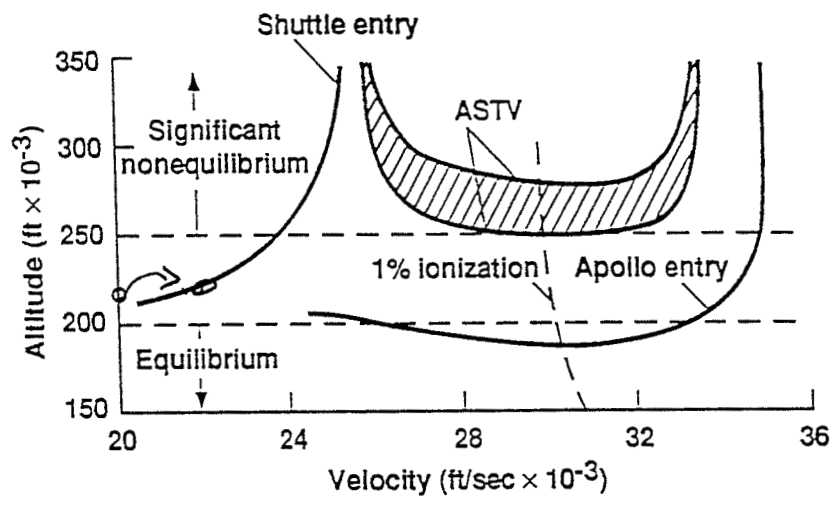
Figure K2.

Portion of VUV survey record in the vicinity of the 130 nm atomic lines to indicate the spectral details available for analysis. The strong atomic oxygen at 130.22 nm is off scale. Not all features have been identified at the present writing.Figure M.

Figure K3

120 nm to 500 nm photographic survey of the surface flux data from the arc-jet wind tunnel test.
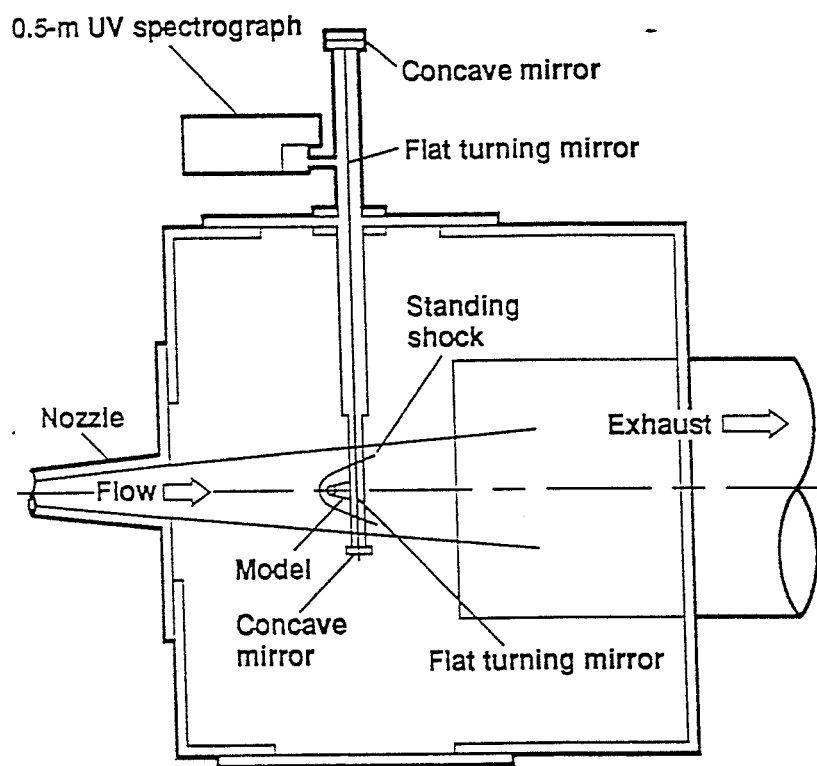
Figure L.

Details of the atomic nitrogen lines at 174 nm. The feature at 174.27 nm is from two lines 0.001 nm apart, and the feature at 174.52 nm is from two lines 0.002 nm apart. The wings from these lines can be seen as a rise in the background continuum.
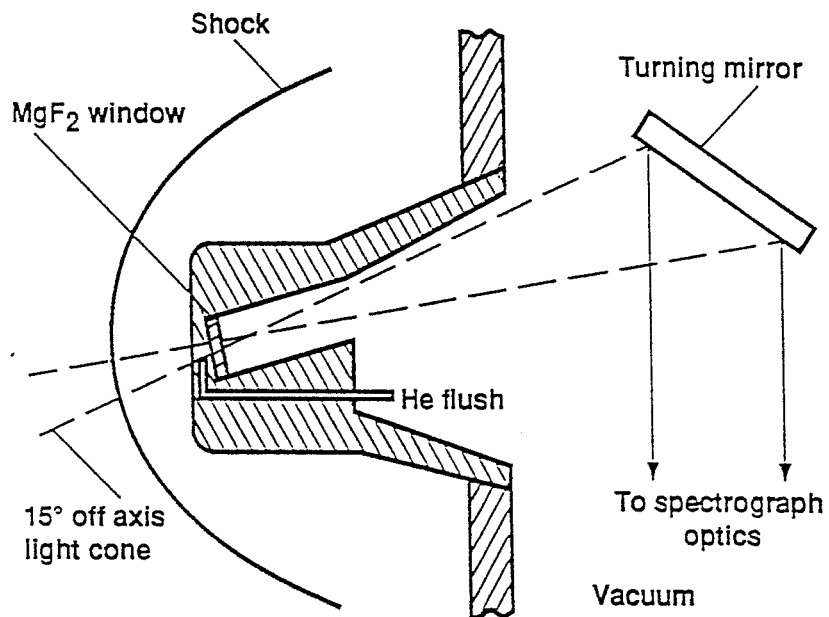
Figure A

0.5-m UV spectrograph

Concave mirror

Flat turning mirror

Standing shock

Nozzle

Exhaust

Flow

Model

Concave mirror

Flat turning mirror

Palumbo-2

Fig B

Shock

MgF_2 window

Turning mirror

He flush

To spectrograph
optics

15° off axis
light cone

Vacuum

Fig C

4

FIG D

5

Fig E

Fig H

F G

Fig I

FIG J

VUV surface flux data from the arc-jet wind tunnel test. Atomic lines from nitrogen and oxygen are well resolved. The strong atomic nitrogen feature at 174 nm is seen to be off-scale. Carbon lines are tentatively identified.

Figure K2.

Portion of VUV survey record in the vicinity of the 130 nm atomic lines to indicate the spectral details available for analysis. The strong atomic oxygen at 130.22 nm is off scale. Not all features have been identified at the present writing.Figure M.

Figure K3

120 nm to 500 nm photographic survey of the surface flux data from the arc-jet wind tunnel test.

Figure L.

Details of the atomic nitrogen lines at 174 nm. The feature at 174.27 nm is from two lines 0.001 nm apart, and the feature at 174.52 nm is from two lines 0.002 nm apart. The wings from these lines can be seen as a rise in the background continuum.

WAVELENGTH, nm

Fig K
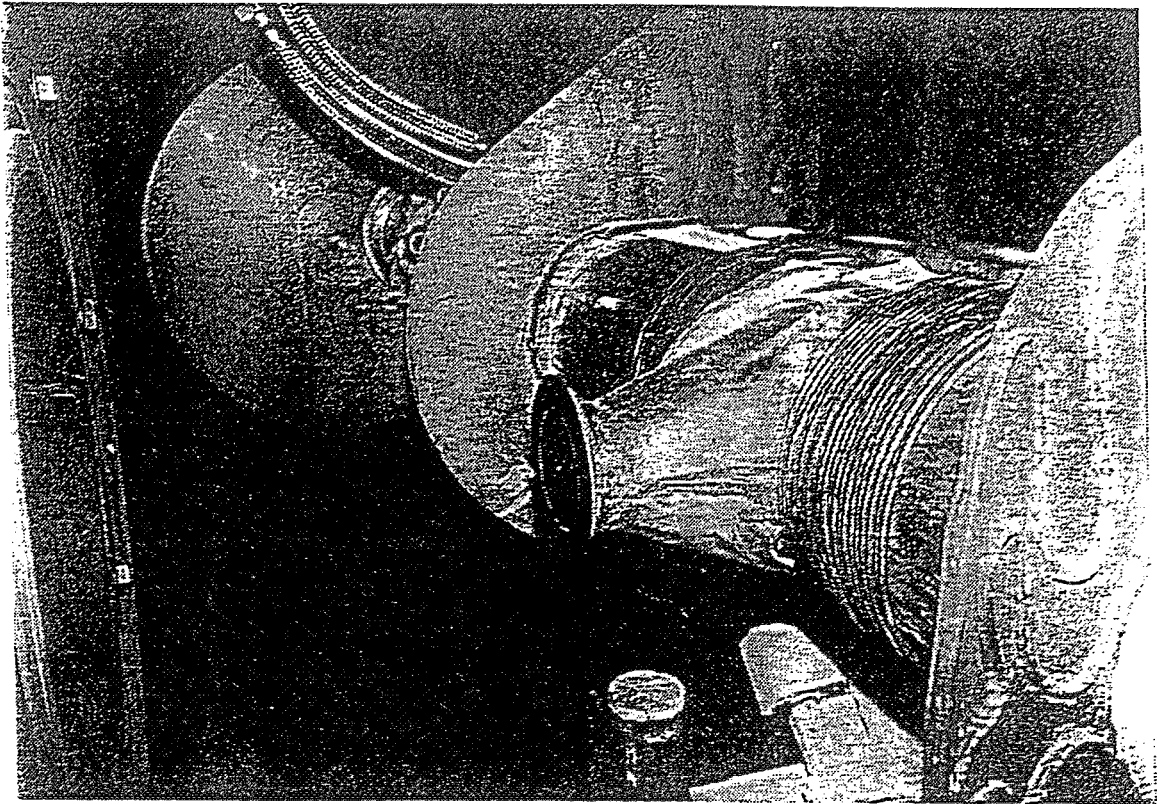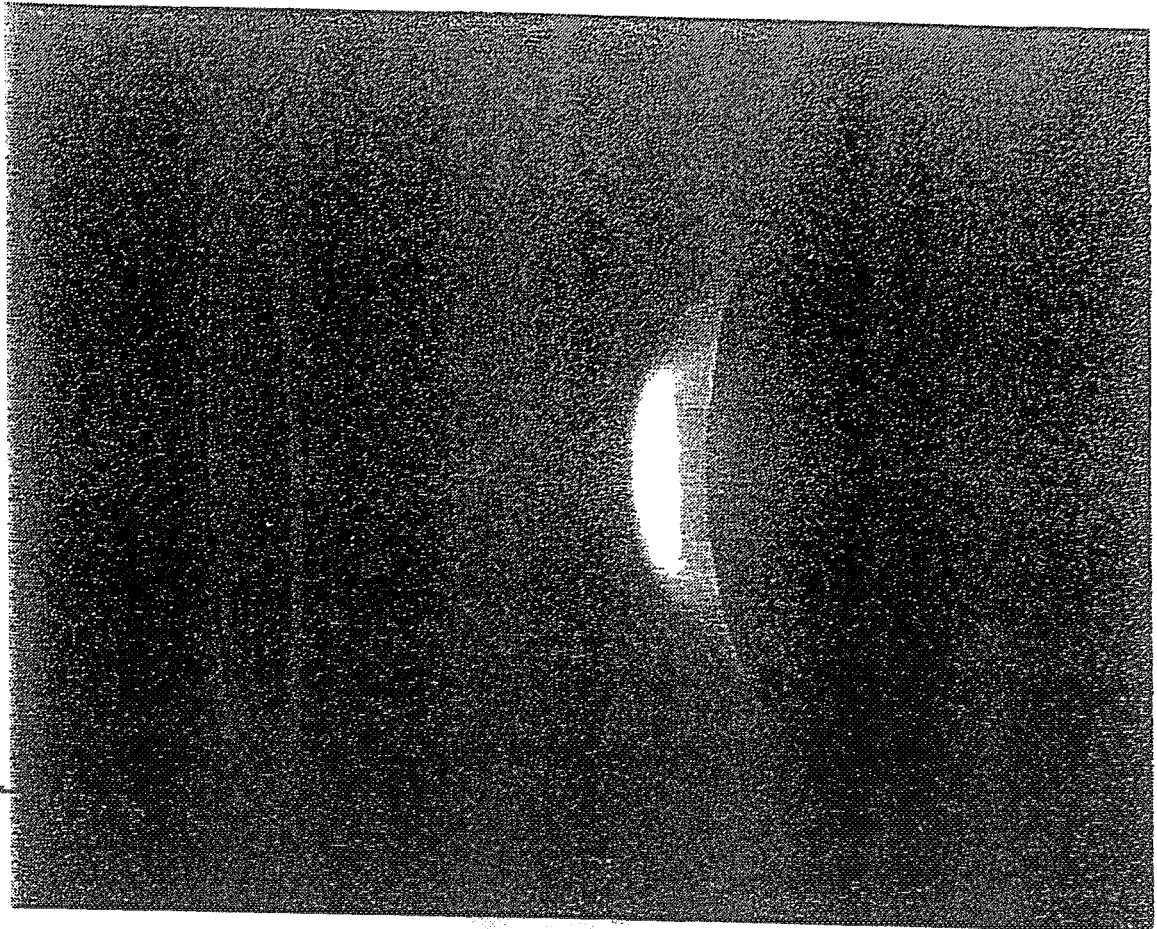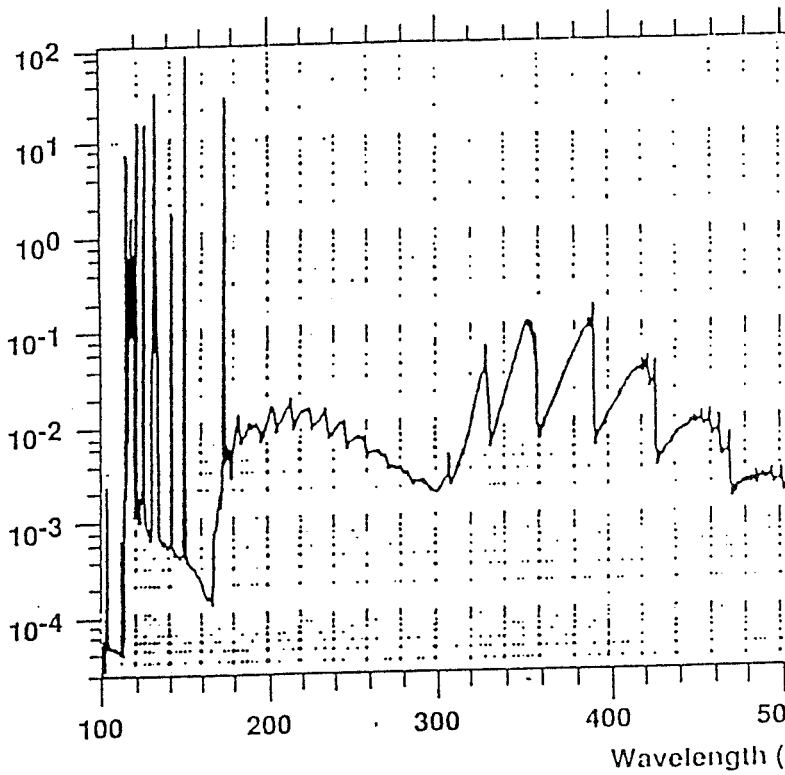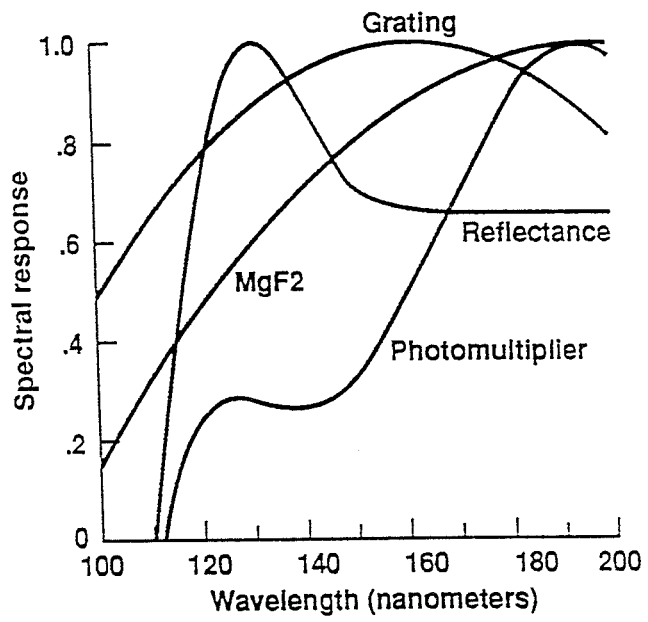
Figure axis labels:

Wavelength (nanometers)

Peak labels:
- C_I { 131.1, 132.8, 132.9 }
- O_I { 130.2, 130.4, 130.6 }
- N_I { 130.9, 131.0, 131.1, 132.1, 132.6 }
- 141.19 N_I
- 146.37, 146.38 C_I
- 149.26, 149.46 N_I lines
- 156.03 → 156.14 C_I (5 lines)
- 165.69 → 165.81 C_I (5 lines)
- 174.2 → 174.4 N_I (4 lines)
- 193.09 C_I
- NO_γ

Palumbo-11

reference fig K

reference for fig K

This is an uncorrected spectrum
These labels will be on fig K

Wavelength (nanometers)

Peaks labeled: 130.22 O₁, 130.49 O₁, 130.60 O₁, 131.10 N₁, 131.90 N₁, 131.97 N₁, 132.66 N₁, 132.79 N₁

FIGURE K3

174.27

174.52

1.0

.1

.01

173   173.5   174   174.5   175   175.5

Wavelength (nanometers)

Palumbo:13
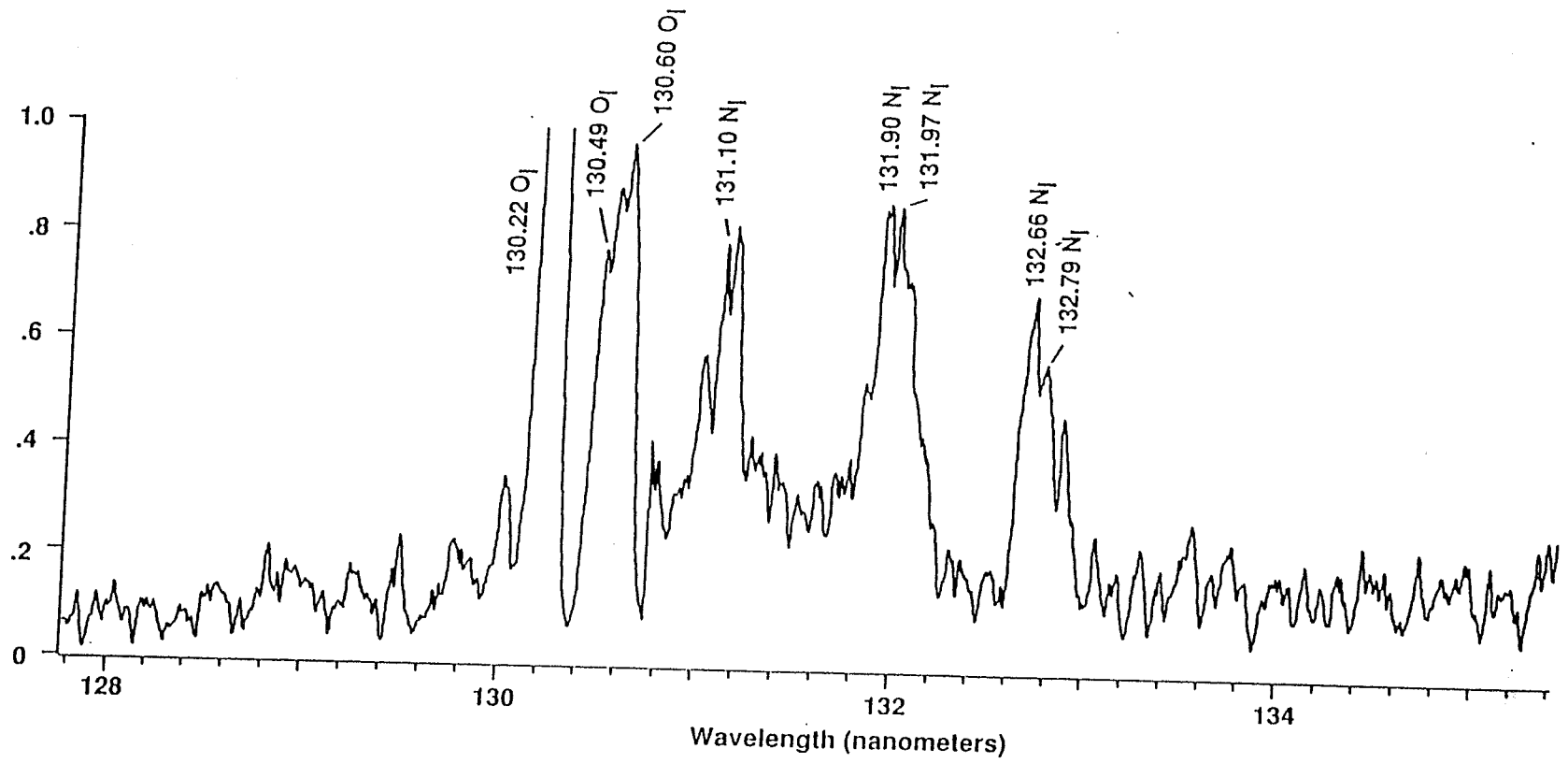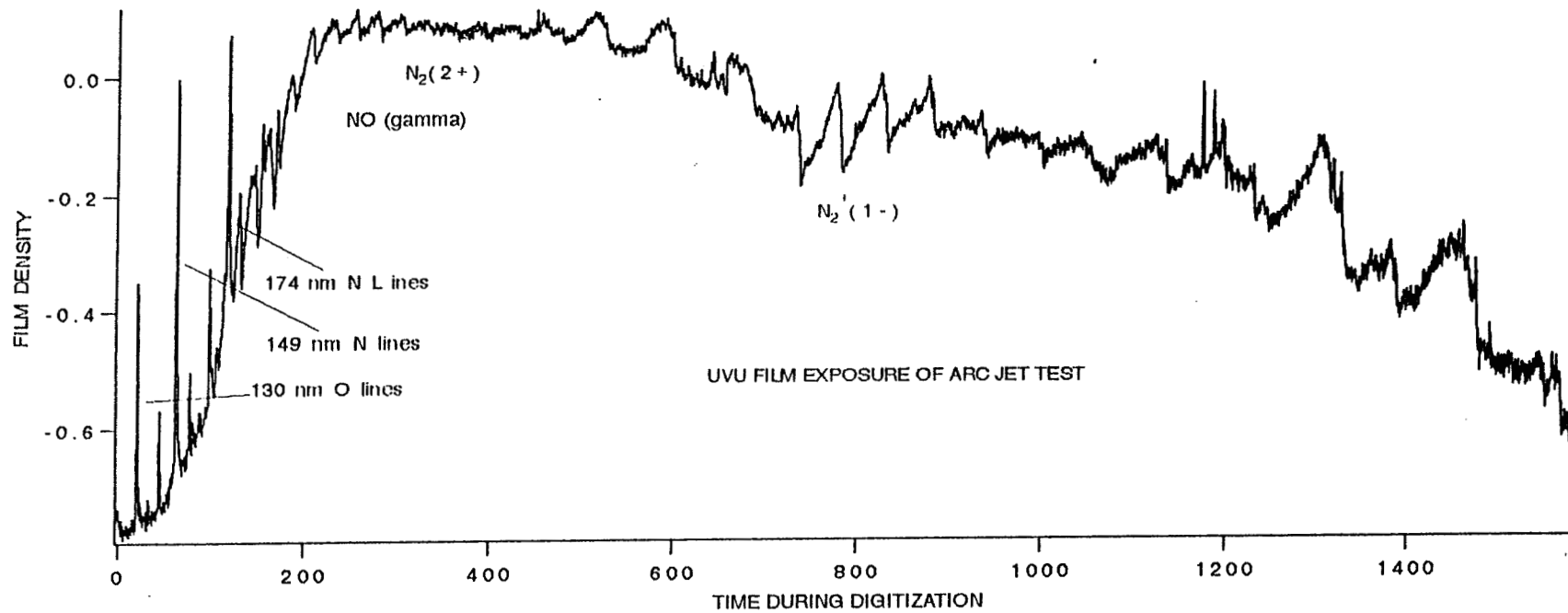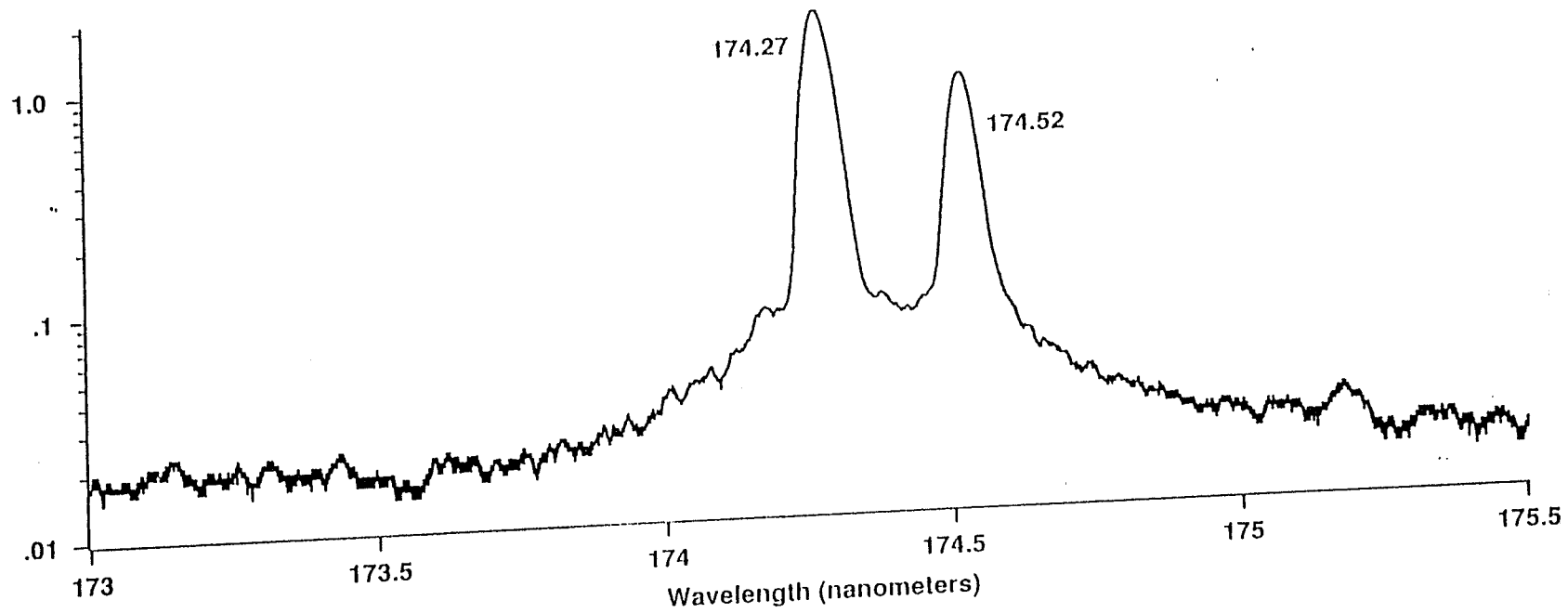
Fig L

APPENDIX - D

AIAA-94-0086

O9307
32276
16P

Measured and Calculated Spectral Radiation from a Blunt Body Shock Layer in an Arc-Jet Wind Tunnel

Roger Craig
MCAT Institute
Moffett Field
California

AIAA 94-0086

Measured and Calculated Spectral Radiation from a Blunt Body Shock Layer in an Arc-Jet Wind Tunnel

Dikran S. Babikian and Giuseppe Palumbo
Eloret Institute
Palo Alto, CA 94303

Roger A. Craig
MCAT Institute
Moffett Field, CA 94035

and

Chul Park, Grant Palmer, and Surendra P. Sharma
NASA Ames Research Center
Moffett Field, CA 94035

AIAA 32nd Aerospace Sciences Meeting
January 10-13,1994 / Reno, Nevada

MEASURED AND CALCULATED SPECTRAL RADIATION
FROM A BLUNT BODY SHOCK LAYER IN AN ARC-JET WIND TUNNEL

Dikran S. Babikian* and Giuseppe Palumbo*
Eloret Institute, Palo Alto, CA 94303
Roger A. Craig**
MCAT Institute, Moffett Field, CA 94035
and
Chul Park[†], Grant Palmer* and Surendra P. Sharma[‡]
NASA Ames Research Center, Moffett Field, CA 94035

Abstract

Spectra of the shock layer radiation incident on the stagnation point of a blunt body placed in an arc-jet wind tunnel were measured over the wavelength range from 600 nm to 880 nm. The test gas was a mixture of 80% air and 20% argon by mass, and the run was made in a highly nonequilibrium environment. The observed spectra contained contributions from atomic lines of nitrogen, oxygen, and argon, of bound-free and free-free continua, and band systems of N_2 and N_2^+. The measured spectra were compared with the synthetic spectra, which were obtained through four steps: the calculation of the arc-heater characteristics, of the nozzle flow, of the blunt-body flow, and the nonequilibrium radiation processes. The results show that the atomic lines are predicted approximately correctly, but all other sources are underpredicted by orders of magnitude. A possible explanation for the discrepancy is presented.

Nomenclature

A = Einstein A-coefficient.
E = Energy level of emitting state, cm.$^{-1}$
g = Statistical weight of the emitting state.
hν = Photon energy, cm^{-1}.
I = Intensity of a spectral line, W/(cm^2-μ-sr).
T = Heavy particle translational temperature, K.
T_e = Electron-electronic temperature, K.
T_v = Vibrational temperatue, K.
V = Flight velocity, km/s.

Introduction

For the last few decades, characterization of the radiation phenomena in the nonequilibrium region of a shock layer over a blunt body flying in high velocity, low density environments has been the focus of the efforts of many researchers. During an atmospheric entry, a spacecraft passes through the regime of altitudes where the flow be-

*Research Scientist; Member AIAA.
**Research Scientist; Senior Member AIAA.
[†]Staff Scientist; Associate Fellow AIAA.
[‡]Research Scientist; Associate Fellow AIAA.

hind the shock wave is in nonequilibrium in both chemical composition and internal thermal modes. It is known that the intensity of the radiation is strongest in the middle of the nonequilibrium zone.[1] For entry speeds in excess of 10 km/s for Earth and 8 km/s for Mars and Venus, nonequilibrium radiation is the major source of heat transfer to the stagnation region.[1,2] For this reason, a flight experiment, called the Aeroassist Flight Experiment (AFE), had been proposed at one time for the purpose of determining the intensity of this radiation.[3,4]

Predicting the flowfield around an entry body for an equilibrium regime and the radiation emitted by the equilibrium flowfield can be done more confidently; predicting nonequilibrium radiation is difficult because of the complex nature of the nonequilibrium radiation phenomena. However, in the last few years, through concerted theoretical[5-8] and experimental[9-12] efforts, it became possible to predict the radiation features in the region of peak nonequilibrium radiation with fair accuracy. This is accomplished by using a computer code named Nonequilibrium (NONEQ),[8] which is an expanded version of the code Nonequilibrium Air Radiation program (NEQAIR),[6] which accounts for the nonBoltzmann populations of electronic states and carries out detailed line-by-line calculation of both atomic and molecular lines.

Questions remain as to how well the NONEQ code predicts the radiation phenomena in the very low density regime where the nonequilibrium peak does not occur in the shock layer. That is, the truncated flow where the available flow time is shorter than the time needed for the flow to reach the peak nonequilibrium radiation point. Recently, two flight experiments, named Bow Shock 1 and Bow Shock 2, have been conducted in which the NO Gamma band radiation incident on the stagnation point was measured at flight speeds of 3.5 and 5.2 km/s, respectively.[13] The results show that the NONEQ code predicts the radiation intensities quite well in the equilibrium and moderately nonequilibrium regimes but underestimates it by many orders of magnitude in severely nonequilibrium regimes. The discrepancy between the theory and measurement is less for the 5.2 km/s flight than for the 3.5 km/s flight. Despite intensive theoretical study of this phenomenon, the discrepancy has not yet been satisfactorily explained.[13]

The flow regime of this large discrepancy is illustrated in Fig. 1. The figure shows the behavior of the trans-

lational temperature T, vibrational temperature T_v, and radiation emission power behind a normal shock wave in a one-dimensional flow computed using the NONEQ code. The freestream conditions are those of the present experiment to be described in detail later. As seen here, the radiation emission peaks. If the shock layer thickness is larger than the distance to the peak radiation point, as indicated in the figure as the AFE vehicle condition, then the flowfield can be said to be in moderate nonequilibrium. The existing NONEQ and similar codes correctly predict the total radiation power emitted in this case. A highly nonequilibrium flowfield is one in which the shock layer thickness is shorter than the distance to the peak radiation point, as indicated in the figure as the present arc-jet test condition. The discrepancy between the measurements and calculations for the Bow Shock flights occurred when the flow environment was in this highly nonequilibrium regime.
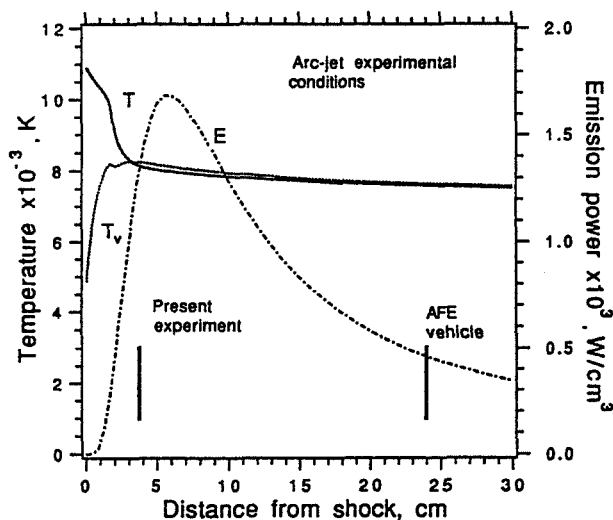

Fig. 1. Comparison between the relaxation distance and flow lengths for the present experimental condition.

The purpose of the present work is to study the radiation phenomena in this highly nonequilibrium regime, where, as shown in Fig. 1, the available flow distance is shorter than the distance needed for the flow to reach peak radiation. The study is conducted at an enthalpy corresponding to a flight speed of 7.8 km/s. If the trend observed in the flight experiment holds true, that the discrepancy is smaller at higher flight velocity, one would hope that there would be little or no discrepancy between the present data and the calculations made using the NONEQ code at this enthalpy level. If the discrepancy between experiment and calculation still exists, the study should contribute to elucidate the nature of the discrepancy.

The experimental work is carried out with a model placed in the test section of an arc-heated wind tunnel. The radiation incident on the stagnation point of a flat circular disk is detected using a grating spectrograph.

Observations were made in the near infrared wavelength range from 600 to 880 nm. This spectral region is chosen because it contains strong and well characterized lines from nitrogen and oxygen atoms and molecular band radiation from the N_2 First Positive system. In addition, there are bound-free and free-free continua that can potentially contribute to the overall background radiation. By comparing the intensities of these different radiation sources, an insight about the nature of the highly nonequilibrium regime can be gained.

In order to produce a synthetic spectrum for the experimental condition, the thermochemical state of the flow in the test section of the arc-jet wind tunnel is calculated using the best available computer code.[14] The enthalpy value input into the code is calculated from the arc heater characteristics[15] and the results of the heat transfer measurements to a sphere placed in the freestream. The nonequilibrium relaxation phenomena in the shock layer are then calculated using both the one-dimensional NONEQ code and a two-dimensional code.[16] Little difference was seen between the results of the one- and the two-dimensional calculations. The radiative transport calculation was then carried out through the shock layer using the NONEQ code.

When the results of the computations are compared with the experimental data, it is found that the computations severely underestimate the intensity of continua and molecular bands by several orders of magnitude. Thus, it is concluded that the trend seen in the flight experiments at 3.5 and 5.2 km/s still prevails at the equivalent flight speed of 7.8 km/s. No satisfactory explanation for this discrepancy has been found.

Experiment

Experimental Setup

The experimental procedures are presented in detail in Refs. 17 and 18. However, a brief description is given here for completeness. Fig. 2 shows the schematic of the overall arrangement of the model and the radiation detection system. The experiment is conducted in a constricted arc wind tunnel at Ames Research Center rated at 20 MW, known as the Aerodynamic Heating Facility. The test was made at one run condition, which is given in Table 1. The area ratio of the nozzle, deduced from Pitot impact pressure measurements at the station where the model was located, is 113.

Table 1. The operating conditions of the arc-heater.

Electrical current	950 amperes
Electrical voltage	1800 volts
Electrical power input	1.71 MW
Test gas mass flow rate	0.034 kg/s
Test gas mixture by mass	80% air, 20% Ar
Arc-heater efficiency	0.43
Mass-averaged enthalpy	21.5 MJ/kg
Centerline enthalpy	57.3 MJ/kg

In addition to air and argon, a small amount of copper is in the stream, which, based on the mass loss of the electrodes, is judged to be about 50 ppm by volume on the average.[14] Vaporization of copper electrodes occurs mostly during the start-up and shut-down processes. During the run, copper vaporization is small when the settling chamber pressure is low. At 1 atm settling chamber pressure maintained in the present study, the copper content in the flow is believed to be much less than 50 ppm. Such low concentration of copper vapor is inconsequential to the flow properties,[14] and therefore the presence of copper is neglected.

In order to determine the flow enthalpy, the characteristics of the arc discharge in the arc-constrictor are first calculated using the code Arc Heater Flowfield (ARCFLO).[15] The code yielded the centerline enthalpy value of 57 MJ/kg at the exit of the constrictor. In the past, the centerline enthalpy values have been compared with the enthalpy values deduced from the heat transfer rates to the stagnation point of a sphere placed in the flow. The heat transfer rate-deduced enthalpy values were slightly more than half the centerline enthalpy value at the exit of the arc constrictor. The difference is believed to be caused by the mixing in the settling chamber placed between the exit plane of the arc constrictor and the nozzle entrance.[20] Based on this observation, the enthalpy in the test section is judged to be approximately 30 MJ/kg. The equilibrium conditions based on this enthalpy value and the known pressure in the settling chamber are given in Table 2.

Table 2. Calculated settling chamber conditions.

Pressure	1.02 atm
Temperature	7780 K
Centerline enthalpy	30 ± 3 MJ/kg
Ar mole fraction	8.88^{-2}
N_2 mole fraction	7.29^{-2}
O_2 mole fraction	0
NO mole fraction	9.20^{-4}
N mole fraction	6.29^{-1}
O mole fraction	2.06^{-1}
Ar^+ mole fraction	8.44^{-5}
N^+ mole fraction	7.23^{-4}
O^+ mole fraction	1.94^{-4}
NO^+ mole fraction	2.22^{-4}
e^- mole fraction	1.22^{-3}

Fig. 3 shows a schematic view of the model. The model face is a flat circular disk 15 cm in diameter with the edge rounded to approximately 3 mm radius. A small aperture centered on the forward face admits the surface radiative flux. The viewing optical axis is canted 15° from the centerline in order to reject the direct irradiation from the arc constrictor. A magnesium-fluoride window, cooled with a flow of helium, is placed in a cavity below the aperture to transmit the radiation signal into the optical

system. The optical system consists of two flat mirrors and two concave mirrors. The first flat mirror turns the direction of the oncoming beam to the first concave mirror (see Fig. 2). The parallel beam produced by this concave mirror is refocused by the second concave mirror. The beam from the second concave mirror is turned by the second flat mirror and directed into the entrance slit of a grating spectrograph. The system is water-cooled, and the optical path was evacuated during the test in order to eliminate the uncertainty caused by absorption.

During the run, a luminous shock layer is visible to the eye. The stand-off distance of the visible shock layer was determined to be approximately 4 cm.
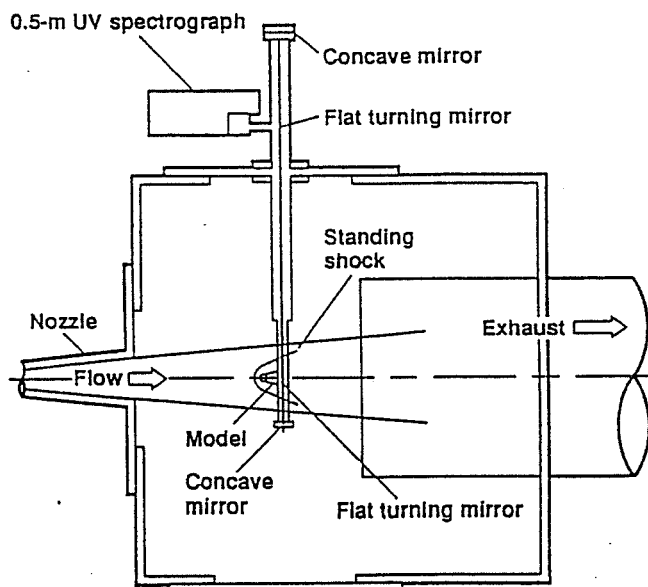

Fig. 2. Schematic of the present experimental setup in the Ames 20 MW Aerodynamic Facility.
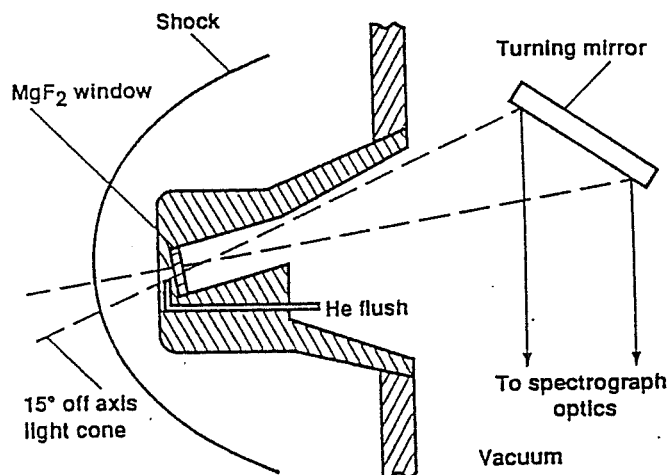

Fig. 3. Schematic of the optical arrangement within the model.

The spectrograph was a McPherson model 216.5 Czerney-Turner instrument with a focal length of 0.5 meter with an exit film plane of a 10 cm span. With a grating of 300 grooves per millimeter, the instrument has a reciprocal dispersion of 6.6 nm/mm and a theoretical resolution of 0.13 nm, and allows a spectral range of 660 nm to be recorded in a single exposure. As mentioned in Introduction, the radiation measurement was made for the near infrared wavelength range from 600 to 900 nm. This region contains a number of spectral lines from nitrogen and oxygen atoms with known transition probabilities and the well-characterized N_2 First Positive band system. The sensitivity of the film used declines rapidly beyond 880 nm. In separate measurements, radiation from the visible range from 300 to 600 nm, and that from the vacuum ultraviolet range from 120 to 300 nm, were also made. Preliminary results for the visible and the vacuum ultraviolet spectra are presented in Refs. 18 and 19, respectively. In addition, spectral measurements were made in the visible wavelength range from the direction normal to the nozzle axis to obtain the radiation intensities from the shock layer as a function of the distance from the model wall. This work will be presented in the future also. The present measurements were made photographically because the radiation signal was too weak to be measured reliably with a photoelectric method while maintaining a sufficiently high wavelength resolution.

A grating with 300 grooves/mm blazed at 500 nm was used for the experiment. In the experiment, an exposure of 8 min was made on a Kodak High Speed Infrared Film. Exposures were also made of a calibrated tungsten ribbon lamp on the same film, all for the same 8 min exposure.
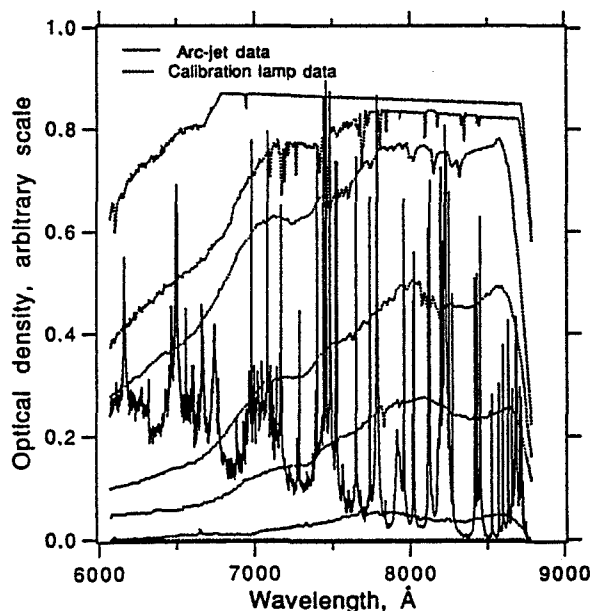

Fig. 4. Microphotodensitometer traces of the spectra obtained in the arc-jet test and the calibration lamp with varying slit widths.

The lamp was placed in front of the model, and the luminous surface of its heated tungsten ribbon was imaged on the stagnation point using a concave mirror. The solid angle of this setup was identical to that of the arc-jet experiment. The exposure from the calibration lamp was controlled by the combination of a neutral density filter and the width of the entrance slit. Second order effect was negligible for the calibration lamp.

Photographic Data

The microphotodensitometer trace of the photographic data of the arc-jet test is compared with those of the calibration lamp in Fig. 4. The ordinates in this figure represent optical densities of the film, that is, the logarithm of the attenuation of a light beam through the film. As seen here, the spectral intensities in the arc-jet data are approximately within the range covered by the calibration traces. The absolute intensity values of the arc-jet data are determined at each wavelength through interpolation between the calibration values. This was done at wavelength intervals of 0.017 nm, resulting in a total of 16862 wavelength points. At each wavelength point, an intensity-optical density curve is constructed as shown in Fig. 5. The calibration points were fitted with a Gaussian curve using a least-square curve-fit method. The radiation intensity is deduced from the optical density of the experimental data using this curve.

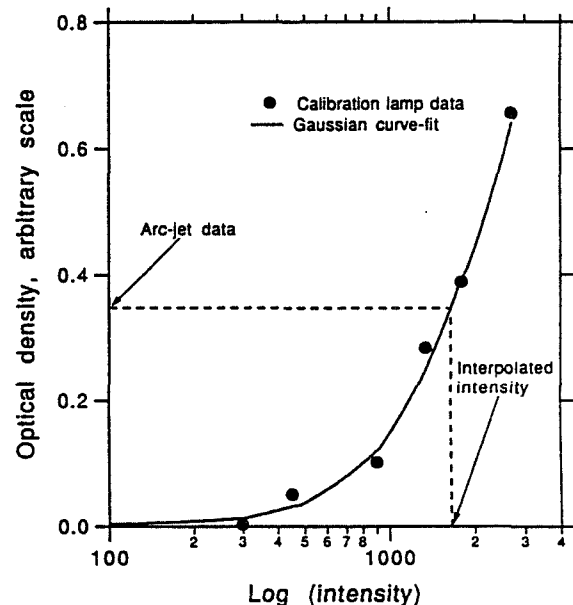Fig. 5. The relationship between optical density and radiation intensity.

The spectrum contains the distinct features of atomic lines and complicated background features. Most of the atomic lines are identified to belong to either nitrogen, oxygen, argon, or copper. There are still unidentified lines, however. Identifiable features of the N_2 First Positive band system were seen throughout the observed wave-

length regions, and a weak feature of the N_2^+ First Negative system was identified at wavelengths below 670 nm. Second-order images were too weak to be identified.

The area under the curve for each atomic line was calculated in order to determine the overall average line intensity over the inhomogeneous shock layer. These intensity values are plotted in an atomic Boltzmann plot in Fig. 6. As seen in the figure, the three atomic oxygen lines give an equivalent average Boltzmann temperature of about 27000 K, whereas the nitrogen lines give about 12000 K. These equivalent temperatures are considerably higher than the equilibrium temperatures listed in Table 2. This is a consequence of strong nonequilibrium phenomenon in the shock layer.
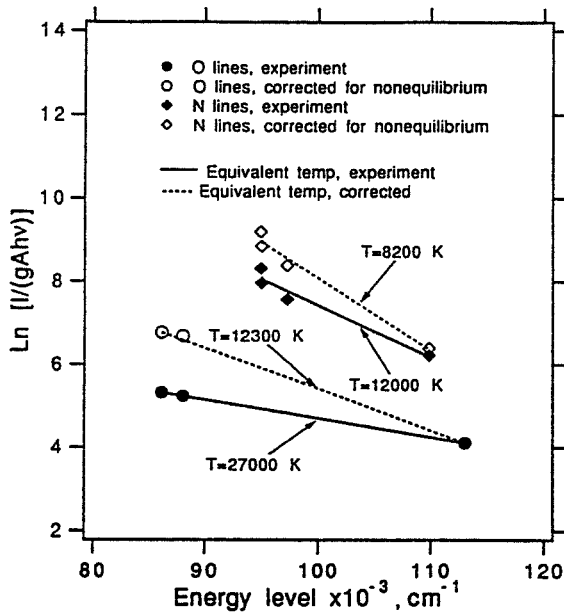

Fig. 6. Atomic Boltzmann plot of the selected atomic oxygen and nitrogen lines obtained from the experiment.

It is known that the lower excited states tend to be underpopulated with respect to the equilibrium values at low densities due to radiative depopulation. This is because (i) the radiative depopulation rate (Einstein A-coefficient) is larger for lower states than for the upper states, and (ii) the upper states tend to be in equilibrium with the free state. The extent of this underpopulation can be calculated using the NONEQ code. The calculation shows that the emitting levels of the oxygen lines in Fig. 6 emanating at energy levels around 87000 cm^{-1} are underpopulated by a factor of 0.23 with respect to the equilibrium value, while the population of the emitting levels around 113000 cm^{-1} is unaffected. For nitrogen, the lower and the upper groups of the levels are depopulated by factors of 0.41 and 0.86, respectively. When this phenomenon is accounted for, the deduced effective average temperatures over the shock layer are 12300 K for oxygen and 8200 K for nitrogen, as shown in the figure. These values are closer to the equilibrium temperature given in Table 2.

Comparison With Calculations

Computational Method

The thermochemical nonequilibrium relaxation processes in the nozzle are calculated using the one-dimensional Nonequilibrium n-Temperature (NOZNT) code.[14] The code recognizes the differences among the vibrational temperatures of different molecules but assumes the electronic excitation to be characterized by the electron temperature. The electron-electronic temperature is not equated to the vibrational temperature of any species. The code has been validated against the existing experimental data in Refs. 14 and 21.

Table 3. Test section freestream conditions (NOZNT solution).

Geometrical area ratio of nozzle	113
Centerline enthalpy	30 ± 3 MJ/kg
Equivalent flight speed	7.75 km/s
Static pressure	9.6^{-5} atm.
Density	5.60^{-5} kg/m^3
Heavy particle temperature	321 K
N_2 vibrational temperature	4100 K
NO vibrational temperature	910 K
Electron-electronic temperature	6170 K
Mean free path	0.123 cm
Equivalent flight altitude	71.6 km
Velocity	4890 m/s
Mach number	10.1
Total number density	2.13^{15} cm^{-3}
Ar mole fraction	9.30^{-2}
N_2 mole fraction	1.22^{-1}
O_2 mole fraction	0
NO mole fraction	2.55^{-3}
N mole fraction	5.66^{-1}
O mole fraction	2.15^{-1}
Ar$^+$ mole fraction	6.88^{-5}
N$^+$ mole fraction	4.93^{-4}
O$^+$ mole fraction	1.53^{-4}
NO$^+$ mole fraction	1.33^{-17}
e$^-$ mole fraction	7.15^{-4}
Model	
Shape	flat circular disk
Diameter	15 cm
Shock standoff distance	≈ 4 cm
Equivalent sphere radius in flight	≈ 60 cm
Knudsen number (for 15 cm)	0.0328
Reynolds number (for 15 cm)	2700

In Figs. 7(a) and (b), the calculated temperatures and species concentrations along the nozzle axis are shown for the present test conditions. Selected numerical values are presented in Table 3 for the nozzle exit conditions. As seen here, the vibrational temperatures of N_2 and NO are considerably different, with N_2 having the higher vibrational temperature. The electron-electronic temperature

is considerably higher than the N_2 vibrational temperature. The flow is virtually frozen in the nozzle. Most of the vibrational energy is contained in N_2. The vibrational energy of N_2 is larger than the electron-electronic energy at the exit of the nozzle.
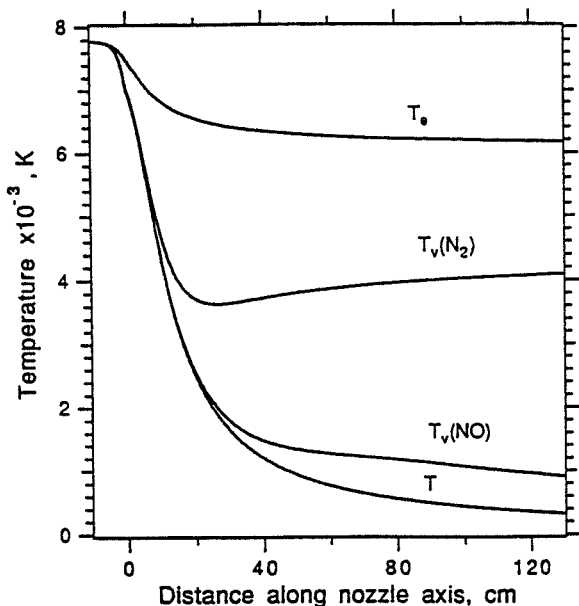

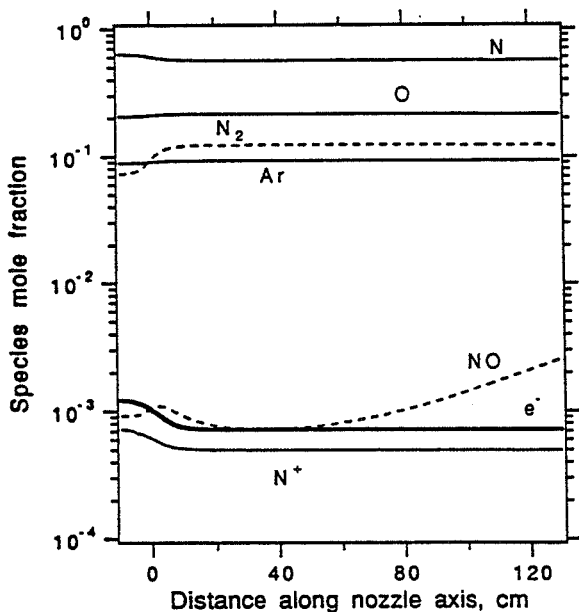Fig. 7. Calculated nozzle flow properties. (a) Temperatures

Fig. 7. (b) Species mole fractions.

The calculated equilibrium conditions in the shock layer are presented in Table 4. The nonequilibrium processes in the blunt body shock layer are calculated using both one- and two-dimensional codes. The one dimensional flow solution is obtained by the flow solver portion of the NONEQ code, which is the same as that identified as STRAP in Ref. 7. The two-dimensional solution is obtained using a code referred to as 2D2T.F described in Ref. 16. Both codes use a two-temperature model in which the vibrational temperatures of the molecules, the electronic excitation temperatures of all species, and the electron thermal temperature are assumed to be the same. The one-dimensional code has been validated against experimental data in Ref. 7. The two-dimensional code has been validated indirectly by comparing with the one-dimensional code. Both these codes were originally written for a freestream flow of undisturbed air. They were modified to accommodate the nonequilibrium freestream conditions of the present flow environment.

Table 4. Calculated equilibrium conditions in the shock layer.

Pressure	0.0118 atm
Temperature	6430 K
Ar mole fraction	8.56^{-2}
N_2 mole fraction	3.44^{-2}
O_2 mole fraction	0
NO mole fraction	1.34^{-4}
N mole fraction	6.79^{-1}
O mole fraction	2.00^{-1}
Ar^+ mole fraction	3.46^{-5}
N^+ mole fraction	5.07^{-4}
O^+ mole fraction	1.59^{-4}
NO^+ mole fraction	1.09^{-4}
e^- mole fraction	8.10^{-4}

The two codes were run for the 30 MJ/kg case and at higher enthalpies. The vibrational temperature of N_2 determined by NOZNT code was chosen as representative of the vibrational-electron-electronic temperature ahead of the shock wave in the one- and the two-dimensional blunt body flow codes. A one-dimensional solution obtained for a constant-area channel is shown in Fig. 1, along with the total radiation emission power calculated using the NONEQ code.

The solution obtained from the one-dimensional code is shown in Fig. 8(a) and (b) for the 30 MJ/kg case. As seen in the figure, there is substantial variation in the temperatures and concentrations of the species across the shock layer. The two-dimensional code yielded approximately the same results.

Spectral Calculation

The spectral intensities are calculated for the flow properties shown in Figs. 8(a) and (b) using the spectral part of the NONEQ code. Presently the code allows calculation of nonequilibrium radiation only for nitrogen, oxygen, and carbon. Therefore presence of argon was neglected in the code. Figure 9 shows the comparison between the measured and the calculated spectra. As seen here, the calculation approximately reproduces the intensities of the atomic lines, but underestimates the background

radiation composed of bound-free and free-free continua and molecular radiation.
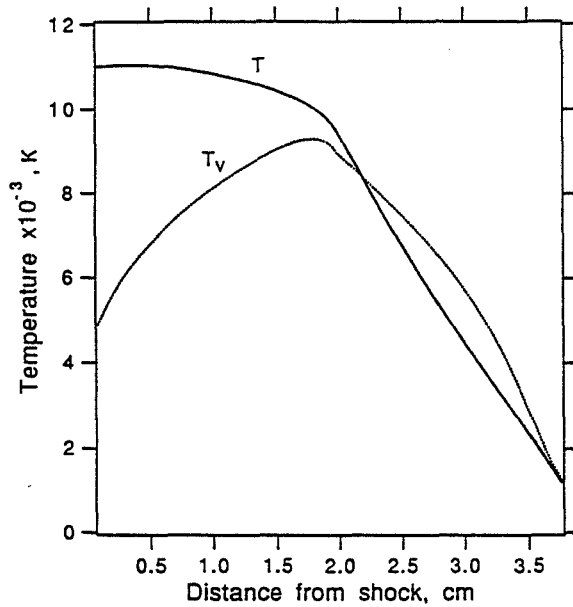

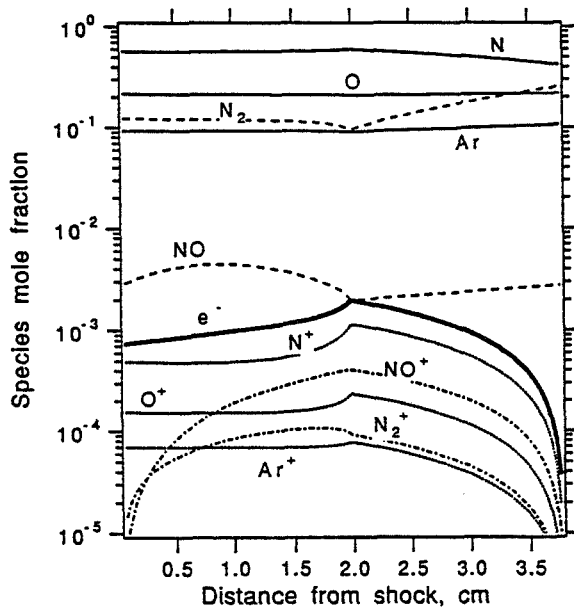Fig. 8. Calculated properties along the stagnation line. (a) Temperatures.

Fig. 8. (a) Species mole fractions.

In order to verify that this large discrepancy is not due to the misjudgment of the enthalpy values, calculations were made also with enthalpy values of 35, 40 and 45 MJ/kg. At these higher enthalpies, the atomic line intensities are calculated to be higher, by a factor within about 3, but the background radiation remained relatively unchanged. This behavior is explained as follows: at higher flow enthalpy, the electron concentration in the nozzle increases. This causes the electron temperature to approach

the lower N_2 vibrational temperature. Thus the initially low vibrational-electron-electronic temperature produces a slow rate of ionization behind the shock wave, which in turn produces only a small increase in electron density and continuum radiation behind the shock wave. Therefore, the low background radiation at higher enthalpy is not unreasonable.
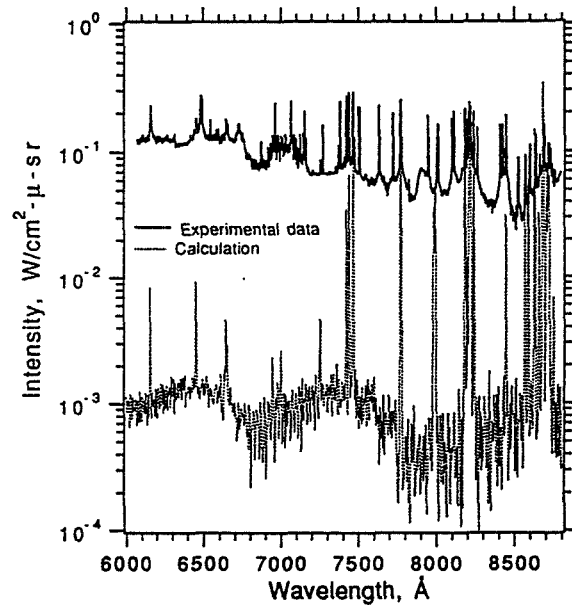
Fig. 9. Comparison between the measured and the calculated spectra.

Discussion

Equivalent Intensities

In order to explain the discrepancy between the experimental and theoretical spectral intensities, it is hypothesized that the ionization phenomena behind the bow shock wave occurs at a rate faster than calculated due to the highly excited freestream. Highly excited species require little energy to vibrationaly excite or ionize. Computationally, this situation is implemented by (i) making the vibrational relaxation times very short, (ii) lowering the magnitude of the energy feedback in electron-impact ionization (the energy depletion in the electron gas as a result of electron-impact ionization), and (iii) increasing the rate coefficients for electron-impact ionization reactions. The vibrational relaxation times are taken to be those corresponding to the elastic collisions; the energy feedback is reduced arbitrarily to 1% of the ionization potential; and the ionization rates are increased one thousand-fold.

In Fig. 10, the solution for the enhanced reaction rates is compared with the original solution. As seen here, there is a significant reduction in electron temperature in the peak region and an increase in total radiated power. Nevertheless, the changes were unable to bring the calculated values of the background radiation into agreement with

the experimental values. In order to quantify the discrepancy between the calculated and the experimental values, the calculation was repeated with the intensities of each radiation sources multiplied by an arbitrary factor.
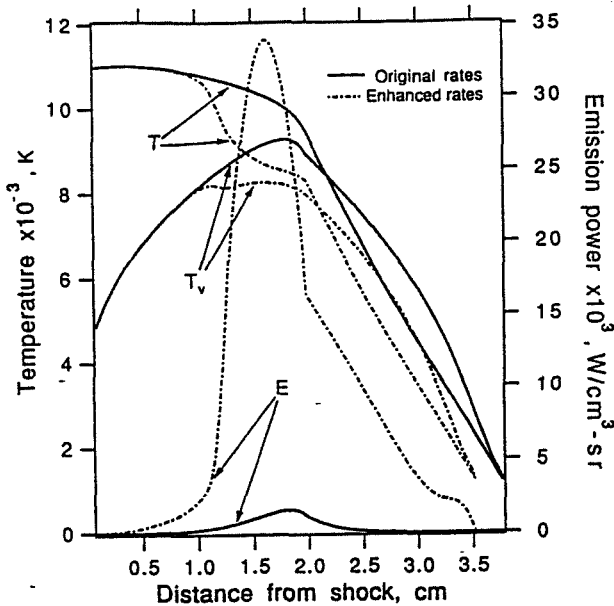

Fig. 10. Comparison between the solution for the enhanced reactions case and the original solution.

Through a trial and error procedure, the factors that gave the best agreement with the experimental data are given in Table 5. The resulting synthetic spectrum is compared with the experimental data in Fig. 11.

Table 5. The multiplicative factors to reproduce the experimental spectrum.

Source	Factor
N lines	1
O lines	1
$N^+ + e^-$ bound-free continuum	6000
$O^+ + e^-$ bound-free continuum	6000
$N^+ + e^-$ free-free continuum	300
$O^+ + e^-$ free-free continuum	300
N_2 First Positive band system	50
N_2^+ First Negative band system	500

Explanation of Discrepancy

As shown in Fig. 1, the present experiment was conducted in a highly nonequilibrium regime where the available flow residence time is too short for the nonequilibrium radiation intensity to reach its peak point. As mentioned in Introduction, the flight experiments, Bow Shock 1 and Bow Shock 2, have demonstrated that calculations tend to severely underestimate radiation intensities in such a regime. In Fig. 12, the present results are compared with

those of the two flight experiments. In the figure, the ratios of the calculated to the measured intensities, the reciprocals of the multiplicative factors in Table 2, are shown as a function of flight altitude. Even though the equivalent flight altitude of the present test is 71.6 km, it is shown as 61.2 km. This is because the shock layer thickness in the present experiment is approximately four times that of the flight experiments, and therefore the equivalent freestream density is four times the experimental value for the same shock layer thickness.
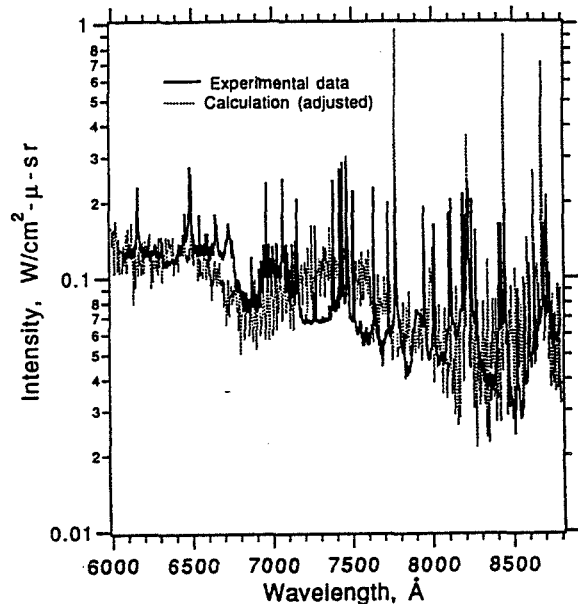
Fig. 11. Comparison between the measured spectra and the spectra calculated with enhanced reaction rates and intensity factors.

As indicated in Fig. 12, the calculated intensities are orders of magnitude smaller than the measured values in both the flight and the present experiments. The discrepancy between the theory and measurement on the intensity of the background radiation in the present experiment is comparable with that found for the NO Gamma band in the flight experiments. A discrepancy of similar extent is found in a shock tube experiment of Ref. 10 between the measured and the calculated intensities of the background radiation at wavelengths above 600 nm.

The large discrepancy between the measurement and the calculation in the intensities of the bound-free and free-free continua might be due to the pseudo-continuum caused by the large numbers of weak atomic lines which are neglected in the calculation. The NONEQ code accounts for atomic lines listed in the NBS Tables.[22] The Tables list only the lines from the states at or below the principal quantum number of 3, and a few of those from the principal quantum number of 4 and 5. However, there are a large number of atomic lines that emanate from the principal quantum number of 4 and all those from the principal quantum number above 4 that are unaccounted

for in the NBS Tables. These neglected lines are mostly in the infrared wavelength region longer than 700 nm. The widths of these lines are so broad that they appear as a continuum. Whether this pseudo-continuum can account for the missing radiation needs to be evaluated.

The discrepancy in the calculated intensities of the N_2 First Positive and N_2^+ First Negative band systems is thought to be caused by the inadequacy of the code of the excitation code. The excitation portion of the NONEQ presently includes only four excited electronic states. The rate coefficients for collisional transitions among the states considered have been obtained mostly by extrapolation from the limited existing experimental data. Errors in the rate coefficients so determined, and the fact that there are transitions from many other electronic states, are believed to be responsible for this discrepancy. Such shortcomings of the NONEQ code can be corrected but it will require considerable additional work.
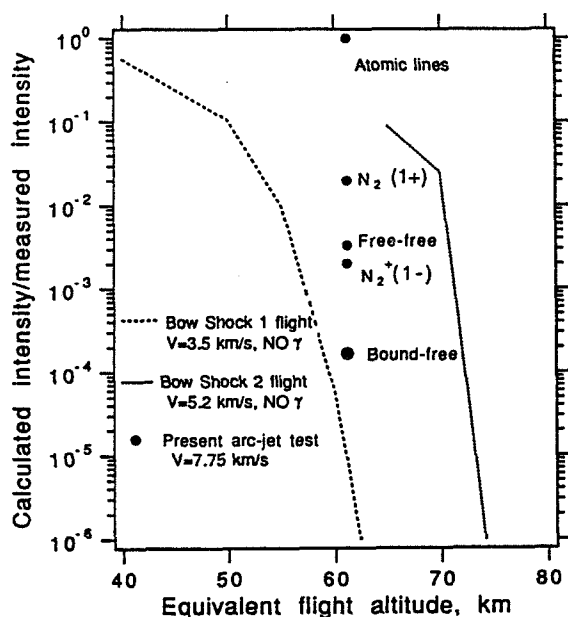

Fig. 12. The ratio between the calculated and the measured intensities of the present experiment compared with those for the Bow Shock 1 and Bow Shock 2 flight experiments.

The present work indicates that the features of the nonequilibrium spectrum seen in an arc-jet wind tunnel test are the same as those in flight or in a shock tube experiment. This is an indication that an arc-jet experiment can be used for the purpose of studying nonequilibrium radiation phenomena. Work is presently in progress to reduce the visible and the vacuum ultraviolet spectral data obtained in the experiments mentioned earlier.

Conclusions

The spectra of the shock layer radiation incident on the stagnation point of a blunt body were measured in an arc-jet wind tunnel in the wavelength range from 600 to 880 nm in a highly nonequilibrium regime using an air-argon mixture as the test gas. Synthetic spectra were produced through the computation of the constricted-arc characteristics, nozzle flow, blunt body flow, and nonequilibrium radiation phenomena. Most of the calculated intensities of atomic lines agree approximately with the measured values, but those for continua and molecular bands are much weaker than the measured values. The discrepancy between the measured and the calculated intensities is similar to that found in two flight experiments and in shock tube data. Possible explanations for the discrepancy are presented. The present work shows also that an arc-jet wind tunnel can be used for the study of nonequilibrium radiation phenomenon.

References

[1]Park, C., "Radiation Enhancement by Nonequilibrium in Earth's Atmosphere," *Journal of Spacecraft and Rockets*, Vol. 22, No. 1, January-February 1985, pp. 27-36.

[2]Park, C., Howe, J.T., Jaffe, R.L., and Candler, G. V., "Chemical Kinetic Problems of Future NASA Missions. 2. Mars Entries: A Review," To be published in *Journal of Thermophysics and Heat Transfer*.

[3]Davy, W., Park, C., Arnold, J. A., and Balakrishnan, A., "Radiometer Experiment For the Aeroassist Flight Experiment," AIAA Paper 85-0967, June 1985.

[4]Craig, R. A., Davy, W. C., and Whiting, E.E., "Science Objectives and Performance of a Radiometer and Window Design for Atmospheric Entry Experiments," to be published as a NASA TMX, 1994.

[5]Park, C., "Calculation of Nonequilibrium Radiation in the Flight Regimes of Aeroassisted Orbital Transfer Vehicles," Thermal Design of Aeroassisted Orbital Transfer Vehicles, *Progress in Astronautics and Aeronautics*, Vol. 96, edited by H. F. Nelson, AIAA, 1985, pp. 395-418.

[6]Park, C., "Nonequilibrium Air Radiation (NEQAIR) Program: User's Manual," NASA TM 86707, July 1985.

[7]Park, C., "Assessment of Two-Temperature Kinetic Model for Ionizing Air," *Journal of Thermophysics and Heat Transfer*, Vol. 3, No. 3, July 1989, pp. 233-244.

[8]Whiting, E. E., and Park, C., "Radiative Heating at the Stagnation Point of the AFE Vehicle," NASA TM 102829, November 1990.

[9]Sharma, S. P., and Gillespie, W., "Nonequilibrium and Equilibrium Shock Front Radiation Measurements," *Journal of Thermophysics and Heat Transfer*, Vol. 5, No. 3, July-September 1991, pp. 257-265.

[10]Sharma, S. P., Gillespie, W. D., and Meyer, S. A., "Shock Front Radiation Measurements in Air," AIAA Paper 91-0573, January 1991.

[11]Sharma, S. P., and Whiting, E. E., "Modelling of Nonequilibrium Radiation Phenomena: An Assessment," AIAA Paper 94-0253, January 1994.

[12]Sharma, S. P., "Assessment of Nonequilibrium Radiation Computation Method for Hypersonic Flows," *International Journal of Modern Physics*, Vol. 4, No. 4, April 1993, pp. 847-881.

[13]Levin, D. A., Candler, G. V., Collins, R. J., Erdman, P. W., Ziph, E. C., and Howlett, C. L., "Examination of Ultraviolet Radiation Theory for Bow Shock Rocket Experiments," AIAA Paper 92-2871, June 1992.

[14]Park, C., and Lee, S. H., "Validation of Multi-Temperature Nonequilibrium Nozzle Flow Code NOZNT," AIAA Paper 93-2862, July 1993.

[15]Nicolet, W. E., Shepard, C. E., Clark, K. C., Balakrishnan, A., Kesselring, J. P., Suchsland, K.E., and Reese, J. J., "Methods for the Analysis of High-Pressure, High Enthalpy Arc Heaters," AIAA Paper 75-0704, June 1975.

[16]Palmer, G., "Explicit Thermochemical Nonequilibrium Algorithm Applied to Compute Three-Dimensional Aeroassist Flight Experiment Flowfields," *Journal of Spacecraft and Rockets*, Vol. 27, No. 5, September-October, 1990.

[17]Palumbo, G., "Shock Layer Vacuum Ultraviolet Spectroscopy in an Arc-Jet Wind Tunnel," NASA TM 02258, January 1990.

[18]Palumbo, G., Craig, R., and Carrasco, A., "Spectral Measurements of Shock layer Radiation in an Arc-Jet Wind Tunnel," Paper 93-145, *Instrument Society of America Meeting*, Albuquerque, NM, April 1993.

[19]Craig, R. C., Palumbo, G., and Carrasco, A., "VUV Shock Layer Radiation in an Arc-Jet Wind Tunnel Experiment," NASA TM 108796, 1994.

[20]Durgapal, P., and Palmer, G., "Strongly Coupled Radiative Transfer and Joule Heating in the Cathode Region of an Arc Heater," AIAA Paper 93-2801, July 1993.

[21]Babikian D. S., Gopaul N. K. J. M., and Park, C., "Measurement and Analysis of Nitric Oxide Radiation in an Arc-Jet Flow," AIAA Paper 93-2800, July 1993.

[22]Wiese, W. L., Smith, M. W., and Glennon, B. M., "Atomic Transition Probabilities. Vol. 1. Hydrogen Through Neon," NSRDS-NBS 4, National Bureau of Standards, May 1966.

APPENDIX - E

07308
322-765
14p

Venusian Atmospheric Equilibrium Chemistry at the Pioneer Venus Anomalous Event Altitude

Roger Craig
MCAT Institute
Moffett Field
California

Venusian Atmospheric Equilibrium Chemistry
at the
Pioneer Venus Anomalous Event Altitude

Roger Craig*

Introduction

No convincing explanation for the anomalous behavior of the Atmospheric Structure Experiment temperature sensors at ~13km altitude has been found. It occured on all of the widely-spaced probes, in a similar fashion. This suggests an interaction between the probe and some property of the 13km atmospheric conditions. Could -the probes have provided local condensation sites for a metallic vapor? Could the probes have picked up static charges from the descent through the cloud layer, and a chemical reaction at 13km result in spallation and loss of charge? Several questions of this nature have been raised. Additional knowledge of the probe environment would surely suggest other possible scenarios, and perhaps offer a basis for evaluation.

A preliminary effort has been made to determine atmospheric chemical species which might be present at 13 km. The purpose of this effort is to initiate suggestions of possible chemical interactions and to explore the effects of the presence of possible metal reactants including condensation. Equilibrium fractions of chemical species were calculated at a variety of conditions. Baseline calculations were made for the altitudes near 13 km. For comparison calculations were also made at 13km but with the introduction of plausible metal atoms.

Assumptions

As a start, chemical equilibrium in the lower portion of the atmosphere is assumed. The high temperatures and pressures of Venus' lower atmosphere makes this reasonable. This assumption, however, does not hold with all species. For example the PVGC measurements indicate higher levels of CO, and lower levels of COS, than the calculated equilibrated amounts. For our purposes the gross, chemically reactive atmospheric constituents were assumed to be reasonably represented by the species

---

mole fractions given in the table below. These values are similar to those recommended and discussed by von Zahn[1].

Table 1

species	mole fraction
CO_2	.965
N_2	.035
CO	20ppm
H_2O	140ppm
SO_2	150ppm
H_2S	3ppm
HCl	0.4ppm
HF	5ppb

The atmospheric equilibrium was determined from the composition defined by this mixture and the local conditions of temperatures and pressures

Results

Baseline Atmosphere
A calculation of the equilibrium species mixture for a baseline atmosphere (i. e., one without the addition of metallic compounds) was determined by calculations[2] of mole fractions as at four altitudes- ground level, the altitude of the anomaly, and the altitudes characterized by $\pm100K$ around the anomaly altitude. The conditions used were are shown below.

Table 2

altitude	temperature	pressure
0 km	740K	93atm
3.8km	700K	8atm
13km	640K	40atm
17km	600K	29.5atm

The resulting species mole fractions are given in figure 1. Carbon dioxide and N_2 are not plotted. The computation considered many more species than shown in the figure but only those whose fractions were greater than

[1] von Zahn et. al., chapter 13 of VENUS, Hunten et. al., editors, page 325, U. of Ariz. Press, 1983
[2] The program used was developed by Gordon and McBride and is described in NASA SP 273, 1971.

1ppb are plotted. The list of species considered but whose fractions were estimated to be less than 1 ppb is given in appendix A.

From this figure it is reasonable to assume, from an equilibrium viewpoint, that there is no unusual chemical dependence on altitude in the region of the anomaly. Additionally no highly reactive, "surprise" species are formed from consideration of equilibrium of the species in appendix A.

The main hydrogen bearing species is H_2O and, in equilibrium, is nominally in the recommended amount in table 1. Other hydrogen bearing species are formed but only in trace. The measurements of HCl and HF, discussed by von Zahn[3], are the values shown in table 1, and are basically the equilibrated values. The only other hydrogen bearing species above 1ppb are H_2S and H_2. The former is less tenuous in equilibrium at 13km than the recommended amount of (0.6ppm vs 3ppm) but is consistent with the upper limit of 2 ppb suggested by the PVGC results. The former is only present in the ppb range and than only at the lower altitudes.

The main sulphur bearing species is SO_2 and, as H_2O, is present in equilibrium at the recommended levels. Other sulphur bearing species are formed, i. e., COS, H_2S, S_2 and S_2O. Although COS has not been measured in the Venusian atmosphere, the PVGC placed an upper limit of a few ppm above 22km. This value is somewhat less than the calculated amount of 8ppb at 17km, but similar enough be consistent with the assumption of equilibrium. H_2S has been discussed. Measurements of the sulphur allotrope S_3 have been made and resulting equilibrium calculations[4] yielded about the same level of S_2 calculated herein. Elemental sulphur should exist mainly as the allotrope S_2 at these lower altitudes. The last sulphur species shown, S_2O, is present in amounts greater than SO and SO_3 but only at about 10ppb.

Addition of Metallic Vapors

The metals chosen for consideration were titanium, the material of which the Atmospheric Structure Experiment temperature sensors were constructed, and metals from the composition measurements by Veneras 13 and 14[5] , viz., Mg, Al, Si, K, Ca, Ti, Mn, and Fe. The species chosen for

[3] von Zahn et. al., chapter 13 of VENUS, Hunten et. al., editors, page 401, U. of Ariz. Press, 1983
[4] von Zahn et. al., chapter 13 of VENUS, Hunten et. al., editors, page 394, U. of Ariz. Press, 1983
[5] Moroz, Chapter 5 of VENUS, Hunten et. al., editors, page 67, U. of Ariz. Press, 1983

initial examination were Ti, Mg, Fe, and K. These species were chosen partly because of the ready availability of thermodynamic data, and the likelihood of forming volatile compounds or aerosols which could reach the probe.

Figures 2-5 are the equilibrium mole fractions calculated for the conditions at 13km. The independent variable is the mole fraction of the volatilized atom. The notion of mole fractions of gas phase metal atoms at 13km over Venus might be not realizable, but the condition of chemical equilibrium does not involve consideration of the specific compounds being used as the reactions. Rather the atomic inventory and the possible compounds being equilibrated define the system.

Perusal of the figures indicates a marked influence on the balance of the trace species. No gas phase metallic compounds are formed. However an assortment of solid phase species are seen. As with the baseline calculations, more species were considered in the calculations. Appendices B through E list the species considered for each metal in addition to those species given in appendix A.

With the additions of the metals the levels of H_2O and HF are unaffected. In each case the levels of SO_2 decrease and CO and H_2 are increased. COS and H_2S are increased with Ti, K and Mg, but decreased slightly with Fe. HCl is unaffected with Ti, Fe and Mg, but with K added eventually exchanges with KCl as the chlorine compound. Graphite occur with Ti and Fe Ti and Fe and trace amounts of CH_4 occur with Ti, Fe and Mg.

The condensed species formed with each metal considered are given in the table below.

metal fraction	Titanium	Iron	Potassium	Magnesium
small	TiO_2	Fe_3O_4 FeS_2	K_2SO_4	K_2CO_3
large	TiO_2	Fe_3O_4 FeS	K_2CO_3 K_2SO_4 KCl	K_2CO_3

Appendix A

Species considered in the calculation of equilibrium composition of the baseline Venus atmosphere, but whose fractions were estimated to be less than 1 ppm.

C	CCL	CCLF3	CCL2
CCL2F2	CCL3	CCL3F	CCL4
CF	CF2	CF3	CF4
CH	CHCL	CHCLF2	CHCL2F
CHCL3	CHF3	CH2	CH2CLF
CH2CL2	CH2F2	CH3	CH3CL
CH3OH	CN	CNN	COCL
COCLF	COCL2	COF	COF2
COOH	CS	CS2	C2
C2CL2	C2CL4	C2CL6	C2F2
C2F4	C2H	C2HCL	C2HF
CHCO,ketyl	C2H2,acetylene	C2H2,vinylidene	
CH2CO,ketene	C2H3,vinyl	CH3CN	
CH3CO,acetyl	C2H4		
C2H4O,ethylen o	CH3CHO,ethanal	CH3COOH	(HCOOH)2
C2H5	C2H6	CH3N2CH3	CH3OCH3
C2H5OH	CCN	CNC	C2N2
C2O	C3	C3H3,propargyl	C3H4,allene
C3H4,propyne	C3H4,cyclo-	C3H5,allyl	
C3H6,propylene	C3H6,cyclo-	C3H6O	
C3H7,n-propyl	C3H7,i-propyl		
C3H8	C3H8O,1propanol	C3H8O,2propanol	C3O2
C4	C4H2	C4H4,1,3-cyclo-	
C4H6,butadiene			
C4H6,2-butyne	C4H6,cyclo-	C4H8,1-butene	
C4H8,cis2-buten	C4H8,tr2-butene	C4H8,isobutene	C4H8,cyclo-
(CH3COOH)2	C4H9,n-butyl	C4H9,i-butyl	C4H9,s-butyl
C4H9,t-butyl	C4H10,isobutane	C4H10,n-butane	C4N2
C5	C5H6,1,3cyclo-	C5H8,cyclo-	C5H10,1-
pentene	C5H10,cyclo-	C5H11,pentyl	C5H11,t-
pentyl	C5H12,n-pentane	C5H12,i-pentane	
CH3C(CH3)2CH3	C6H2	C6H5,phenyl	
C6H5O,phenoxy	C6H6	CL	CLCN
CLF	CLF3	CLO	CLO2
CL2	CL2O		
F	FCN	FO	FO2

F2	F2O	FS2F,fluorodisu	H
HCN	HCO	HCCN	HNC
HNCO	HNO	HNO2	HNO3
HOCL	HOF	HO2	HSO3F
HCHO,formaldehy	HCOOH	H2F2	H2O2
H2SO4	H3F3	(HCOOH)2	H4F4
H5F5	H6F6	H7F7	N
NCO	NF	NF2	NF3
NH	NHF	NHF2	
NH2	NH2F	NH3	NH2OH
NO	NOCL	NOF	NOF3
NO2	NO2CL	NO2F	NO3
NO3F	NCN	N2F2	N2F4
N2H2	NH2NO2	N2H4	N2O
N2O3	N2O4	N2O5	N3
N3H	O	OH	O2
O3	S	SCL	SCL2
SF	SF2	SF3	SF4
SF5	SF6	SH	SN
SO	SOF2	SO2CLF	SO2CL2
SO2F2	SO3	S2CL	S2CL2
S2F2,thiothiony	S8	C(gr)	H2O(s)
H2O(L)	H2SO4(L)	NH4CL(a)	NH4CL(b)
S(cr1)	S(cr2)	S(L)	SCL2(L)
S2CL2(L)			

Appendix B
Addition of Metallic Iron

Species considered in addition to those of Appendix A in the calculation of equilibrium composition of the Venus atmosphere with addition of metallic iron, but whose fractions were estimated to be less than 1 ppm.

Fe	FeC5O5	FeCL	FeCL2
FeCL3	FeO	Fe(OH)2	Fe2CL4
Fe2CL6	Fe(a)	Fe(a)	Fe(c)
Fe(d)	Fe(L)	FeC5O5(L)	FeCL2(s)
FeCL2(L)	FeCL3(s)	FeCL3(L)	FeO(s)
FeO(L)	Fe(OH)2(s)	Fe(OH)3(s)	FeS(a)
FeS(b)	FeS(c)	FeS(L)	FeSO4(s)
Fe2O3(s)	Fe2S3O12(s)	Fe(a)	Fe(c)
Fe(d)	Fe(L)	FeC5O5(L)	FeCL2(s)
FeCL2(L)	FeCL3(s)	FeCL3(L)	FeO(s)
FeO(L)	Fe(OH)2(s)	Fe(OH)3(s)	FeS(a)
FeS(b)	FeS(c)	FeS(L)	FeSO4(s)
Fe2O3(s)	Fe2S3O12(s)		

Appendix C
Addition of Metallic Titanium

Species considered in addition to those of Appendix A in the calculation of equilibrium composition of the Venus atmosphere with addition of metallic titanium, but whose fractions were estimated to be less than 1 ppm.

Ti	TiCL	TiCL2	TiCL3
TiCL4	TiO	TiOCL	TiOCL2
TiO2	Ti(a)	Ti(b)	Ti(L)
TiC(s)	TiC(L)	TiCL2(s)	TiCL3(s)
TiCL4(L)	TiN(s)	TiN(L)	TiO(a)
TiO(b)	TiO(L)	TiO2(L)	Ti2O3(1)
Ti2O3(2)	Ti2O3(L)	Ti3O5(a)	Ti3O5(b)
Ti3O5(L)	Ti4O7(s)	Ti4O7(L)	

Appendix D
Addition of Metallic Potassium

Species considered in addition to those of Appendix A in the calculation of equilibrium composition of the Venus atmosphere with addition of metallic potassium, but whose fractions were estimated to be less than 1 ppm.

K	KCN	KCL	KF
KH	KO	KOH	K2
K2C2N2	K2CL2	K2F2	K2O2H2
K2SO4	K(cr)	K(L)	KCN(s)
KCN(L)	KCL(s)	KCL(L)	KF(s)
KF(L)	KHF2(a)	KHF2(b)	KHF2(L)
KOH(a)	KOH(b)	KOH(L)	KO2(s)
K2CO3(s)	K2CO3(L)	K2O(s)	K2O2(s)
K2S(1)	K2S(2)	K2S(3)	K2S(L)
K2SO4(b)	K2SO4(L)		

Appendix E
Addition of Metallic Magnesium

Species considered in addition to those of Appendix A in the calculation of equilibrium composition of the Venus atmosphere with addition of metallic magnesium, but whose fractions were estimated to be less than 1 ppm.

Mg	MgCL	MgCLF	MgCL2
MgF	MgF2	MgH	MgN
MgO	MgOH	MgO2H2	MgS
Mg2	Mg2F4	Mg(cr)	Mg(L)
MgCL2(s)	MgCL2(L)	MgF2(s)	MgF2(L)
MgO(s)	MgO(L)	MgO2H2(s)	MgS(s)
MgSO4(s)	MgSO4(L)		

LOWER ATMOSPHERE OF VENUS

R. CRAIG, 5/94

EFFECTS ON EQUILIBRIUM CHEMISTRY
BY ADDITION OF 100 PPM OF AlF2O
FROM VOLCANIC INPUT

FUNCTION OF ALTITUDE

H2O

SO2

AlF3(a)

SO3

Al2O3(a)

HF

HCl

H2SO4

AlF2O(g)

O2

HSO3F(g)

ALTITUDE, KM